2012

Evaluation of Live-Load Distribution Factors (LLDFs) of Next Beam Bridges

Abhijeet Kumar Singh

University of Massachusetts Amherst, aksingh@engin.umass.edu

EVALUATION OF LIVE-LOAD DISTRIBUTION FACTORS (LLDFs)

OF NEXT BEAM BRIDGES

A Thesis Presented

By

ABHIJEET KUMAR SINGH

Submitted to the Graduate School of the
University of Massachusetts Amherst in partial fulfillment
Of the requirement for the degree of

MASTER OF SCIENCE IN CIVIL ENGINEERING

May 2012

CIVIL AND ENVIRONMENTAL ENGINEERING

EVALUATION OF LIVE-LOAD DISTRIBUTION FACTORS (LLDFs)

OF NEXT BEAM BRIDGES

A Thesis Presented

by

ABHIJEET KUMAR SINGH

Approved as to style and content by:

_____

Breña, Sergio, Chairperson

_____

Lardner, Thomas, Member

_____

Civjan, Scott, Member

_____

Richard N. Palmer, Department Head
Civil and Environmental Engineering Department

ACKNOWLEMDGEENT

I would like to extend my thanks to my advisor, Dr Sergio Breña for his guidance and support throughout the project. It is his guidance and support because of which I am able to complete my thesis. I would also like to say thank to my committee members, Dr Lardner and Dr Civjan for their assistance and feedback on the research. I am also thankful to the guidance provided by Kalayacki Emre in learning the advance tools SAP 2000 V14.2 in a very short duration of time. I am also thankful to my parents who were always with me in my good and bad time and helped me to look at life in more comprehensive and balanced manner

ABSTRACT

EVALUATION OF LIVE-LOAD DISTRIBUTION FACTORS (LLDFs)

OF NEXT BEAM BRIDGES

MAY 2012

ABHIJEET KUMAR SINGH, M.S.C.E.

UNIVERSITY OF MASSACHUSETTS AMHERST

Directed by: Professor Sergio Breña

A new precast-prestressed cross section was recently developed by a consortium of engineers from the six New England states, New York and members of the northeast region of PCI. The northeast extreme Tee (NEXT) beam is efficient for medium Bridge spans (50 to 80 ft long). Field formwork savings are introduced by having a flange cast integrally during fabrication of the beams at the precasting plant. Job safety is increased because a working platform is created. The flange width of the NEXT Beams can be adjusted during fabrication to accommodate roadways of different widths and skew angles. Because the section is new with complexity in its shape, the present design guidance cannot be used to evaluate LLDFs for NEXT beams within the context of the AASHTO LRFD. In particular, the use of live-load distribution factors (LLDFs) equations in LRFD for NEXT beams is not straightforward. The distance between the beam webs is variable depending on whether it is measured within a beam module or between adjacent modules. In absence of detailed information a PCI technical committee evaluated LLDFs (through AASHTO 2010 Bridge specification) for the NEXT beams used in the Brimfield Bridge by two different approaches and found one of them conservative. The conservative approach was single stem which uses the average spacing

(between webs ([S1+S3]/2)) for use in the LLDF equations.. The committee expressed concerns about whether trends of LLDFs would be similar for other parametric sets, and would like to standardize the methodology for the Bridge projects in Massachusetts with NEXT beam as the girder. To verify the conservativeness of single stem methodology (for the evaluation of LLDFs) for other parameters this research project was initiated. LLDFs are evaluated based on the two approaches and compared with the LLDFs obtained through finite element modeling.

The results of 40-3D finite element models have been used to compare the LLDFs obtained from AASHTO 2010 Bridge design specification. The results were also used to compare different parameters that affect LLDFs of NEXT beams including span, skew angle, and beam end fixity. The finite element models were created using a Bridge prototype that is being instrumented for future field verification of the analyses. The models were created using frame elements for the beams and shell elements for the cast in place deck. The integral abutment and foundation of the Bridges was included in the models in which piles are created using frame elements and abutments are created using shell elements. The results indicate that the approach taken for the design of NEXT beams is in general conservative for interior girders of the Bridge. On the contrary such the adopted approach was not yielding the higher value of LLDFs. The variation in strains due to losses are compared by two methods (strains variation obtained from field data and strain variation obtained based on AASHTO equation of losses) to verify the AASHTO equation of losses.

TABLE OF CONTENTS

LIST OF TABLES

LIST OF FIGURES

xv

CHAPTER 1

INTRODUCTION

This chapter provides an introduction and benefits associated with the use of a newly developed prestressed concrete beam section for use in short to medium span Bridges. Because the beam does not fall into typical cross sections included in the AASHTO LRFD specification (2010), recommendations about its design, specifically the appropriate live-load distribution factors, need to be provided to engineers. This new section provides several safety and economic benefits making attractive for use within the span range for which it was intended.

1.1 NEXT Beam Introduction and Benefits

The northeast extreme tee (NEXT) beam is a prestressed double T-beam recently developed by a consortium of engineers from all six New England states, New York and members of the northeast region of prestressed concrete institute (PCI). Its efficient design minimizes cost and labor in both manufacturing plant and at the job site. It also eases the construction process and improves the safety for the workers. The lack of draped (harped) strands is a significant benefit during fabrication. The elimination of deck forming in the field due to its top flange (Figure 1.1a) saves significant time during construction and also provides an instant platform for work. The need of a diaphragm near the supports or intermediate diaphragms is eliminated as the top flange provides sufficient lateral stability to the NEXT beam while placing fresh concrete. The cantilever portion of the NEXT beam (outside the stem Figure 1.1b) provides space in the exterior girder to erect parapet wall which keeps designers and contractors away from creating false work for the erection of parapet wall. The NEXT beam (Figure1.1c) can

1

accommodate multiple utilities such as drainage pipe and electrical wire between the stems and there is no need to create any false work to hide them. The widths of the NEXT beams can be adjusted readily in fabrication to accommodate roadways which are tapered in plan. Moreover its flange can be modified readily to accommodate gentle curve of the highway alignment. The NEXT beam is available for skew angle up to 30°.
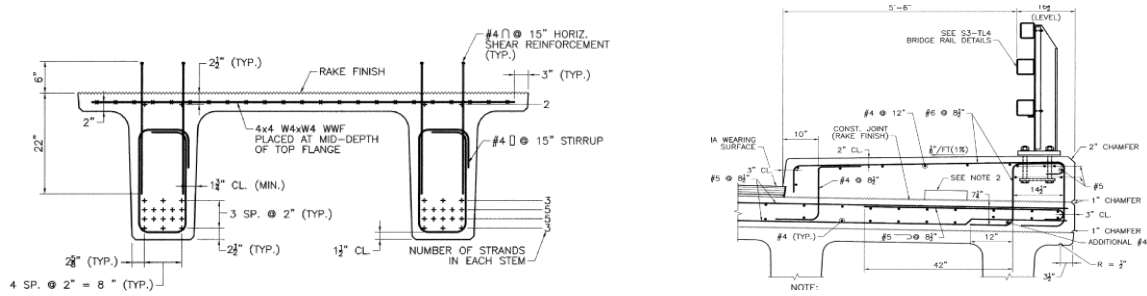
(a) No Need of Formwork and diaphragm   (b) No Need of false work

to cast deck and Parapet
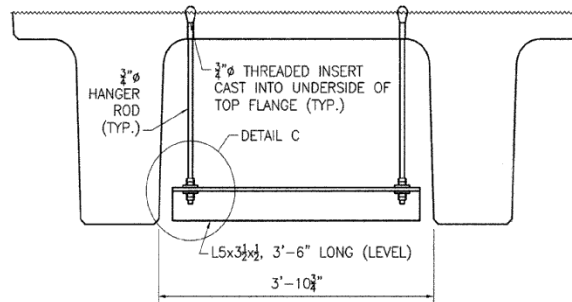
(c) No Need of false arrangement to hide multiple utilities

Figure1.1 Benefits of NEXT Beam

1.2 Motivation of Thesis

The numerous benefits associated with the NEXT beam are going to make it a wide spread choice for the owners in the future for the spans ranging between 50 ft (15.24 m) to 80 ft (24.38m). Apart from the consortium states, which developed the NEXT beam

2

other states have also accepted NEXT beam due to its versatility. But the complex shape of NEXT beam creates confusion among the members of PCI technical committee at the front of live load analysis based on live load distribution factors (LLDFs). It is very important to investigate all the concerns pertaining to NEXT beam so that it can be used at widespread level in the future. To formulate the problem statement it is important to explain LLDF, its type and formulations mentioned in AASHTO (2010 Bridge design specification).

1.2.1 LLDF Introduction

The effect of live load in terms of actions (bending moment and shear force) on the girder of the Bridge is obtained through LLDFs. The LLDFs make live load analysis simpler and keeps designer of the Bridge away from complex three dimensional live load analyses. The use of LLDFs is based on equation 1.1 in which F_I the maximum force at particular section of the girder of the Bridge, which can be obtained through influence line method.

$$F_s = g * F_I$$ ..... Equation 1.1

Where,

F_s = the maximum force at the section of concern in the girder in terms of action (bending moment and shear force).

g = LLDFs.

F_I = the maximum force at the section of concern obtained by running the live load of interest on simply supported girder (only).

3

1.2.2 LLDF Types

The LLDFs can be of different types. Based on action it can be for bending moment and shear force. Based on the division of lane it can be for one lane loaded and two or more lanes loaded. Based on the arrangement of girders it can be for interior and exterior girder. So there are eight different types of LLDFs and all of them are considered while evaluation, verification and conclusion about the problems related to LLDFs of the NEXT beams. Notation and definition of all the eight types are as follow.

gM_1^{i-} = LLDF for bending moment for interior girder for one lane loaded.

gM_2^{i-} = LLDF for bending moment for interior girder for two or more lanes loaded.

gM_1^{e-} = LLDF for bending moment for exterior girder for one lane loaded.

gM_2^{e-} = LLDF for bending moment for exterior girder for two or more lanes loaded.

gV_1^{i-} = LLDF for shear force for interior girder for one lane loaded.

gV_2^{i-} = LLDF for shear force for interior girder for two or more lanes loaded.

gV_1^{e-} = LLDF for shear force for exterior girder for one lane loaded.

gV_2^{e-} = LLDF for shear force for exterior girder for two or more lanes loaded.

1.2.3 NEXT Beam Spacings and Problem Statement

Live load distribution factors in AASHTO LRFD require the use of spacing between girders to determine values that can be used for design of Bridge girders. In NEXT beams the spacing between girders is not uniquely defined, resulting in uncertainty about the most appropriate value.

Figure 1.2 is one of the Bridge cross section using NEXT beams as the girder. The nearest structure to NEXT beam is "I" type of cross section which is mentioned in *table 4.6.2.2.1-1* of AASHTO (2010 Bridge design specification).

4
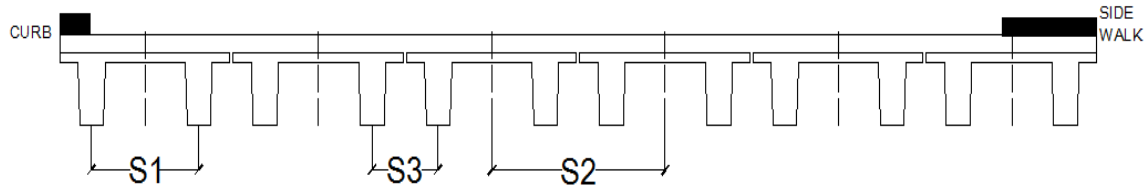
Figure1.2: NEXT Beam with Varying Spacing Between Stems.
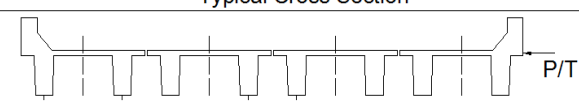
Supporting Components	Type of Deck	Typical Cross Section
Precast Concrete Double T Section With Shear Keys and With or Without Post Tensioning.	Integral Concrete	P/T

Figure1.3: I type of Girder (Double T Beam Girder)

In the mentioned *table* of "I" type girder the spacing between the stem of individual double T beam is similar to the spacing between the stem of adjacent double T beam. Moreover the horizontal spacing (between the center of gravity of two adjacent girders) is also similar to the spacing between the stems. This constant spacing has been used for the evaluation of LLDF for double T beam.

But if we look at Bridge cross section with NEXT beam as girder in Figure 1.2 the three spacings are different. S1 is the spacing between the stems of same NEXT beam. S2 is the spacing between the c.g (horizontal center of gravity of NEXT beam) of two adjacent NEXT beams, whereas S3 is spacing between stems of two adjacent NEXT beams. The equations (Equation 3.1, 3.2, 3.4 & 3.5) mentioned in AASHTO (2010 Bridge design specification) to evaluate LLDFs in interior girders contain only one S, the spacing between the girder. The equations are also mentioned in Chapter 3 by Equation 3.1, 3.2, 3.4 and 3.5

The three different spacings (S1, S2, S3 Figure 1.2) in NEXT beams create a concern among members of PCI technical committee, that what spacing should be taken while

evaluation of LLDFs. Based on the concern related to spacing, PCI technical committee has contacted the original authors of the AASHTO Bridge design specification and found that NEXT beam type of structure with varying spacing *(Figure 1.2)* was not specifically investigated through any of the advanced form of analysis during development of code. In the absence of detailed verification of LLDFs of NEXT beam type the PCI technical committee evaluated the LLDFs for the Bridge (with NEXT beam as the girder) by single (*Type K* Figure 1.4) stem (SST) approach and by double (*Type I* Figure 1.3) stem approach (DST) using 2010 AASHTO Bridge design specification. In SST approach each stem of NEXT beam was considered as *K type* (Figure 1.4) whereas in DST approach NEXT beam was considered as *I type* (Figure 1.3). AASHTO formulation of LLDFs contains spacing between the girders. The spacing considered in SST approach was average spacing ([S1+S3]/2) whereas spacing considered for DST approach was S2 (spacing between horizontal center of gravity between NEXT beam).
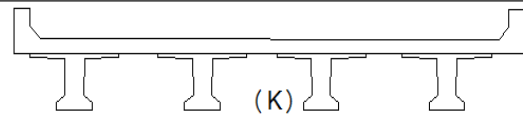
Supporting Components	Type of Deck	Typical Cross Section
Precast Concrete I or Bulb T section.	Cast in Place Precast Concrete	

Figure1.4: K type of Girder (I Beam Girder)

Based on the results PCI technical committee concluded that SST approach is more conservative for some of the particular case investigated. Further verification for other sets of parameters (varying spans and varying skew angles) is required so that the method can be standardized for the LLDFs evaluation of NEXT beams.

The primary objective of the thesis is to ascertain whether the conclusion of PCI technical committee extends to other sets of parameters or not. The verification has been

done in Chapter three in which LLDFs has been evaluated for K type (Figure1.4 SST approach) of girder as well as for I type (Figure 1.3 DST approach) of girder. In the last of chapter the evaluated values from both methods have been compared. It is also important to verify the LLDFs through advance form of analysis. Chapter four is all about creation of finite Element Model (FEM), evaluation of LLDFs for different set of parameters and to compare the obtained LLDFs to the LLDFs obtained through latest AASHTO (2010 Bridge design specification). The comparison will help us to check whether the variation of LLDFs for different set of parameters obtained through FEM analysis is in congruence with AASHTO formulations or not. The comparison will also help us to ascertain the method to get the most conservative value of LLDFs.

The NEXT beam is a prestressed beam and therefore subjected to complex long term effects of creep, shrinkage and relaxation of strands. It is important to verify whether the losses taking place in the NEXT beam is in congruence with latest AASHTO (2010 Bridge design specification) or not. Instrumentation of the NEXT beam will give us strain measurement at different stages. The strain values along the depth of NEXT beam will help us to ascertain the behavior of NEXT beams in terms of creep and shrinkage. Strains at different stage will also include the loss component due to long term effect of creep, shrinkage and relaxation. Future work is based on comparison of strain component obtained at various stages from analytical calculation and instrumentation outcome. This comparison between strains will also help us to compare analytically evaluated value of long term losses with long term losses obtained through instrumentation.

1.3 Brimfield Bridge Project

7

For this research, a prototype Bridge located in Brimfield, Massachusetts was selected in order to establish typical characteristics of a NEXT beam Bridge. The Brimfield Bridge is an integral abutment Bridge (IAB) that can be divided in to three main components: - super structure, sub structure and foundation. The super structure portion has six NEXT 32 beams cast integrally in to the abutments. Abutments are supported on the foundation which encompasses six HP 10x 57 piles. The Bridge is skew with 30° skew angle. Using the Brimfield Bridge characteristics, three parameters importantly affecting live-load distribution factors of NEXT beam Bridges were selected and varied systematically. The three parameters chosen are span length, skew angle and end support conditions. The effects of these parameters on live-load distribution factors are discussed in Chapter three to five. Full details of the Brimfield Bridge are provided in Chapter 3.

1.4 Scope of Research

The core scope of the research can be divided in to three parts. Firstly the evaluation of AASHTO (2010 Bridge design specification) live load distribution factor for the NEXT beam to verify the outcome of PCI technical committee. Secondly it is important to verify the AASHTO (2010 Bridge design specification) formulation through some advance from of analysis in terms of variation of LLDFs with parameters and conservativeness. Therefore FE models are created to get the LLDFs for the NEXT beam. Details from instrumentation will be used to verify complex long term behavior of Bridge pertaining to creep, shrinkage and relaxation. Different types of losses (short term as well as long term) at the level of the center of prestressing force of strands has been evaluated in terms of strains from FEM analysis and then compared from the strains obtained from field data.

1.4.1 Evaluation of LLDFs from Latest AASHTO Specification

LLDFs for the NEXT beam have been evaluated based on latest AASHTO (2010 Bridge design specification) for K type (DST approach Figure 1.3) and I type (SST approach Figure 1.4) of the girder and the obtained value has been compared for different parametric sets. The evaluation of LLDFs has been done for five of the parametric sets to study LLDF with varying span and skew angle of the Bridge. The spans considered are 50ft (15.24m), 66.67ft (20.32m) and 80ft (24.38m), and the skew angle considered are 0°, 30° and 45°. Spacing between the girders has not been considered as a parameter, as it is fixed and marginally more than the flange width of girder. The comparison of LLDFs obtained from both the methods will help us to ascertain whether the outcome of PCI technical committee for particular case can be generalized for wide spectrum of parameters or not. This whole evaluation and comparison has been done in Chapter three.

1.4.2 Evaluation of LLDF from FEM Methods

It is important to verify the LLDFs of NEXT beam with an advanced form of analysis. LLDFs have been evaluated with the help of FEM analysis in Chapter five. Chapter five describes the creation of two different type of FEM model with different sets of parameters and to evaluate the LLDFs. The first model is simply supported model which is very near to the LLDFs value obtained from the AASHTO (2010 Bridge design specification). The second model is integral abutment Bridge model which is similar to the actual Brimfield Bridge. Again the parametric study of LLDFs of the NEXT beam has been done based on two of the important parameters i.e. span of the Bridge and skew angle of the Bridge. The spans considered are similar to the previous subsection i.e. 50ft (15.24m), 66.67ft (20.32m) and 80ft (24.38m) and the skew angle considered are 0°, 30°

9

and 45°. Spacing between the girders has not been considered as parameter, as spacing is fixed as and marginally more than the flange width of girder. Under FEM verification 40 FEM's are generated to evaluated LLDF for the NEXT beam with different parameter. Out of 40 FEM's,20 FEM's are for simply supported Bridge and 20 FEM's are for IAB models. The FEM LLDFs are evaluated for three different cases.

Evaluation of LLDFs for simply supported Bridge through AASHTO (2010 Bridge design specification).

Evaluation of LLDFs for simply supported Bridge through linear FE analysis.

Evaluation of LLDFs for Integral Abutment Bridge through non linear FE analysis in which soil has been modeled as non liner spring.

The obtained values of LLDFs from two of the FEM have been compared in Chapter five to ascertain the effect of inclusion of sub structure and foundation. In Chapter five LLDFs obtained from all the four approaches are compared to verify whether the variation of LLDFs obtained from FEM have the same nature of variation or not. The comparison will further help us to find out which method will gives us the higher value of LLDFs for different type of forces (bending moment and shear forces) and for different type of components (interior girders and exterior girders).

1.4.3 Field Test

The scope of field test is to monitor the Bridge in the span of 3 years through various strain gauges fixed at numerous locations with the intent of its long term behavior such as Creep, Shrinkage, deflection and crack width. The strain gauge data will give the strains at different stages of fabrication, erection and service period of the girder. These strain

values will be useful to evaluate creep and shrinkage loss at different time interval. Through field testing strains were obtained before and after the following stages.

At gage installation.

20 hrs after pouring of concrete.

At the time of detentioning of strands.

At the time of placing of girder on temporary support in casting yard.

After placing the girder over abutment.

After pouring slab concrete.

At the time of live load testing.

At the interval of each three months.

In Chapter six the strain values has been evaluated from the FEM for the actual Bridge at different stages and then compared with the strains obtained from the field instrumentation. The strains at different stages and at different height of the girder will help us to ascertain the behavior of NEXT beams at different stages. Moreover the strain values obtained from the field data can help us to get the long term loss (creep loss, shrinkage loss, relaxation loss) in the strands. This loss will be compared with the loss obtained from analytical formulation of long terms effects from AASHTO (2010 Bridge design specification). The comparison will help us to verify AASHTO (2010 Bridge design specification) equations of losses in the NEXT beam.

CHAPTER 2

LITERATURE REVIEW

In the past many studies had been done in the area of skew Bridge. The major concerns of the studies were to establish the behavior of skew Bridges, determine LLDF, evaluate the influence of numerous parameters, and investigate the validity of design assumption and many more. The studies were done through field and laboratory tests to compare the outcome through numerical approaches which were based on advance FEM analysis from available advanced tools. The intent of this section is to put forward all the details of those investigations and their outcome and further utilize them in the investigation of LLDF evaluation of NEXT beam bridges for different parametric sets.

2.1 Field Testing

Bishara et al (1993) conducted a field test of a 137feet (41.75m) span four lane composite steel-concrete Bridge with skew angle of 58.5^o. The main intent was to investigate the validity of wheel load distribution factor expressions mentioned in AASHTO (2010 Bridge design specification) from FEM analyses of 36 Bridges of varying geometry. The Bridge located in Columbus, Ohio, was tested using six dump trucks with known axle loads. Once the field test was complete, sensitivity studies were conducted using various parameters such as skew angles, varying spans, number of lane loaded and slab width. It was found that skew angle has the highest impact on the wheel - load distribution factor. However, the skew effect is negligible when the skew angle is less than 30°. Distribution factors for interior and exterior girder were derived from field studies and compared to the FEM modeling and AASHTO (2010 Bridge design specification). For skew angle greater than 30° the LLDF derived from equations were found to be 5-25% higher than

12

the resulting factors from the FEM models. The LLDF for the interior girder were found to be 30-85% that of the AASHTO specified factor of S/5.5 and 30-70% of the AASHTO factors for the exterior girders.

Barr et al (1999): In this paper with the help of live load testing reliability of FEM model of three span continuous Bridge was evaluated. After establishing the reliability the model, this was used to evaluate LLDFs for flexure for 24 different variations in terms of diaphragm, their locations, lifts, continuity and skew angles. Based on study it was concluded that lifts, end diaphragm and skew angles affect the LLDFs whereas the effect of intermediate diaphragm and continuity was insignificant.

Civjan et al (2007) – The recent studies in 2007 were done to appreciate the behavior of sub structure and foundation of IAB with respect to interaction with soil and to verify various assumptions used while analysis and construction of the IAB. A three span Bridge in Orange- Wendell, Mass. (OW) was used as the parametric study to determine the influence of Bridge design which allows the effects of parameters to be directly evaluated. The Bridge was extensively instrumented to provide data on the various movements, pressures, and strains experienced by the Bridge over time. The non-Linear FEM analysis with the help of GT STRUDL has also been used to check the congruence of Bridge behavior with respect to output obtained from field data. The parameters used in the paper were abutment backfill, degree of pile restraint in the top 3.0m of pile and methods of obtaining abutment soil-spring properties and distribution of backfill pressure.

Brena et al (2007)- In the similar line Brena et al have used various field data collected in the span of three years of service of an integral Bridge constructed in Massachusetts for

13

better understanding of lateral movement of abutment and piles corresponds to long terms loadings such as temperature variation along with soil structure interaction. This paper was useful in getting the idea of related to effect of backfill and soil restraints on the piles deformation and forces.

2.2 Laboratory testing and Analytical Modeling

Apart from various field tests laboratory studies in coordination with analytical modeling have also been performed in the past to better appreciate the behavior of skew Bridges. The approach was to utilize laboratory testing to validate an analytical model and to include sensitivity studies to predict the effects of specific parameter.

Newmark et al (1948) – Reported on a series of laboratory tests on straight and skewed Bridges and based on experiments performed it was concluded that the skewed Bridge with skew angle of 60° was critical in terms of shear in comparison of Bridge with straight configuration. In addition it was concluded that the maximum moments in the beam decreased for large angle of skew and positive moment at the centre of a panel increased.

Helba and Kennedy et al (1995, 1996) performed laboratory studies of girder moments and shear distribution of six simply supported skew composite steel concrete Bridges with skew angle of 45°. After series of experiments and based on various experiments it was concluded that skew angle is the most critical parameter for the distribution of shear force and controlling factor for the design of exterior girder.

Yochia Chen (1999): This paper considered different types of Bridges (Steel I girder-with cross bracings, prestressed concrete box girder with diaphragm, prestressed I girder with diaphragm) for AASHTO LLDFs and FEM LLDFs. It explains the detailed process

14

to prepare the FEM model in Adina (FEM tool). Based on comparison it concluded that FEM LLDFs are lesser than the AASHTO LLDFs and incorporating the advanced FEM tools does not affect the sizing of the girder. The most important finding was that the load distribution factor is not affected by the type of load considered.

Khaloo et al (2003) : This paper studied the LLDFs for simply supported skew Bridges for varying parameters such as skew angle (0-60°) , varying spacing (1.8m ,2.4m ,2.7m) between girders, varying span (25m, 30m, 35m) and different arrangement of interior transverse diaphragm (parallel to support line, perpendicular to girder, diaphragm with different spacing) . The comparison between AASHTO LLDFs and FEM LLDFs are in congruence to other evaluations. For flexure, LLDFs was not varying till 30°. Beyond 30° the LLDFs for flexure reduce and variation between two comparisons was different for interior and exterior girders. With increased spacing it was observed that LLDFs increase. For span parameter the flexure LLDFs for interior girder was not sensitive whereas for exterior girder it was increasing. The transverse diaphragm perpendicular to the girder was found to be the best arrangement for even distribution of load. For this type of diaphragm varying spacing between them does not affect the load distribution factor.

Yousif et al (2007): A comprehensive study on LLDFs, dependent parameters (span, slab thickness, spacing between girders, longitudinal stiffness) and range of applicability of the mentioned parameters were studied on all the six type of PCI beam I to VI. Under study LLDFs obtained from AASHTO LRFD (2004) were compared to the LLDFs obtained from FEM analyses in terms of their ratio. The study was done with twelve different span between (6m to 73m) , four spacing (1.1m , 2.2m, 2.99m, 4.9m) and four different slab thicknesses (110mm, 190mm, 240mm, 300mm) through creation of 886

15

FEM Bridge model. The study was done on the same data base of the Bridge considered by the Zokie et al (1991). The study concluded the ration for the flexure moment to be greater as well as less than 1.0 for different types of PCI beam in different range of spans. Zokaie et al (2007) – This paper brief out the development of present LLDF for the AASHTO (2010 Bridge design specification), which was based on extensive study of previously adopted S/D formulae along with studies on several hundred actual Bridges through numerical approach of FEM analysis. This paper was helpful in establishing various super structure parameters such as span of the Bridge, spacing between the girder, and skew angle of the Bridge.

Murat et al (2008): This paper was based on investigation of the effect of soil-structure interaction on different component of IAB. Apart from soil-structure interaction variation different properties of super structure such as stiffness of girder, spacing between the girders were also considered. Soil properties were varied with respect to soil stiffness of foundation. The effect of backfill and its compaction level were not considered. Sub structure properties of abutment were varied by varying its depth and thickness. The presence and absence of wing wall were also considered. The results from various 2 dimensional and 3 dimensional FEM model were used for the evaluation of LLDF. Through the outcome it was concluded that varying properties in soil stiffness, sub structure and foundation properties has negligible effect on the LLDF on the super structure portions. However the effect was significant on sub structure and foundation.

Devin K Harris (2009): This paper discuss different type of methodologies (beam line method, load fraction approach, S over approach, AASHTO LRFD design specification approach, lever arm approach, in service assessment, FEM approach), used to evaluate

16

the distribution factor. It critically analyzed the strength and shortcomings of different methods through comparison and validation through FEM. Based on study, comparison were made on the appropriateness of different type of neutral axis for composite bridge to get the true response are discussed. The comparison and conclusion also considered the effect of secondary members and boundary conditions.

17

CHAPTER 3

CALCULATION OF AASHTO LIVE LOAD DISTRIBUTION FACTOR

Live load distribution factors (LLDFs) are used to calculate the live load bending moment and shear force on Bridge girders caused by moving loads. LLDFs make not only live load analysis simpler but also keep designers away from having to develop complex 3-D models of simple Bridges. This chapter mainly contains the evaluation of LLDFs for the recently developed North East Extreme Tee (NEXT) beam cross section using AASHTO LRFD Specifications (2010).

Evaluation of LLDFs in this chapter was conducted using two generic cross sections included in the AASHTO LRFD (2010): Type i (Figure 3.1) and Type k (Figure 3.2). In this project, evaluation of LLDFs of a type k cross section is termed the single stem (SST) approach, whereas evaluation of a type I cross section is termed the double stem (DST) approach. The objective for evaluating LLDFs using two different approaches is to verify the recommended procedure proposed by the prestressed concrete institute (PCI) Bridge technical committee for designers. These recommendations indicated that a SST approach would result in conservative estimates of moments and shears for most of the cases typically encountered in practice.
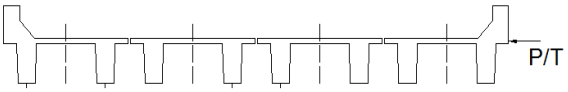
Supporting Components	Type of Deck	Typical Cross Section
Precast Concrete Double T Section With Shear Keys and With or Without Post Tensioning.	Integral Concrete	P/T

Figure3.1: Type I Girder (Double T Beam Girder)
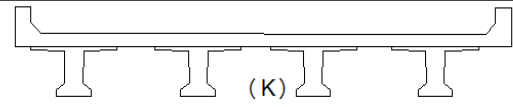
Supporting Components	Type of Deck	Typical Cross Section
Precast Concrete I or Bulb T section.	Cast in Place Precast Concrete	(K)

Figure3.2: Type K Girder (I Beam Girder)

The effect of parametric variation such as of varying span and skew on LLDFs are studied based on actual prototype Bridge model i.e. Brimfield Bridge model which has span of 66.67ft (20.34m) with 30° skew angle. Section 3.1 and 3.2 explains the detail of Brimfield Bridge's super structure, sub structure and foundation details.

3.1 Super Structure Brimfield Bridge

The super structure portion of the Bridge has six NEXT 32 beam (Figure 3.2) as shown in Figure 3.3. The Bridge has safety curbs on the east side having the width of 1.42ft (0.43m) and side walk in the west side with width of 4.37ft (1.33m).The spacing between the girders is 8.08ft (2.44m). The total width of the Bridge is 48.5ft (14.78m). All the details of mentioned dimensions are shown in Figure 3.3.
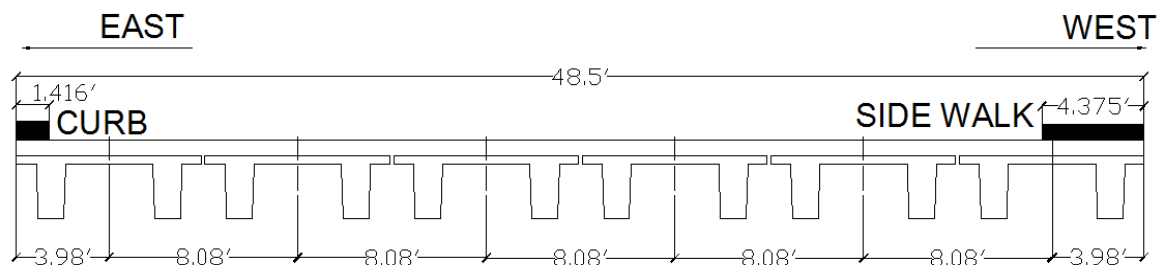
Figure3.3: Bridge Cross Section- Brimfield Bridge

The Bridge is spanning from North to South and having the span of 66.67ft (20.34m) between the centers of gravity of the Abutment. Figure 3.5 and Figure 3.6 are showing arrangement plan and elevation of the Bridge with other minute details. The NEXT beam

is further topped by 0.67ft (0.20m) thick concrete deck slab which will act compositely with the NEXT beam.
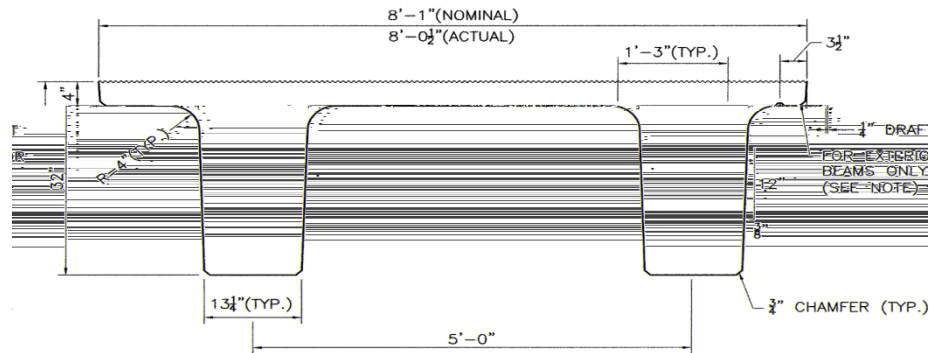
Figure3.4: NEXT 32 Beam
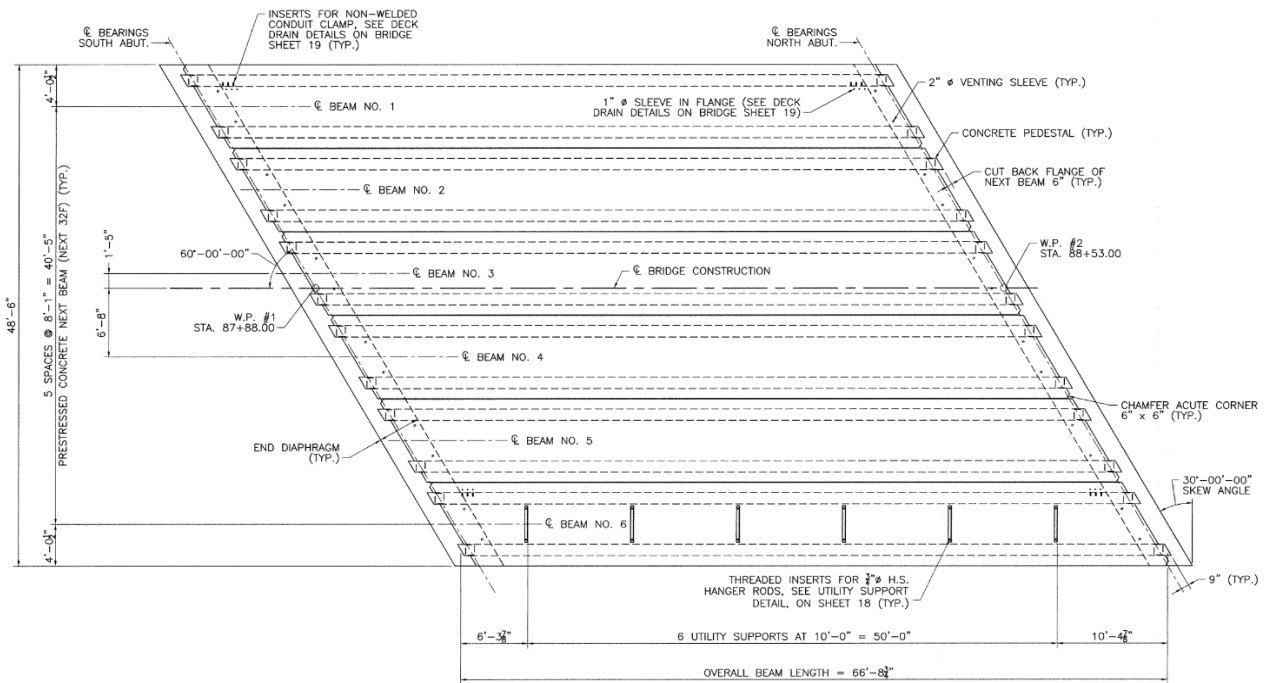
Figure3.5: Arrangement Plan of the Bridge
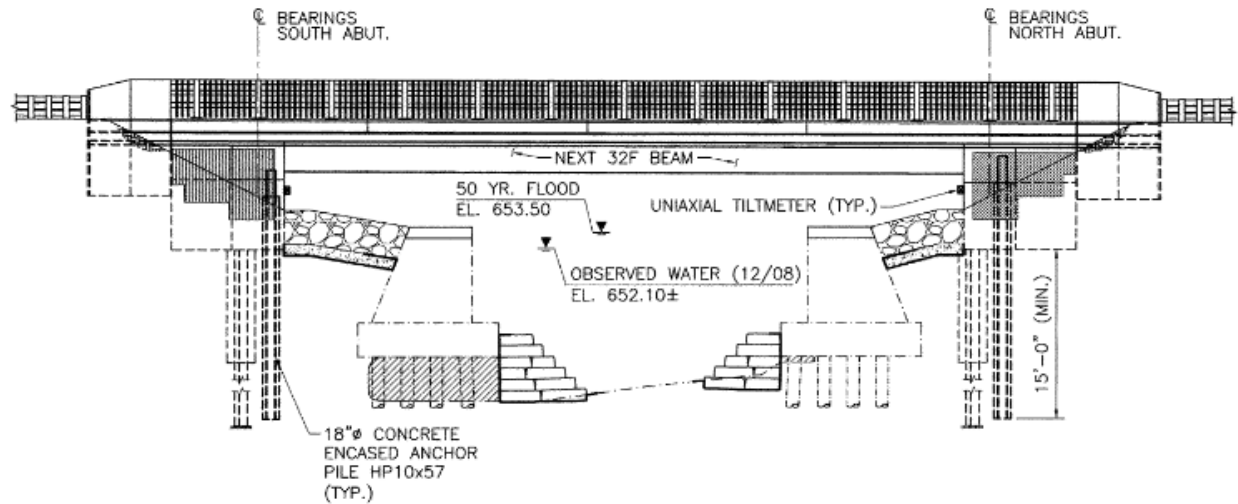
Figure3.6: Elevation of the Bridge

3.2 Sub Structure and Foundation Brimfield Bridge

The NEXT beam is supported over the abutment (sub structure) in North and South side. The abutment is reinforced cement concrete (RCC). The abutment's thickness, length and height are 4ft (1.22m), 56.97ft (17.36m) and 10.08ft (3.07m) respectively. The abutment is attached to the wing wall (sub structure) which provides extra rigidity to the abutment along with retaining the soils. The wing wall's thickness, length and height are 1.623ft (0.49m), 3.44ft (1.04m) and 10.08ft (3.07m) respectively. The abutment is further supported on six HP 10x57 piles in both sides as shown in Figure 3.7 (abutment on the North side) and Figure 3.8 (abutment of South side). Six piles of HP 10x57 sizes are used under each abutment and are not in line with road's skew, but perpendicular to the abutment.

21
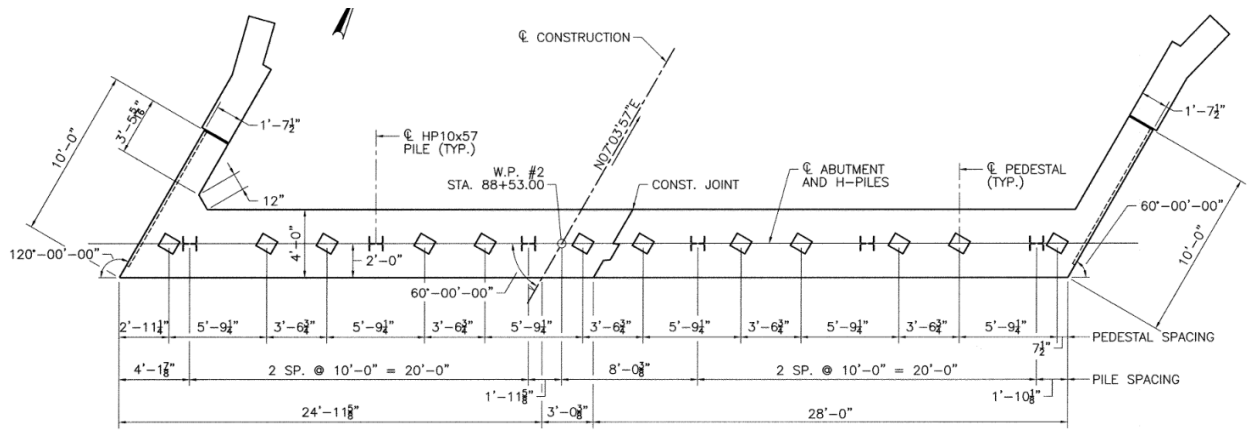
Figure 3.7: Abutment on North Side
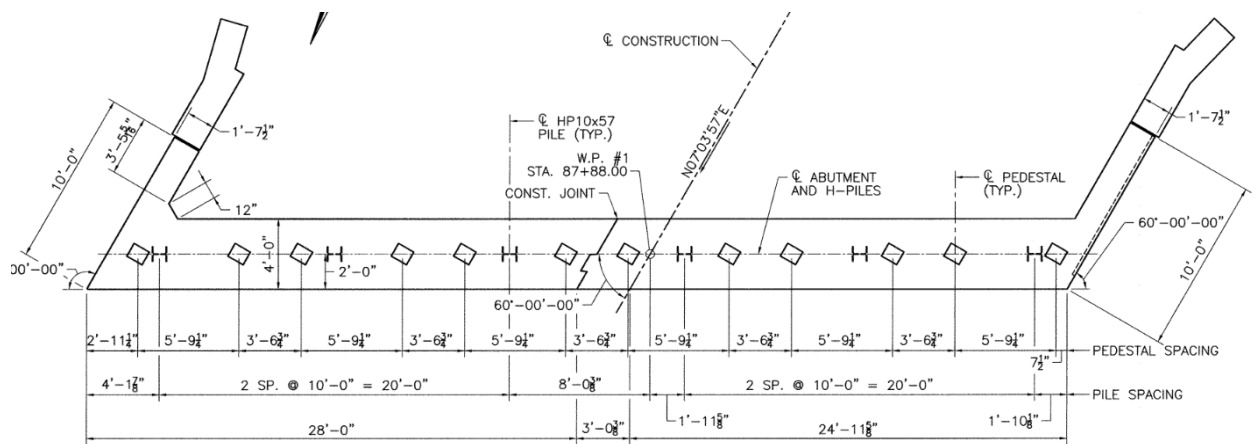
Figure 3.8: Abutment on South Side

3.3 Calculation of LLDFs for NEXT Beam Bridge

LLDFs for typical NEXT beam Bridges were calculated for bending moment and shear force for interior and exterior girders. These calculations were repeated assuming one lane loaded and two or more lanes loaded. The critical LLDFs for design is taken as the maximum of these two lane loading cases. AASHTO equations for LLDFs (Equation 3.1 to 3.1o) are dependent on various parameters. Spacing between the girders and Bridge span are the most important parameters as seen in these equations. NEXT beam Bridges can be efficiently used in the range of 50 to 80ft (15.24 to 24.38m), and because of this

22

LLDFs are calculated for three different spans in the following section (50, 66.67, and 80ft [15.24, 20.32, and 24.38m]). For an individual NEXT beam, the width of the flange is set so spacing between NEXT beams is determined by the flange width. Therefore, girder spacing was not chosen as a parameter that could vary significantly. Bridge skew angle was another important parameter chosen for calculation of LLDFs in NEXT beam Bridges. Three different skew angles 0°, 30° and 45° have been considered for LLDFs evaluation. A Bridge with span equal to 66.67ft (20.32m) and a skew angle of 30° represents a prototype Bridge from which basic structural details were drawn for this project (Brimfield Bridge). Nine combinations of parameters were studied to assess their influence on LLDFs. All these parameters were studied on the base model of Brimfield Bridge which has three portions of super structure sub structure and foundation.

3.4 Calculation of LLDFs - Single Stem Approach (SST-type k)

The single stem approach (SST) was proposed by the PCI Northeast Bridge technical committee as the conservative approach for design of NEXT beams Bridges. In a type k cross section approximation (AASHTO 2010), each individual stem is considered as a girder (Figure 3.2). Calculation of LLDFs must consider the spacing between stems, which for NEXT beam Bridges is taken as the average ([S1+S3]/2) of the spacing between stems in the same NEXT beam unit (S1-5ft [1.52m]) and the spacing between the stems of adjacent NEXT beam units (S3-3ft [0.91m]). The value of LLDFs obtained in this manner is multiplied by two to get the LLDFs for design of a NEXT beam.

The Brimfield Bridge is made up of six NEXT beams, of which two are exterior girders and four are interior girders. For the SST approach, the Bridge is considered to contain

23

twelve girders, with stems B2 to B11 are representing interior girders, and B1 and B12 are representing exterior girders (Figure. 3.2).
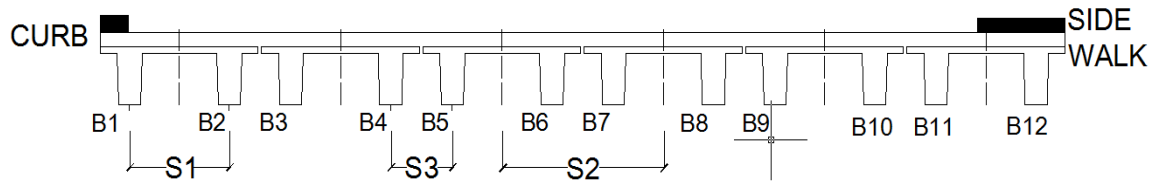
Figure3.9: Beam Numbering Used in Single Stem Approach

The design LLDF computed for interior girder is the maximum value of LLDFs of the ten interior girders (B2 to B11), whereas the design LLDF for exterior girder is computed from the maximum value determined for the two exterior girders (B1 and B12).

3.5 Calculation of LLDFs - Double Stem Approach (DST - type i)

Calculation of LLDFs using the double stem approach (DST) considers the entire NEXT beam unit as a single beam. The spacing (S2) between the center of gravity of two adjacent NEXT beams (Figure 3.9) is used for the spacing parameter in the LLDF equations. The LLDF values thus obtained are used directly in design for individual NEXT beams. Using again the prototype Bridge discussed earlier (Brimfield Bridge), a total of six NEXT 32 beams are considered making up the Bridge cross section, of which two are exterior girders and four are interior girders (Figure 3.10). Under the DST approach B2 to B5 are interior girders, whereas B1 and B6 are exterior girders.
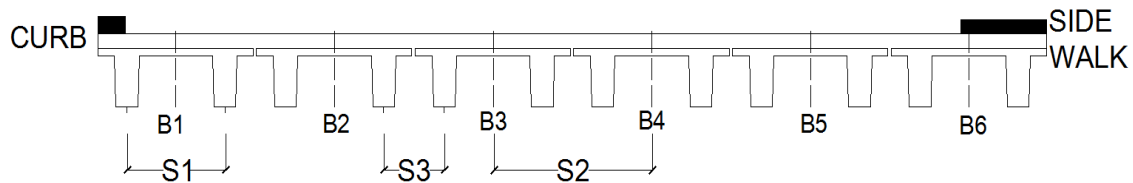
Figure 3.10: Beam Numbering Used in Double Stem Approach

24

3.6 Calculation of LLDFs for Interior Girders

Calculation of LLDFs for interior girders follows equations in AASHTO LRFD (2010), with the assumption that girder spacing in those equations is taken as the average spacing of stems when using the SST approach (type k section), or the spacing between NEXT beams when using the DST approach (type I section). The equations for LLDFs for bending moment for interior girders with one lane loaded is given in Equation 3.1, and for two or more lanes loaded by Equation 3.2.

$$gM_1^{i-} = 0.06 + [S/14]^{0.4}[S/L]^{0.3}[K_g/(12Lt_s^3)]^{0.1} \quad \dots \quad \text{Equation 3.1}$$

$$gM_{2+}^{i-} = 0.075 + [S/9.5]^{0.6} [S/L]^{0.2}[K_g/(12Lt_s^3)]^{0.1} \quad \dots \quad \text{Equation 3.2}$$

$$K_g = n(I + Ae_g^2)$$

$$n = E_{Beam}/E_{Slab}$$

Where,

gM_1^{i-} = LLDF for bending moment for interior girder with one lane loaded.

gM_{2+}^{i-} = LLDF for bending moment for interior girder with two or more lanes loaded.

K_g = longitudinal stiffness parameter for the composite girder (in^4).

S = respective spacing between the girders (ft) for different approach.

L = span of the Bridge (ft).

t_s = thickness of deck slab (in).

n = modular ratio between the material of girder and material of deck.

e_g = the distance between center of gravity of NEXT beam and deck slab (in).

A = Cross sectional area of the girder (in^2).

I = Moment of inertia of NEXT beam (in^4).

E_{Beam} = Modulus of elasticity of NEXT beam (ksi).

25

E_{Slab} = Modulus of elasticity of deck slabs (ksi).

To evaluate LLDFs, NEXT beams with different depths (24, 32, and 36in. [610, 813, and 914mm]) were considered typical for use in three different spans being investigated (50, 66.67, and 80ft [15.24, 20.32, and 24.38m]). These depths were determined using the span ranges of different NEXT beam cross sections from available load tables. The SST and DST approaches used to evaluate LLDFs result, therefore, in different values of K_g depending on the cross section used. Table 3.1 lists the different values of K_g and relevant parameters used to calculate K_g.

26

Table3.1: Cross section properties for Use in AASHTO LLDF equations

Details	Unit	SST			DST		
NEXT Beam		24F	32F	36F	24F	32F	36F
K_g	in^4 (m^4)	158,318 (0.06)	310,661 (0.13)	417,440 (0.17)	316,635 (0.13)	621,323 (0.26)	834,881 (0.35)
N		1.41	1.41	1.41	1.41	1.41	1.41
I	in^4 (m^4)	26,481 (0.01)	58,050 (0.024)	80,142 (0.033)	52,962 (0.022)	116,100 (0.048)	160,284 (0.066)
A	in^2 (m^2)	492 (0.317)	583 (0.375)	640 (0.412)	984 (0.633)	1,166 (0.750)	1,280 (0.824)
e.g	in (mm)	13.18 (334.77)	16.65 (422.91)	18.33 (465.58)	13.18 (334.77)	16.65 (422.91)	18.33 (465.58)
E_{Beam}	ksi (Mpa)	5,098 (35176)	5,098 (35176)	5,098 (35176)	5,098 (35176)	5,098 (35176)	5,098 (35176)
E_{Slab}	ksi (Mpa)	3,605 (24874)	3,605 (24874)	3,605 (24874)	3,605 (24874)	3,605 (24874)	3,605 (24874)

Notes : fc'$_{Beam}$ =8000 psi, E_{Beam} = 57000*sqrt (fc'$_{Beam}$)/1000 ksi, fc'$_{Slab}$ =4000 psi, E_{Slab} = 57000*sqrt(fc'$_{Beam}$)/1000 ksi

To consider the effect of skew angle on LLDFs for bending moment AASHTO LRDF gives a correction factor (C_M) as indicated by Equation 3.3. From Equation 3.3 it is clear that LLDFs for bending moment decrease with increase in skew angle. This result is consistent with results obtained from FEM analyses as discussed later.

$$C_M = 1.25][(K_g/(12Lt_s^3)]^{0.25}][S/L]^{0.5}(\tan\alpha)^1 \quad ….. \text{ Equation 3.3}$$

Where,

α = skew angle of the Bridge (degree).

L = span of the Bridge (ft).

t_s = thickness of deck slab (not including flange of NEXT beam(ft) .

S = spacing between the girders (ft).

LLDFs for the design shear force of interior girders with one lane loaded are calculated using Equation 3.4, whereas with two or more lanes loaded is given by Equation 3.5.

$$gV_1^{i-} = 0.36+[S/25] \quad\quad\quad ….. \text{ Equation 3.4}$$

$$gV_{2+}^{i-} = 0.2+[S/12] - [S/35]^2 \quad\quad\quad ….. \text{ Equation 3.5}$$

Where,

gV_1^{i-} = LLDF for shear force for interior girder with one lane loaded.

gV_{2+}^{i-} = LLDF for shear force for interior girder with two or more lanes loaded.

S = spacing between the girders (ft).

To consider the effect of skew angle on LLDFs for shear force, the LLDF shear force correction factor (C_S) given in Equation. 3.6 is used (AASTHO LRFD 2010). Equation 3.6 clearly shows that LLDFs for shear force increase with an increase in skew angle. This also matches results obtained from FE analyses as discussed in Chapter 5.

$$C_S = 1+ [0.2] (12Lt_s^3/K_g)^{0.3}(\tan\alpha)] \quad\quad\quad ….. \text{ Equation 3.6}$$

28

3.7 Calculation of LLDFs for Exterior Girders

LLDFs for exterior girder are computed using the lever rule according with AASHTO LRFD (2010). The lever rule is a method of computing the distribution factors by taking moments about the first interior girder to get the reaction at the exterior girder, assuming there is a notional hinge in the Bridge deck directly above the first interior girder. The design truck is placed as far away from the first interior girder towards the edge of the Bridge to maximize the reaction computed in the exterior girder. The design truck may be positioned transversely on the Bridge deck such that center of any wheel is not closer than 2ft (0.94m) from the edge of the design lane.

The LLDFs for bending moment for exterior girders with one lane loaded are calculated by the lever rule; for two or more lanes loaded the LLDFs are calculated using Equation 3.7, which is based on the LLDFs for two or more lanes loaded of interior girders.

$$gM_1^{e-} = \text{Lever Rule}$$

$$gM_{2+}^{e-} = e_M * gM_{2+}^{i-} \qquad \qquad ….. \text{ Equation 3.7}$$

$$e_M = 0.77 + d_e/9.1 \qquad \qquad ….. \text{ Equation 3.8}$$

Where,

gM_1^{e-} = LLDF for bending moment for exterior girder with one lane loaded.

gM_{2+}^{e-} = LLDF for bending moment for exterior girder with two or more lanes loaded.

gM_{2+}^{i-} = LLDF for bending moment for interior girder with two or more lanes loaded.

e_M = correction factor for distribution, distance between design lane and the center of gravity of girders (ft).

d_e = horizontal distance from the centerline of the exterior web of the exterior beam at the deck level to the interior edge of the curb or traffic barrier (in).

29

The equations for LLDF for shear force for exterior girders with one lane loaded and two or more lanes loaded are given by lever rule and Equation 3.9 respectively.

$$gV_1^{e-} = \text{Lever Rule}$$

$$gV_{2+}^{e-} = e_V * gV_{2+}^{i-} \qquad \text{..... Equation 3.9}$$

$$e_V = 0.6 + d_e/10 \qquad \text{..... Equation 3.10}$$

Where,

e_V = Correction factor for distribution, distance between design lane and the center of gravity of girders (ft).

To consider the effect of skew angle of the Bridge these LLDFs are multiplied by the respective skew angle correction factors as indicated above (Equation 3.3 and 3.6).

3.7.1 Load Position for LLDF Calculation of Exterior Girders - SST Approach

For calculation of exterior girder LLDFs using the SST approach, a small curb was considered on the edge of the Bridge to allow transverse placement of the design truck as close to the edge as possible to maximize the reaction of the exterior girder. The width of the curb considered was 17in. (0.43m). The first wheel of an HS20 truck load was positioned 25.9in (0.65m) away from the edge of curb (Figure. 3.11). The second wheel of the design truck does not appear in Figure 3.11 because it falls in the first interior NEXT beam. The assumed location of the notional hinge above B11. The reaction obtained in B12 in Figure 3.11 (exterior girder) is multiplied by two to determine the LLDF for the exterior NEXT beam.

30
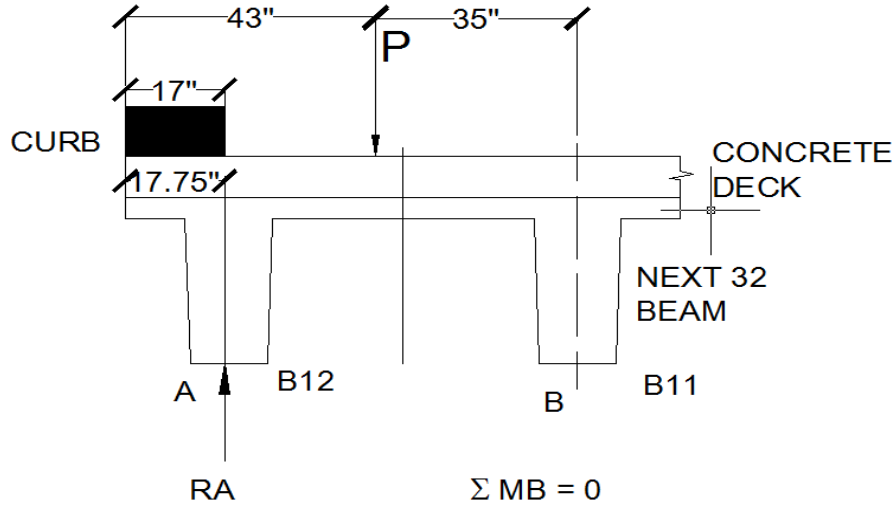
Figure3.11: Wheel Loading in Exterior Girder for LLDF Calculation - Single Stem

Approach

For the case of one lane loaded Applying,

$$\Sigma MB = 0 \qquad\qquad\qquad ….. \text{ Equation 3.11}$$

R_A Reaction at the center of gravity of the exterior stem $= 0.58P$

L_F kips The Lane fraction carried by exterior stem $(0.58*P/2)$ $= 0.29P$

$$sM_1^{e-} = m*L_F \qquad\qquad ….. \text{ Equation 3.12}$$

$$gM_1^{e-} = gV_1^{e-} = 2*sM_1^{e-} \qquad\qquad ….. \text{ Equation 3.13}$$

Where,

sM_1^{e-} = LLDF for bending moment of exterior Stem B12

$gM_1^{e-} = 2*sM_1^{e-}$ = LLDF for bending moment for exterior NEXT beam

gV_1^{e-} is LLDFs for shear force for exterior NEXT beam

m   is multiple lane presence factor = 1.2 for single lane loaded.

Using Equation 3.11, Equation 3.12, Equation 3.13 we get,

$$gM_1^{e-} = gV_1^{e-} = 0.7$$

31

For the case of two or more lanes loaded Equations 3.7 and 3.8 are used. The eccentricity of the center of gravity of the exterior stem to the interior edge of the curb is 0.75in (19.05mm). The factors e_M and e_V for bending moment and shear force respectively, are calculated as:

d_e = 30.75 in.

e_M = 0.77+d_e/9.1 = 1.05ft (0.32m)

e_V = 0.6+d_e/10 = 0.88ft (0.27m)

$gM_{2+}^{e-} = e_M*gM_{1-}^{i-}$

$gV_{2+}^{e-} = e_V*gV_{1-}^{i-}$

These values are then used in Equations 3.7 and 3.9 to calculate the LLDFs for moment and shear of exterior girders for two or more lanes loaded. These LLDF values have to be adjusted by the respective skew angle correction factor from Equation 3.3 and Equation 3.6 for moment and shear, respectively. Results of calculated LLDFs for bending moment and shear force are presented in tabular form in Section 3.7 (Table 3.3 and 3.5, respectively).

3.7.2 Load Position for LLDF Calculation of Exterior Girders - DST Approach

For the evaluation of LLDFs of exterior girders using the DST approach, a narrow curb was again assumed to allow the wheel from the design truck to be placed in a position that generates a high force on the exterior girder. The width of the curb considered was 17in. (0.43m). The first wheel of an HS20 truck load was placed 26in. (0.65m) from the edge of the curb. The notional hinge for application of the lever rule was placed at the centroid of the first interior NEXT beam unit. The reaction in the exterior NEXT beam unit is determined at the centroid of that unit as illustrated in Figure 3.12. This figure

32

illustrates B6 as a typical exterior girder; the figure also shows the notation used for calculation of the exterior girder LLDF for a single lane loaded.
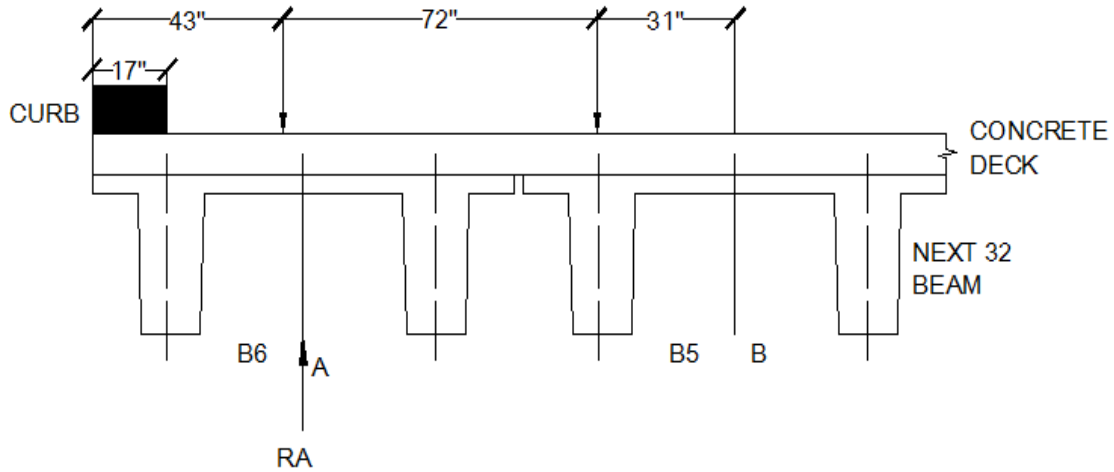
Figure3.12: Loading Exterior Girder Double Stem Approach

For the case of one lane loaded Applying,

$\Sigma MB = 0$ ….. Equation 3.14

R_A Reaction at the center of gravity of the exterior NEXT Beam   = 1.37 P

L_F The lane fraction carried by exterior stem (1.37*P/2)   = 0.68

$$gM_1^{e-} = gV_1^{e-} = m*L_F$$ ….. Equation 3.15

Where,

gM_1^{e-} = LLDFs for bending moment for exterior NEXT beam

gV_1^{e-} = LLDFs for shear force for exterior NEXT beam

m   = multiple lane presence factor = 1.2

Solving Equation 3.17, with m=1.2 we get,

$$gM_1^{e-} = gV_1^{e-} = 0.82$$

33

Similar to the SST for two or more lanes loaded analytical equations mentioned in AASHTO LRFD specifications (2010) are used. The eccentricity of the center of gravity of the exterior girder to the interior edge of the narrow sided curb de is 30.75in (0.78m). Similarly e_M and e_V correction factors for bending moment and shear force respectively have been evaluated in this section. These values have to be multiplied by the respective LLDFs of the interior girder.

d_e = 30.75 in

e_M = 0.77+de/9.1 = 1.05ft (0.32m)

e_V = 0.6+de/10 = 0.88ft (0.27m)

$gM_{2+}^{e-} = e_M*gM_{1-}^{i-}$

$gV_{2+}^{e-} = e_V*gV_{1-}^{i-}$

These LLDFs have to be also multiplied by the respective skew angle correction factors when applicable. Results of LLDFs for bending moment and shear force are listed in Section 3.8.

3.8 LLDF Values Computed Using Single Stem Approach (type k)

This approach is assumed to be the conservative approach proposed by the PCI Bridge technical committee and used currently by designers for design of NEXT beam Bridges. An 8in (203.2mm). thick deck has been considered acting compositely with the NEXT beam. Tables 3.2 through 3.5 list LLDFs for bending moment and shear force for different assumed spans and skew angles. The spans considered are 50, 66.67, and 80ft [15.24, 20.32, and 24.38m]. The skew angles considered are 0°, 30° and 45°.

34

Table 3.2: LLDFs-Bending Moment-Interior Girder

One lane loaded (gM_1^{i-})				Two or more lanes loaded (gM_{2+}^{i-})			
Span	Skew			Span	Skew		
ft (m)	0°	30°	45°	ft (m)	0°	30°	45°
50 (15.24)	0.66	0.63	0.62	50 (15.24)	0.83	0.80	0.77
66.67 (20.32)	0.63	0.61	0.59	66.67 (20.32)	0.81	0.79	0.76
80 (24.38)	0.61	0.59	0.57	80 (24.38)	0.80	0.77	0.75

Notes : 1=one lane loaded whereas, **2+**= for two or more lanes loaded, i- interior girder, **e-** represent

exterior girder respectively, M = Bending Moment

Table 3.3: LLDFs-Bending Moment-Exterior Girder

One Lane Loaded (gM1e -)				Two or more Lanes Loaded (gM2+e -)			
Span	Skew			Span	Skew		
ft (m)	0°	30°	45°	ft (m)	0°	30°	45°
50 (15.24)	0.70	0.68	0.66	50 (15.24)	0.63	0.62	0.60
66.67 (20.32)	0.70	0.68	0.66	66.67 (20.32)	0.63	0.61	0.59
80 (24.38)	0.70	0.68	0.66	80 (24.38)	0.63	0.60	0.58

Notes : 1=one lane loaded whereas, **2+**= for two or more lanes loaded, i- interior girder, **e-** represent
exterior girder respectively

Table 3.4: LLDFs-Shear Force-Interior Girder

gV_1^{i-}				gV_{2+}^{i-}			
Span	Skew			Span	Skew		
ft (m)	0°	30°	45°	ft (m)	0°	30°	45°
50 (15.24)	1.04	1.06	1.07	50 (15.24)	1.05	1.06	1.07
66.67 (20.32)	1.04	1.17	1.27	66.67 (20.32)	1.05	1.18	1.27
80 (24.38)	1.04	1.17	1.26	80 (24.38)	1.05	1.17	1.27

Notes : 1=one lane loaded whereas, 2+= for two or more lanes loaded, i- interior girder, e- represent exterior girder respectively

Table 3.5: LLDFs-Shear Force- Exterior Girder

One Lane Loaded (gV_1^{1-})				Two or more Lanes Loaded (gV_{2+}^{1-})			
Span	Skew			Span	Skew		
ft (m)	0°	30°	45°	ft (m)	0°	30°	45°
50 (15.24)	0.70	0.78	0.84	50 (15.24)	0.64	0.71	0.76
66.67 (20.32)	0.70	0.77	0.82	66.67 (20.32)	0.64	0.70	0.75
80 (24.38)	0.70	0.77	0.82	80 (24.38)	0.64	0.70	0.74

Notes : 1=one lane loaded whereas, **2**+= for two or more lanes loaded, i- interior girder, **e-** represent exterior girder respectively.

3.9 LLDF Values Computed Using Double Stem Approach (type i)

A NEXT beam unit has been considered as the girder in these calculations, including an 8 in. (203.2mm) thick deck acting compositely with the beam. The spacing S between girders is taken as the horizontal distance between the center of gravity of two adjacent NEXT beams 8.08ft (2.43m).

Tables 3.6 to 3.9 list LLDFs that have been calculated for bending moment and shear force for three different span lengths and three different skew angles. As before, the spans considered are 50, 66.67, and 80ft [15.24, 20.32, and 24.38m] and the skew angles considered are 0°, 30° and 45°.

Table 3.6: LLDFs-Bending Moment-Interior Girder

One Lane Loaded (gM_1^{1-})				Two or more Lanes Loaded (gM_{2+}^{1-})			
Span	Skew			Span	Skew		
ft (m)	0°	30°	45°	ft (m)	0°	30°	45°
50 (15.24)	0.53	0.49	0.47	50 (15.24)50	0.71	0.67	0.64
66.67 (20.32)	0.50	0.48	0.46	66.67 (20.32)	0.70	0.66	0.63
80 (24.38)	0.49	0.46	0.44	80 (24.38)	0.68	0.65	0.62

Notes : 1=one lane loaded whereas, **2+**= for two or more lanes loaded, i- interior girder, e- represent exterior girder respectively.

Table 3.7: LLDFs-Bending Moment-Exterior Girder

One Lane Loaded (gM_1^{e-})				Two or more Lanes Loaded (gM_{2+}^{e-})			
Span	Skew			Span	Skew		
ft (m)	0°	30°	45°	ft (m)	0°	30°	45°
50 (15.24)	0.82	0.77	0.74	50 (15.24)	0.74	0.70	0.67
66.67 (20.32)	0.82	0.78	0.74	66.67 (20.32)	0.73	0.69	0.65
80 (24.38)	0.82	0.77	0.75	80 (24.38)	0.72	0.68	0.65

Notes :1=one lane loaded whereas, **2**+= for two or more lanes loaded, i- interior girder**, e-** represent exterior girder respectively.

Table3.8: LLDFs-Shear Force-Interior Girder

One Lane Loaded (gV_1^{i-})				Two or more Lanes Loaded (gV_{2+}^{i-})			
Span	Skew			Span	Skew		
ft (m)	0°	30°	45°	ft (m)	0°	30°	45°
50 (15.24)	0.68	0.76	0.82	50 (15.24)	0.82	0.91	0.98
66.67 (20.32)	0.68	0.75	0.80	66.67 (20.32)	0.82	0.90	0.96
80 (24.38)	0.68	0.75	0.80	80 (24.38)	0.82	0.90	0.96

Notes :1=one lane loaded whereas, **2**+= for two or more lanes loaded, i- interior girder**,** e- represent exterior girder respectively.

Table3.9: LLDFs-Shear Force- Exterior Girder

One Lane Loaded (gV_1^{e-})				Two or more Lanes Loaded (gV_{2+}^{e})			
Span	Skew			Span	Skew		
ft (m)	0°	30°	45°	ft (m)	0°	30°	45°
50 (15.24)	0.82	0.92	0.98	50 (15.24)	0.70	0.78	0.84
66.67 (20.32)	0.82	0.91	0.97	66.67 (20.32)	0.70	0.77	0.83
80 (24.38)	0.82	0.90	0.96	80 (24.38)	0.70	0.77	0.82

Notes :1=one lane loaded whereas, **2+=** for two or more lanes loaded, i- interior girder, e- represent exterior girder respectively

3.10 Comparison between Single and Double Stem Approach

A comparison of the results of LLDFs calculated using the two different assumed cross sections (SST and DST) described above was conducted to determine which approach yielded more conservative values. This comparison has been done for the various spans included in the study (Table 3.10 and 3.11) and the various skew angles (Tables 3.12 and 3.13).

3.10.1 Comparison of Results for Various Spans - 0° Skew

Tables 3.10, 3.11 list the LLDFs computed using the SST and DST approaches .From the results we can conclude that the SST approach gives higher LLDF values for interior girders and as assumed by the PCI Bridge technical committee. However, the exterior girder LLDFs computed using the DST approach are higher than those computed with the

SST approach. Higher LLDFs would result in higher design live-load moments for NEXT beams. This comparison is illustrated graphically in Figure 3.13.

Table 3.10: Bending Moment LLDFs - Different Spans, (0° Skew)

Span	50 ft (15.24 m)		66.67 ft (20.32 m)		80 ft (24.38 m)	
	SST	DST	SST	DST	SST	DST
gM_1^{i-}	0.66	0.53	0.63	0.50	0.61	0.49
gM_{2+}^{i-}	0.83	0.71	0.81	0.70	0.80	0.68
gM_1^{e-}	0.70	0.82	0.70	0.82	0.70	0.82
gM_2^{e-}	0.64	0.74	0.63	0.73	0.62	0.72

Notes :1=one lane loaded whereas, **2**+= for two or more lanes loaded, i- interior girder, e- represent exterior girder respectively

Table 3.11: Shear Force LLDFs - Different Spans, (0° skew)

Span	50 ft (15.24 m)		66.67 ft (20.32 m)		80 ft (24.38 m)	
	SST	DST	SST	DST	SST	DST
gV_1^{i-}	1.04	0.68	1.04	0.68	1.04	0.68
gV_{2+}^{i-}	1.05	0.82	1.05	0.82	1.05	0.82
gV_1^{e-}	0.70	0.82	0.70	0.82	0.70	0.82
gV_2^{e-}	0.63	0.70	0.63	0.70	0.63	0.70

Notes:1=one lane loaded whereas, **2**+= for two or more lanes loaded, i- interior girder, e- represent exterior girder respectively

(a)

(b)

(c)

(d)
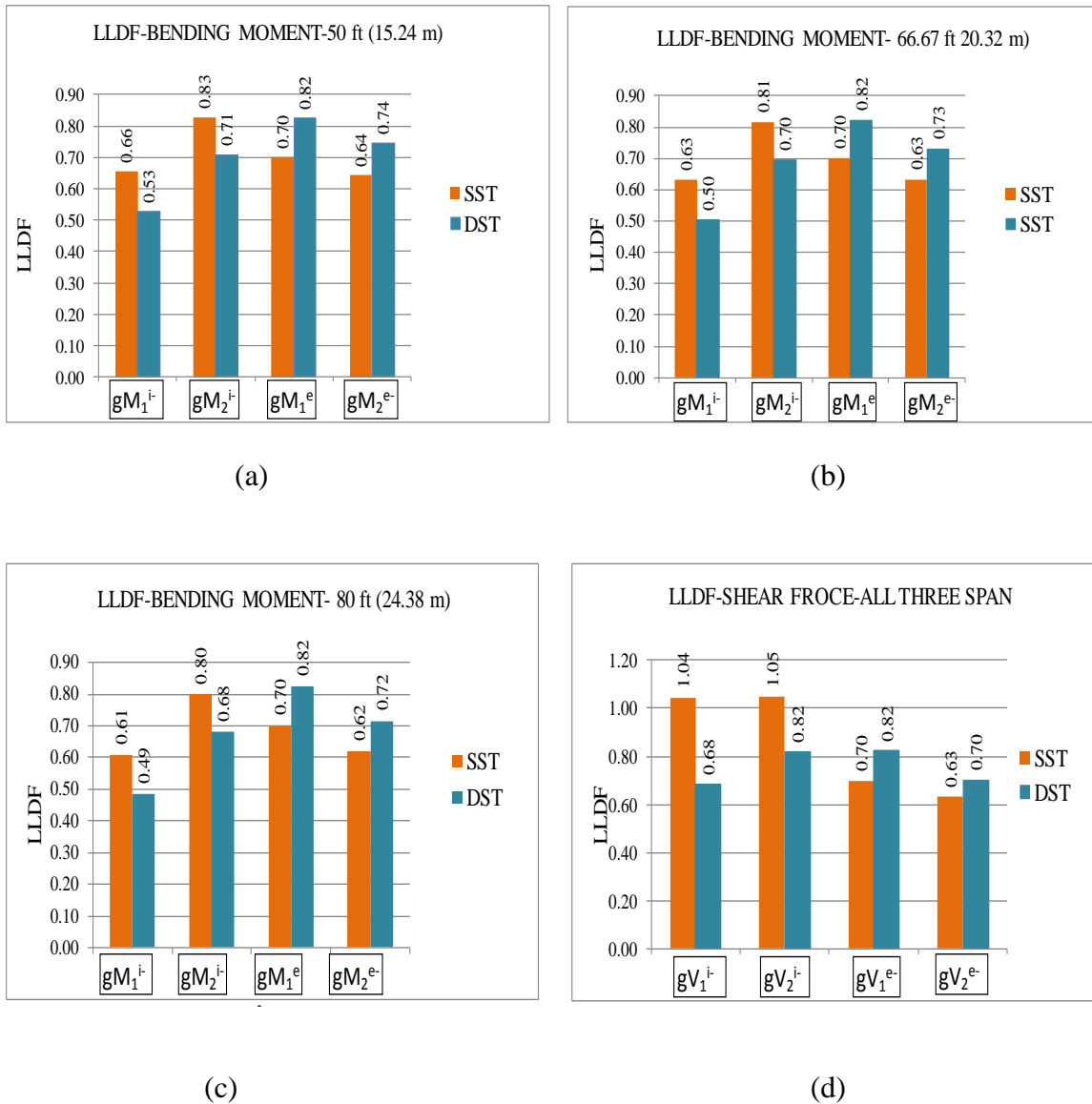
Figure 3.13(a-d) Comparisons of LLDFs for Span Parameter

3.10.2 Comparison of Results for Various Skew Angles -66.67ft (20.32m)

The LLDF values obtained from using the SST and DST approaches for various skew angles are compared in Tables 3.12 and 3.13. This comparison is listed for the span 66.67 ft (20.32m). From the results we can conclude that SST approach gives higher value of LLDFs for the interior girder which is as per the outcome of PCI technical committee. On

41

the contrary for the exterior girder DST is giving higher value for the LLDFs. The comparisons between the two approaches are mentioned in Figure 3.14.

Table 3.12: Bending Moment LLDFs – Different Skew Angles (Span = 66.67 ft (20.32 m))

Skew Angle	0°		30°		45°	
	SST	DST	SST	DST	SST	DST
gM_1^{i-}	0.63	0.50	0.61	0.48	0.59	0.46
gM_{2+}^{i-}	0.81	0.70	0.79	0.66	0.76	0.63
gM_1^{e-}	0.70	0.82	0.68	0.78	0.66	0.74
gM_2^{e-}	0.63	0.73	0.61	0.69	0.59	0.65

Table3.13: Shear Force LLDFs – Different Skew Angles (66.67 ft (20.32 m) Span)

Skew Angle	0°		30°		45°	
	SST	DST	SST	DST	SST	DST
gV_1^{i-}	1.04	0.68	1.17	0.75	1.27	0.80
gV_{2+}^{i-}	1.05	0.82	1.18	0.90	1.27	0.96
gV_1^{e-}	0.70	0.82	0.77	0.91	0.82	0.97
gV_2^{e-}	0.63	0.70	0.70	0.77	0.74	0.83
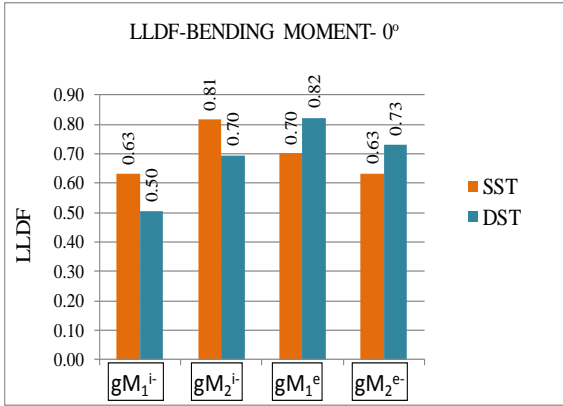
(a)
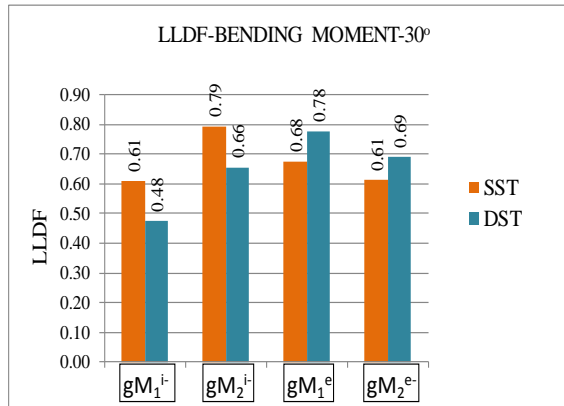
(b)
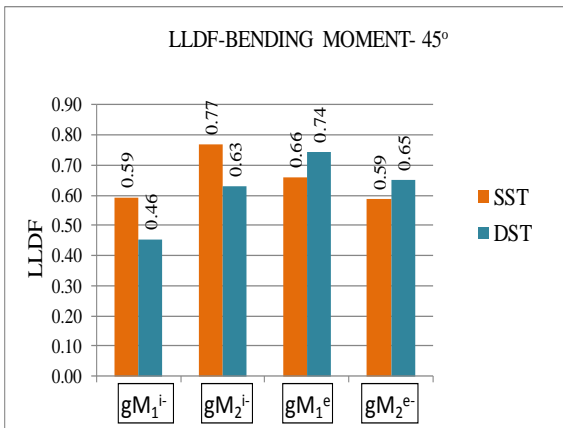
(c)
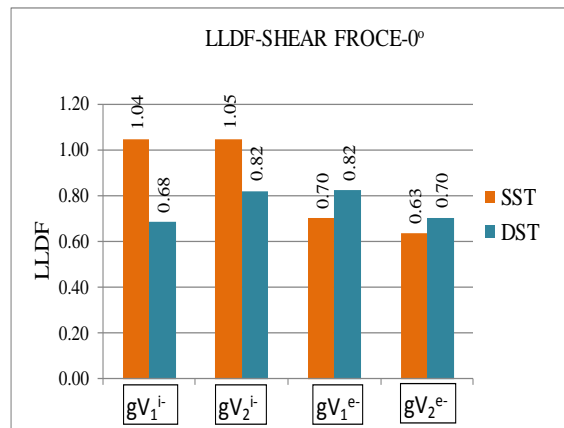
(d)
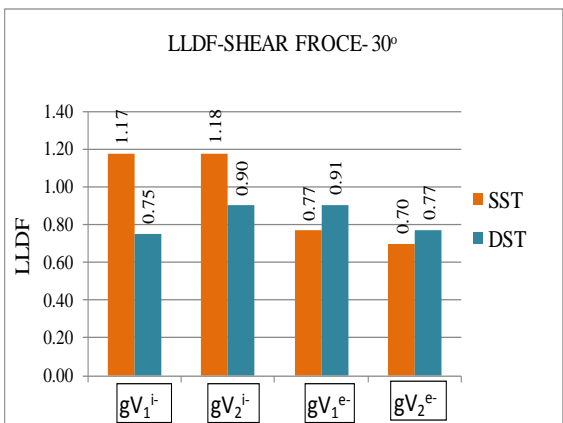
(e)
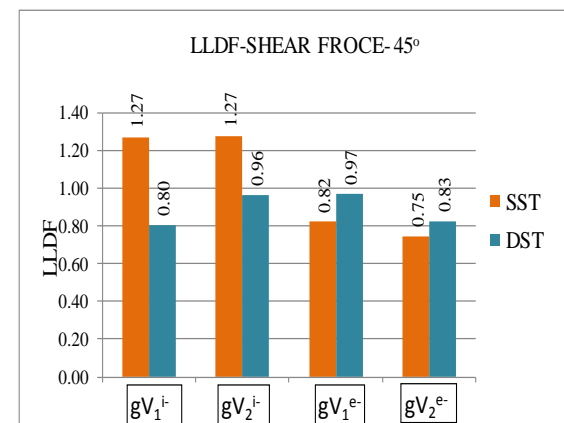
(f)

Figure 3.14(a-f) Comparisons of LLDFs for Skew Angle

3.11 Summary

This chapter presents calculation of LLDF values of NEXT beam Bridges having three different lengths and three different skew angles. The calculations are based on current AASHTO LRFD equations (2010) assuming two different Bridge cross section types (Type K and Type I). Based on these calculations and the comparisons presented in previous sections of this chapter we can conclude the following:

- LLDFs for interior girders determined using the SST approach are higher than those computed using the DST approach.

- LLDFs for exterior girders are higher when using the DST approach compared with the SST approach.

- Interior girder LLDFs for bending moment and shear forces are governed by two or more lanes loaded case for all the parametric sets considered. .

- Exterior girder LLDFs for bending moment and shear force are governed by one lanes loaded case.

The LLDFs computed in this chapter will be compared with values determined from detailed FEM models of the Bridges in Chapter four. These comparisons will give information about the most appropriate cross section type to use in design.

CHAPTER 4

FINITE ELEMENT ANALYSIS OF NEXT BEAM BRIDGES

The objective of this chapter is to provide details of the FEM model used to evaluate live load moment and shear force distribution factors (LLDFs) for NEXT beam Bridges. These LLDFs obtained from FEM analysis of typical NEXT beam Bridges are compared with LLDFs obtained from the AASHTO LRFD equations presented in Chapter 3. The PCI-NE Bridge Technical Committee recommendations to determining LLDFs of NEXT beams can then be evaluated in detail.

Three different spans and three different skew angles have been included in this investigation and verification. The three different spans are 50, 66.67 and 80 ft ([15.24, 20.32 and 24.38m]) and the three different skew angles are 0°, 30° and 45°. These two sets are considered as parameters that are varied in turn to increase applicability of results to a wide range of Bridge geometries. Additionally, Bridge models also include integral abutment configurations even though AASTHO LRFD does not differentiate between non-integral and integral abutments in LLDF equations. Each model with a given span and skew angle was analyzed using a simply supported end and integral abutment end condition. In the past LLDFs for IAB has been explored with straight configuration (0° skew angle, (Dicleli 2008).) but not for the varying skew angle.

4.1 Modeling of Bridge

The FEM analysis program used to model the Bridges was SAP 2000 V14.2. Details of the Bridge model are divided into super structure, sub structure and foundation. The following sections discuss the modeling aspects for each of these components.

45

4.1.1 Modeling of the Super structure

A base model was built using the characteristics of an actual (Brimfield Bridge) NEXT beam Bridge, which is considered to by the prototype for this study (Brimfield Bridge). The configuration of Brimfield Bridge are detailed in section 3.2 and 3.3. After defining the prototype, parameters were varied (span length, skew angle, end fixity) to investigate the effect of these changes on LLDFs. The prototype Bridge has a span length of 66.67ft (20.32m) and a skew angle of 30° degrees. The prototype Bridge super structure consists of six NEXT beams 32 (depth equal to 32in 812.8mm) with an 8 in (203.2mm) concrete deck slab. Because it is unlikely that 32 in. NEXT beams would be used in the other spans included in this study, other NEXT beam depths were chosen to closely reflect what might be used in other spans. Therefore, Bridge models for the 50 and 80ft [15.24 and 20.32m] spans included NEXT 24 and NEXT 36 beams, respectively. The deck thickness of 8in(203.2mm) remained the same in all the models.

NEXT beams were modeled as 3D frame elements with 6 degrees of freedom per node. The cross sectional properties were determined using the section designer feature available in SAP 2000 14.2 to accurately reflect the geometry of the NEXT beams.

The curved chamfer between the web and flange of the NEXT beams could not be easily captured. The modeled section (Figure 4.1) has section properties that are similar to the actual one. In Table 4.1 the comparison of section properties for actual sections and section prepared in section designer are shown. The maximum differences in calculated and actual section properties are below 2%.

Table4.1: Section Property comparison

NEXT 24 Beam Comparison				
Section Property	Unit	Section Designer	Actual Property	Deviation (% Age)
Area	$in^2(m^2)$	984(0.63)	966(0.62)	1.83
I_{33}	$in^4(m^4)$	52962(0.02)	51823(0.02)	2.15
Y_T	in(mm)	9.18(233.17)	9.05(229.87)	1.42
Y_B	in(mm)	14.82(376.42)	14.95(379.73)	0.87
S_T	$in^3(m^3)$	5769	5726(0.09)	0.74
S_B	$in^3(m^3)$	3573.68	3466(0.06)	3.00
NEXT 32 Beam Comparison				
Area	$in^2(m^2)$	1,182(0.76)	1,166(0.75)	1.35
I_{33}	$in^4(m^4)$	115,813(0.048)	116,100(0.047)	-0.25
Y_T	in(mm)	12.49(317.24)	12.65(321.31)	-1.28
Y_B	in(mm)	19.51(495.50)	19.35(491.49)	0.82
S_T	$in^3(m^3)$	9,272(0.152)	9,180(0.15)	0.99
S_B	$in^3(m^3)$	5,936(0.097)	5,998(0.098)	-1.04
NEXT 36 Beam Comparison				
Area	$in^2(m^2)$	1280(0.82)	1287(0.83)	0.54
I_{33}	$in^4(m^4)$	160284(0.067)	160240(0.07)	0.03
Y_T	in(mm)	14.33(363.98)	14.23(361.44)	0.70
Y_B	in(mm)	21.67(550.42)	21.77(552.96)	0.46

S_T	in^3(m^3)	11185(0.18)	11261(0.18)	0.47
S_B	in^3(m^3)	7396(0.12)	7361(0.012)	0.54

Notes: I_{33}=Major moment of Inertia of the NEXT Beam; Y_B= Depth of bottom fiber of the NEXT beam from center of gravity of NEXT beam; Y_T = Depth of top fiber of NEXT beam from center of gravity of NEXT beam; S_T = Section modulus for top fiber of NEXT Beam; S_B =Section modulus for bottom fiber of NEXT beam.

The deck was modeled using 4-node quadrilateral thin shell elements. Nodes of shell elements resulting from meshing coincided in space and were connected to nodes in the NEXT beam frame elements. Each segment along the length of the NEXT beams was approximately 1.67ft (0.5m) long. The concrete deck element dimensions were defined to be consistent with nodes on the beam frame elements and to have a width to length ratio of shell elements of approximately 1.2. This same aspect ratio was maintained for abutment elements in the case of an IAB model.

The beam and shell elements nodes were initially defined on the same plane. Shell nodes were then offset to the top of the NEXT beam flange using the insertion point command in SAP 2000. The insertion point defines the eccentricity between beam element centroid and the top of the flange where shells should be connected. Because different NEXT beam depths were used for the three different spans studied 50, 66.67 and 80ft ([15.24, 20.32 and 24.38m]), the eccentricities changed accordingly. Eccentricities of 13.18in. (1.09m), 16.65in (1.39m) and 18.83in (1.57m) correspond to geometries of NEXT 24, NEXT 32, and NEXT 36 beams, respectively. Figure 4.1 shows the FEM model with only NEXT beams shown, and Figure 4.2 shows the addition of the shell elements on the top flange of the NEXT beams to simulate the actual composite deck action.

48
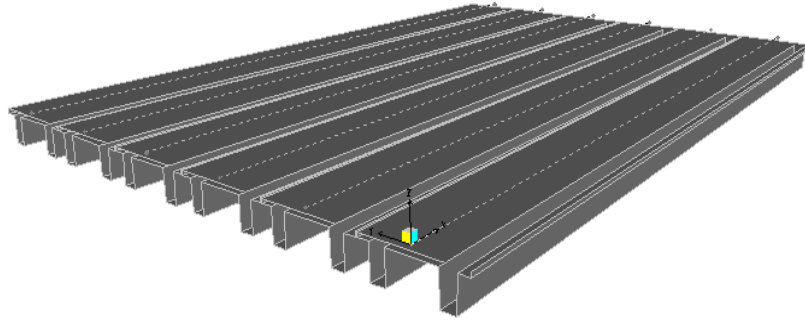
Figure 4.1 FE model illustrating NEXT beams
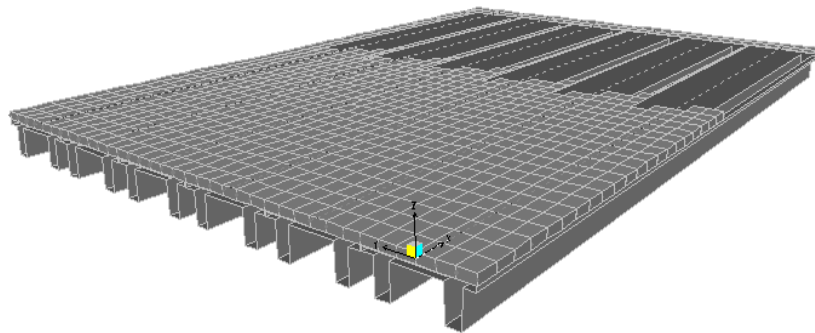
Figure 4.2 FEM model illustrating composite deck

4.1.2 Deck width and division of lane

The total width of the Bridge is 48.5ft (14.78m). The width of the sidewalk is 4.37ft (1.33m) whereas the width of the curb on other side is 1.42ft (0.43m). The roadway therefore has a clear width of 42.73ft (13.02m). As per the AASHTO (2010 Bridge design specification) stipulation clear width of Bridge has to be divided with 12ft (3.66 m) as lane width. After division the integral part of the obtained number is used for the number of lanes. For the actual prototype number of lane is three with 14.24ft (4.34m) as

lane width. The obtained number of lane which is as per the AASHTO (2010 Bridge design specification) stipulation is different from the actual case of two lanes.
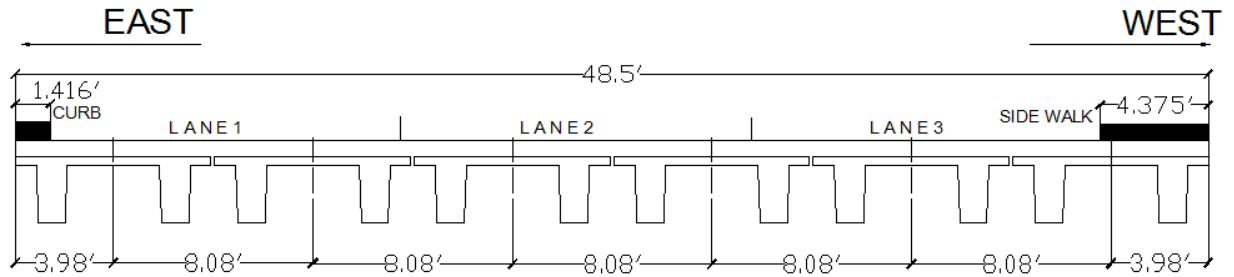
Figure 4.3 Bridge Section with lane division

4.1.3 Modeling of Foundation

The sub structure of the prototype Bridge consists of abutments at both ends supported on steel HP-piles. The sub structure response influences the Bridge response importantly, particularly for the integral abutment Bridge models. If the NEXT beams were supported on bearings that allow rotation and translation, it would be sufficient to simply model the super structure to capture the live-load response of the Bridge. The following sections describe the modeling techniques used to represent the sub structure of the integral abutment Bridge models.

4.1.3.1 Modeling of Abutment

The abutment of the prototype Bridge is 4ft (1.21m) thick and 4.74ft (3.07m) thick. The abutment on each side of the Bridge is supported on six HP 10x57 (metric equivalent) steel piles. The steel pile's weak axis is skew with 30° to the road alignment. The abutment was modeled using four noded thick shell elements with length-to-width ratio

50

very similar to the deck slab (1.2). The depth of the abutment was divided in to six equal shell elements.

4.1.3.2 Modeling of Piles

Piles were modeled using twenty 2-node 3D-frame elements for a total pile length of 20ft (6.09m). The piles were pinned at their bases and made continuous with abutment elements at the top. Pile deformations are largest within the top portion of the pile and the influence of soil-pile stiffness beyond 15ft (4.57m) was minimal. Therefore the considered depth of the pile is adequate to consider the soil structure interaction.

B. Modeling of Soil-Structure Interaction

The effect of soil-structure interaction between abutment and backfill soil has been found to be negligible in calculation of LLDFs (Dicleli 2008). Based on this finding and because the current study focuses on calculation of LLDFs, the FEM models did not model the abutment backfill soil stiffness. Soil-structure interaction between piles and surrounding soil, however, was included because pile restraint affects the degree of fixity developed under live-load at end of NEXT beams. Nonlinear soil springs were attached to the end nodes of each frame element used to model the piles as described by Civjan et al (2008).

Nonlinear modeling of the soil was achieved using force-displacement curves for the soil at different depths. The length of each pile segment was set at 1ft (0.30m). A force-displacement curve at each depth was calculated using the hyperbolic tangent method, discussed in detail in Civjan et al (2008). The equations used are discussed in detail in Appendix A.

Based on the analysis it was observed that link deformation due to live loads are very less. The forces in the link are 0 and based on that it was concluded that links are not active in the model. The link deformation are the deformation of the joints attached to the link.

Figure 4.5 is representing nonlinear P-Y soil resistance modeling at three different depth of 5 ft (1.52 m), 10 ft (3.04 m) , and 20 ft (6.09 m).
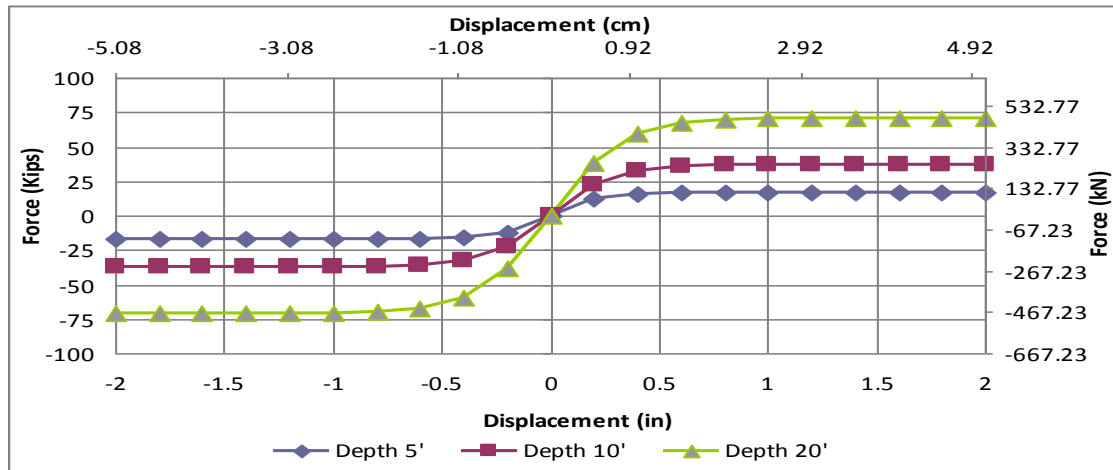
Figure 4.4 Non Linear Soil Modeling at three
Different depths

4.2 Methodology for the Parametric Evaluation of LLDFs using FEM Analysis

LLDFs were evaluated using FEM models for different combinations of parameters as listed in Table 4.2. Spacing between the girders was not considered as a varying parameter because widths of NEXT beams vary only within a narrow range mostly by changing the width of the top flange. This small variation in spacing of beams does not affect LLDF results significantly. The three spans that were considered are 50, 66.67 and 80 ft [15.24, 20.32 and 24.38m] and the three different skew angles are 0°, 30° and 45°. The total set parametric variations considered resulted in nine different FEM models. The

models having a span of 66.67 ft (20.32m) and a 30° skew angle corresponds exactly to the parameters of the prototype Bridge (Brimfield Bridge). This particular FEM model is further used in Chapter 6 for evaluation of strain evaluation at different construction stages and comparison of these strains with analytical modeling and field measurements.

Table 4.2: Different parameteric sets for LLDF Evaluation

Span ft (m)	Skew Angle	Span ft (m)	Skew Angle	Span ft (m)	Skew Angle
	0°		0°		0°
50 (15.24)	30°	66.67 (20.32)	30°	80 (24.38)	30°
	45°		45°		45°

NEXT beam LLDFs were calculated near sections producing the maximum corresponding action. Bending moment LLDFs were determined at mid span, and shear force LLDFs were determined at a section at a distance equal to the depth of the NEXT beams from the supports. In all FEM models, six NEXT beams were included assuming a Bridge width similar to the Brimfield Bridge. These beams are identified as B1 to B6.
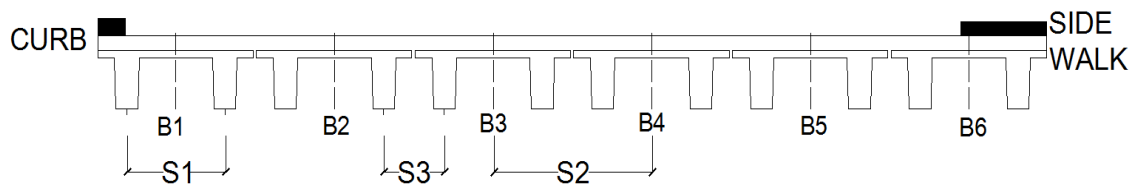
Figure 4.5: FEM Model of Bridge used in FEM method

LLDF were calculated including for four possible loading conditions for the Bridge width selected. According to AASTHO LRFD, up to three design lanes should be considered for the Bridge width subject of this study. Therefore analyses had to be performed to

determine the maximum moment and shear in interior and exterior NEXT beams for live loading applied to lane 1, lane 2, or lane 3; for live loading applied in pairs of lanes (three possible combinations); and for live loading applied to all three lanes. A multiple presence factor, m = 1.2, was used to scale results when live loading was applied to only single lanes in accordance with the AASHTO LRFD Specifications (2010).

The LLDF for interior NEXT beams was determined using the maximum value of moment or shear calculated in beam B2 to B5, whereas LLDFs for exterior NEXT beam was based on results for NEXT beams B1 and B6.

4.2.1 Bending Moment and Shear Force in Line Model

In order to determine LLDFs from 3D-FEM analyses, bending moments and shear forces are needed from a line model subjected to lane loading. Results from line models are commonly used in combination with LLDF equations in AASHTO LRFD to estimate actions in individual girders of Bridge super structures. Only the HS-20 truck portion (Figure 4.8) of the HL-93 lane loading model in the AASHTO LRFD was used for this study. Including the lane loading portion or the tandem arrangement was not believed to influence results significantly. To evaluate LLDFs for bending moment and shear force mid span and supports are respectively considered.

Figure 4.6 and 4.7 show the axle placement on the line model of NEXT beam with influence line ordinates for bending moment and shear force.
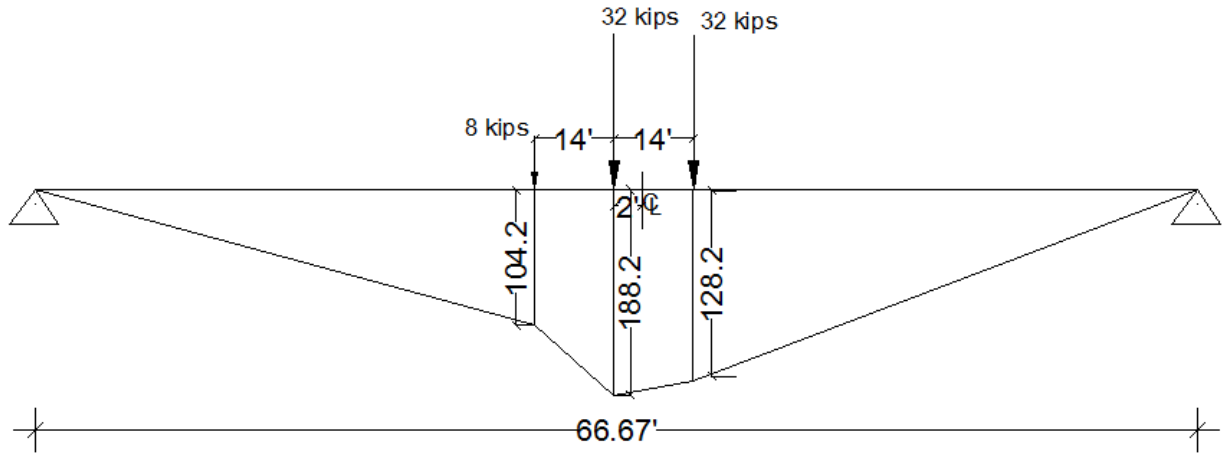
Figure 4.6: Axle Placement for Maximum Bending Moment near Mid Span
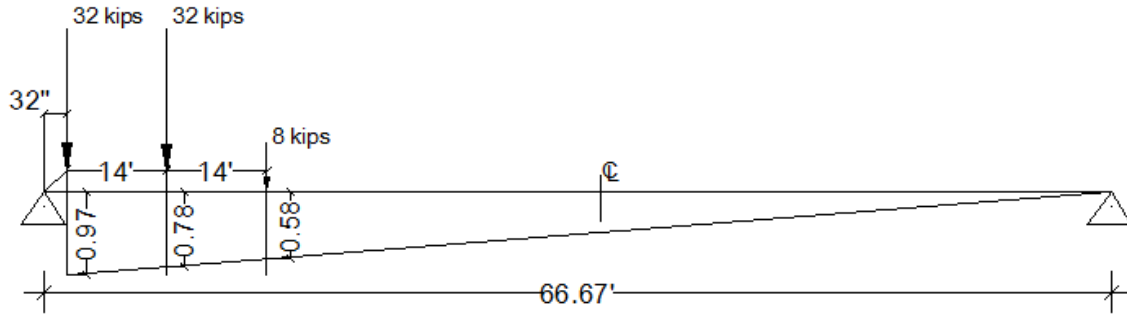
Figure 4.7: Axle Placement for Maximum Shear Force near Support
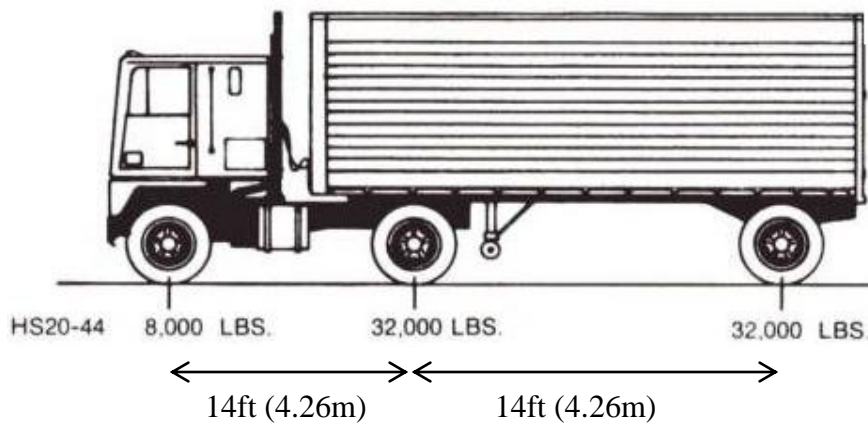
Figure4.8: HS 20 truck

55

Table 4.3 lists the live load moment and shear force computed at midspan and near the support (at depth depth h of NEXT beam from the support) respectively, for different spans of the line model. Because line models are typically two dimensional representations of the Bridge structure, these same actions are used to evaluate LLDFs calculated from Bridge models including skew.

Table 4.3: Maximum Action for Line Model

Span	Moment At Mid Span	Shear Force near Support (h)
ft(m)	Kip-ft (kN-m)	Kips (kN)
50(15.24)	814.17 (1104)	58.56 (260.47)
66.67(20.33)	1241.58 (1646)	62.00(275.77)
80(24.38)	1532.16 (2077)	64.56(287.16)

4.2.2 Evaluation of LLDFs

From FEM analysis we can get the forces (bending moment, shear forces) at critical locations (mid span for bending moment and at depth d from the support for the shear forces) for the NEXT beam. The obtained force has to be divided by the force obtained from influence line method (as per Table 4.3). The obtained value will be the LLDF for the actions (bending moment and shear force).In this section LLDFs are evaluated for 66.67ft (20.32m) span with 30° skew angle. The same steps will be applicable for other parametric sets.

4.2.2.1. LLDFs for Simply Supported Bridge

The first series of models that were considered assumed NEXT beams to be simply supported on top of the abutments. In these models, the effects of the super structure on LLDFs were considered negligible so the sub structure was not modeled and pin supports were provided at the ends of each NEXT beam. Table 4.4 to Table 4.7 list the results of ratios for bending moment and shear force in interior beams (B2 to B5) and exterior beams (B1 and B6). These ratios are defined as the ratio of the action (bending moment and shear force) obtained from FEM analysis to the maximum values of actions (bending moment and shear force)   listed in Table 4.3. These values were obtained through influence line method. These ratios are listed for one lane loaded and for two or more lanes loaded. The LLDFs for the interior NEXT beams for one lane loaded will be the maximum value of the LLDFs of B2 to B5 in Table 4.4 to 4.6. Similarly for the exterior NEXT beam it will be the maximum value among B1 and B2. For LLDFs of NEXT beams with two or more lanes loaded Table 4.7 will be used.

Table 4.4 : LLDFs-Simply Supported Condition (Lane 1 Loaded)

Beam Number	Bending Moment		LLDF (Particular Case)	Shear Force			LLDF (Particular Case)	
	FEA	M_{max}		Acute	Obtuse	V_{max}	Acute	Obtuse
	Kip-in (kN-m)	Kip-in (kN-m)		Kips (kN)	Kips (kN)	Kips (kN)		
B1	234 (26.44)	14,575 (1646.7)	0.01	12.0	73.0 (324.7)	62 (275.79)	0.19	1.18
B2	355 (40.11)	14,575 (1646.75)	0.02	2.0	51.0 (26.86)	62 (275.79)	0.08	0.82
B3	1,288 (145.52)	14,575 (1646.75)	0.08	30.0	19.0 (84.51)	62 (275.79)	0.11	0.31
B4	3,503 (395.79)	14,575 (1646.75)	0.24	21.0	29.0 (129.00)	62 (275.79)	0.37	0.47
B5	6,132 (692.82)	14,575 (1646.75)	0.42	39.0	36.0 (160.14)	62 (275.79)	0.82	0.58
B6	9,531(1072.86)	14,575 (1646.75)	0.65	51.0	52.0 (231.31)	62 (275.79)	0.92	0.84

Table 4.5: LLDFs-Simply Supported Condition (Lane 2 Loaded)

Beam Number	Bending Moment		LLDF (Particular Case)	Shear Force			LLDF (Particular Case)	
	FEA	M_{max}		Acute	Obtuse	V_{max}	Acute	Obtuse
	Kip-in (kN-m)	Kip-in (kN-m)		Kips (kN)	Kips (kN)	Kips (kN)		
B1	958 (108.24)	14,575 (1646.7)	0.06	2.0	38.0	62 (275.79)	0.03	0.61
B2	2,883 (325.74)	14,575 (1646.75)	0.19	17.0	18.0	62 (275.79)	0.27	0.29
B3	5,346 (604.02)	14,575 (1646.75)	0.36	35.0	30.0	62 (275.79)	0.56	0.48
B4	5,773 (652.26)	14,575 (1646.75)	0.39	39.0	37.0	62 (275.79)	0.63	0.60
B5	3,921	14,575 (1646.75)	0.27	46.0	27.0	62 (275.79)	0.74	0.44
B6	1,468 (165.86)	14,575 (1646.75)	0.10	50.0	6.0	62 (275.79)	0.81	0.10

Table 4.6: LLDFs-Simply Supported Condition (Lane 3 Loaded)

Beam Number	Bending Moment		LLDF (Particular Case)	Shear Force			LLDF (Particular Case)	
	FEA	M_{max}		Acute	Obtuse	V_{max}	Acute	Obtuse
	Kip-in (kN-m)	Kip-in (kN-m)		Kips (kN)	Kips (kN)	Kips (kN)		
B1	7109 (803.17)	14,575 (1646.7)	0.48	2.0	39.0	62 (275.79)	0.03	0.63
B2	6215 (702.24)	14,575 (1646.75)	0.42	17.0	18.0	62 (275.79)	0.27	0.29
B3	4555 (514.59)	14,575 (1646.75)	0.31	35.0	30.0	62 (275.79)	0.56	0.48
B4	1949 (220.20)	14,575 (1646.75)	0.13	39.0	37.0	62 (275.79)	0.63	0.60
B5	610 (68.95)	14,575 (1646.75)	0.042	10.0	24.0	62 (275.79)	0.16	0.39
B6	215 (24.25)	14,575 (1646.75)	0.01	50.0	9.0	62 (275.79)	0.81	0.15

Table 4.7: LLDFs-Simply Supported Condition (Two or more Lanes Loaded)

Beam Number	Bending Moment		LLDF (Particular Case)	Shear Force			LLDF (Particular Case)	
	FEA	M_{max}		Acute	Obtuse	V_{max}	Acute	Obtuse
	Kip-in (kN-m)	Kip-in (kN-m)		Kips (kN)	Kips (kN)	Kips (kN)		
B1	7,127 (805.24)	14,575 (1646.7)	0.49	36	29.0	62 (275.79)	0.58	0.47
B2	7,584 (856.88)	14,575 (1646.75)	0.52	56	46.0	62 (275.79)	0.90	0.74
B3	8,261 (933.37)	14,575 (1646.75)	0.57	55	63.0	62 (275.79)	0.89	1.02
B4	7,960 (899.36)	14,575 (1646.75)	0.55	61	55.0	62 (275.79)	0.98	0.89
B5	8,363 (944.89)	14,575 (1646.75)	0.57	47	51.0	62 (275.79)	0.76	0.82
B6	9,676 (1093.24)	14,575 (1646.75)	0.66	99	52.0	62 (275.79)	1.60	0.84

Table 4.8: LLDFs for Bending Moment and Shear Force

gM_1^{i-}	gM_{2+}^{i-}	gM_1^{e-}	gM_{2+}^{e-}
One Lane	Two or more Lanes	One Lane	Two or more Lanes
0.42	0.57	0.65	0.66
gV_1^{i-}	gV_{2+}^{i-}	gV_1^{e-}	gV_{2+}^{e-}
One Lane	Two or more Lanes	One Lane	Two or more Lanes
0.82	1.02	1.18	1.60

4.2.2.2 LLDFs for Integral Abutment Bridge Models

As before, only the models corresponding to a 66.67ft (20.32m) span and a 30° skew are presented in detail here. Results of other Bridge models are presented in Table 4.14 (c to d). LLDFs for integral abutment Bridge models were calculated assuming that NEXT beams were connected to the abutment at each end of the Bridge. The FEM model of the sub structure is shown in Figure 4.9, where the abutment and piles are illustrated. Table 4.9 to 4.12 summarize results of bending moment and shear force ratios used to determine LLDFs for interior (B2 to B5) and exterior beams (B1 and B6).

10 ft (3.04m)   10 ft (3.04 m) 10.5ft(3.2m)   10 ft (3.04m) 10.0 ft (3.04m)
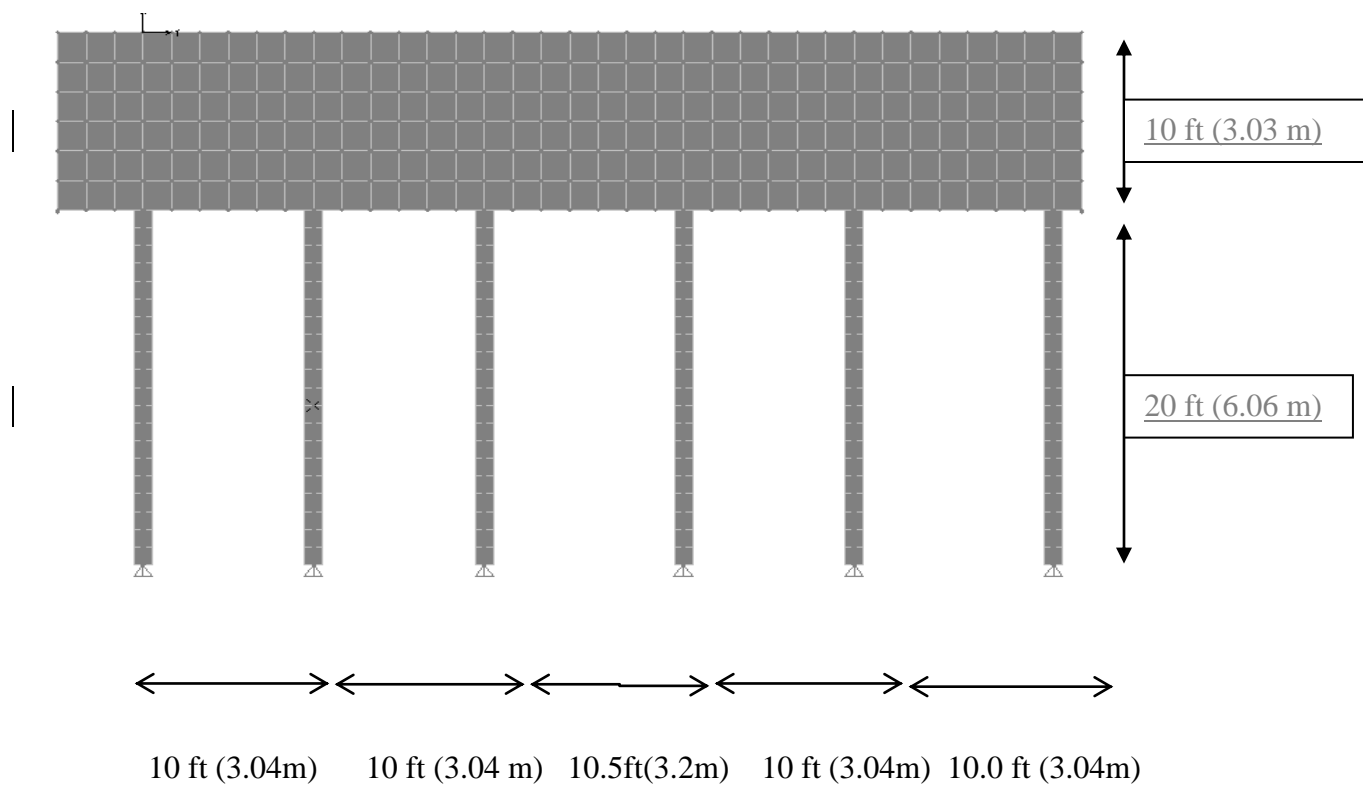
Figure4.9: FEM Model For Integral Abutment Bridge (Side Elevation)

Table 4.9: LLDF-IAB (Lane 1 Loaded)

Beam Number	Bending Moment		LLDF (Particular Case)	Shear Force			LLDF (Particular Case)	
	FEA	M_{max}		Acute	Obtuse	V_{max}	Acute	Obtuse
	Kip-in (kN-m)	Kip-in (kN-m)		Kips (kN)	Kips (kN)	Kips (kN)		
B1	1263 (142.70)	14,575 (1646.7)	0.08	3.0	14.0	62 (275.79)	0.05	0.23
B2	1299 (146.77)	14,575 (1646.75)	0.09	3.0	41.0	62 (275.79)	0.05	0.66
B3	1658 (187.33)	14,575 (1646.75)	0.11	7.0	26.0	62 (275.79)	0.11	0.42
B4	2960 (334.43)	14,575 (1646.75)	0.21	18.0	21.0	62 (275.79)	0.29	0.34
B5	4673 (527.98)	14,575 (1646.75)	0.32	34.0	31.0	62 (275.79)	0.55	0.50
B6	6447 (728.41)	14,575 (1646.75)	0.44	42.0	50.0	62 (275.79)	0.68	0.81

Table 4.10: LLDF-IAB (Lane 2 Loaded)

Beam Number	Bending Moment		LLDF (Particular Case)	Shear Force			LLDF (Particular Case)	
	FEA	M_{max}		Acute	Obtuse	V_{max}	Acute	Obtuse
	Kip-in (kN-m)	Kip-in (kN-m)		Kips (kN)	Kips (kN)	Kips (kN)		
B1	1,507 (170.27)	14,575 (1646.7)	0.10	4	6.0	62 (275.79)	0.06	0.10
B2	2,527 (285.51)	14,575 (1646.75)	0.17	13	21.0	62 (275.79)	0.21	0.34
B3	4,275 (483.01)	14,575 (1646.75)	0.29	32	28.0	62 (275.79)	0.52	0.45
B4	4,624 (522.41)	14,575 (1646.75)	0.32	33	34.0	62 (275.79)	0.53	0.55
B5	3,254 (367.65)	14,575 (1646.75)	0.22	24	21.0	62 (275.79)	0.39	0.34
B6	1,769 (199.87)	14,575 (1646.75)	0.12	36	4.0	62 (275.79)	0.58	0.06

Table 4.11: LLDF-IAB (Lane 3 Loaded)

Beam Number	Bending Moment		LLDF (Particular Case)	Shear Force			LLDF (Particular Case)	
	FEA	M$_{max}$		Acute	Obtuse	V$_{max}$	Acute	Obtuse
	Kip-in (kN-m)	Kip-in (kN-m)		Kips (kN)	Kips (kN)	Kips (kN)		
B1	5,012 (566.28)	14,575 (1646.7)	0.34	13	27.0	62 (275.79)	0.21	0.44
B2	4,855 (548.54)	14,575 (1646.75)	0.33	32	37.0	62 (275.79)	0.52	0.60
B3	3,720 (420.30)	14,575 (1646.75)	0.25	33	27.0	62 (275.79)	0.53	0.44
B4	1,980 (223.71)	14,575 (1646.75)	0.14	23	8.0	62 (275.79)	0.37	0.13
B5	1,366 154.34)	14,575 (1646.75)	0.09	37	2.0	62 (275.79)	0.60	0.03
B6	1,261 (142.47)	14,575 (1646.75)	0.08	1	2.0	62 (275.79)	0.02	0.03

Table 4.12: LLDF- IAB (Two or more than Lanes Loaded)

Beam Number	Bending Moment		LLDF (Particular Case)	Shear Force			LLDF (Particular Case)	
	FEA	M_{max}		Acute	Obtuse	V_{max}	Acute	Obtuse
	Kip-in (kN-m)	Kip-in (kN-m)		Kips (kN)	Kips (kN)	Kips (kN)		
B1	5500 (621.42)	14,575 (1646.7)	0.37	33.0	25.0	62 (275.79)	0.53	0.40
B2	6148 (694.63)	14,575 (1646.75)	0.42	43.0	57.0	62 (275.79)	0.69	0.92
B3	6828 (771.46)	14,575 (1646.75)	0.47	51.0	62.0	62 (275.79)	0.82	1.00
B4	6757 (763.44)	14,575 (1646.75)	0.46	58.0	53.0	62 (275.79)	0.94	0.85
B5	6617 (747.62)	14,575 (1646.75)	0.45	50.0	46.0	62 (275.79)	0.81	0.74
B6	6831 (771.80)	14,575 (1646.75)	0.47	38.0	46.0	62 (275.79)	0.61	0.74

Table 4.13 lists the LLDFs for IAB case with span 66.67 ft (20.32m) and skew angle 30°, obtained from tables 4.8-4.11 as the maximum value of all ratios for a specific category.

Table 4.13: LLDF for Moment and Shear Force

gM_1^{i-}	gM_{2+}^{i-}	gM_1^{e-}	gM_{2+}^{e-}
One lane	Two or more lanes	One lane	Two or more lanes
0.33	0.47	0.44	0.47
gV_1^{i-}	gV_{2+}^{i-}	gV_1^{e-}	gV_{2+}^{e-}
One lane	Two or more lanes	One lane	Two or more lanes
0.66	0.81	1.00	0.74

1=one lane loaded whereas, 2+= for two or more lanes loaded, i- interior girder, e- represent exterior girder respectively, M=Bending Moment, V=Shear Force.

From the Table 4.8 (LLDFs for simply supported Bridge) and Table 4.13 (LLDFs for IAB) we conclude that the LLDF for the SS case is conservative. This seems to be plausible as in IAB modeling, sub structure and foundation components are added with their stiffness due to which it restrained rotation in the beam and alleviate mid span-moments. The reduction in forces in the girder will further results in reduction of LLDFs of the girder.

4.3 Summary

Section 4.2.2 explains the evaluation of LLDFs for actual Brimfield Bridge prototype with span 66.67ft (20.32m). For other sets of parameter the LLDFs are evaluated in the similar manner. Table 4.14 (a-d) lists the LLDFs for span and skew parameters.

68

Table4.14(a-d): LLDFs Obtained From FEM

(a) LLDFs-Bending Moment –Span Parameter

Set of Parameter	50ft (15.24m) Skew 0°		66.67 ft (20.32m) - Skew 0°		80 ft (24.38m) - Skew 0°	
LLDFs	FE_{SS}	FE_{IAB}	FE_{SS}	FE_{IAB}	FE_{SS}	FE_{IAB}
gM_1^{i-}	0.51	0.31	0.42	0.33	0.40	0.33
gM_{2+}^{i-}	0.58	0.46	0.57	0.47	0.55	0.49
gM_1^{e-}	0.64	0.41	0.62	0.43	0.60	0.44
gM_2^{e-}	0.64	0.44	0.63	0.46	0.62	0.48

(b)LLDFs-Shear Force-Span Parameter

Set of Parameter	50ft (15.24m)Skew Skew 0°		66.67 ft (20.32m) Skew 0°		80ft (24.38m) Skew 0°	
LLDFs	FE_{SS}	FE_{IAB}	FE_{SS}	FE_{IAB}	FE_{SS}	FE_{IAB}
gV_1^{i-}	0.67	0.63	0.71	0.68	0.60	0.65
gV_{2+}^{i-}	0.72	0.75	0.79	0.82	0.73	0.79
gV_1^{e-}	0.75	0.79	0.82	0.85	0.79	0.74
gV_2^{e-}	0.75	0.75	0.82	0.85	0.79	0.74

(c) LLDFs-Bending Moment-Skew Parameter

Set of Parameter	66.67 ft (20.32m) - Skew 0°		66.67 ft(20.32m) - Skew 30°		66.67 ft (20.32m) - Skew 45°	
LLDFs	FE_{SS}	FE_{IAB}	FE_{SS}	FE_{IAB}	FE_{SS}	FE_{IAB}
gM_1^{1-}	0.42	0.33	0.42	0.33	0.39	0.31
gM_{2+}^{i-}	0.57	0.47	0.57	0.47	0.52	0.46
gM_1^{e-}	0.62	0.44	0.65	0.44	0.64	0.42
gM_2^{e-}	0.63	0.47	0.66	0.47	0.65	0.44

(d) LLDFs-Shear Force- Skew Parameter

Set of Parameter	66.67 ft (20.32m) Skew 0°		66.67 ft (20.32m) Skew 30°		66.67 ft (20.32m) Skew 45°	
LLDFs	FE_{SS}	FE_{IAB}	FE_{SS}	FE_{IAB}	FE_{SS}	FE_{IAB}
gV_1^{1-}	0.71	0.68	0.82	0.66	1.21	0.68
gV_{2+}^{i-}	0.79	0.82	1.02	1.00	1.32	0.89
gV_1^{e-}	0.82	0.85	1.18	0.81	2.73	1.10
gV_2^{e-}	0.82	0.85	1.60	0.74	2.76	1.48

Notes 1=one lane loaded whereas, 2+= for two or more lanes loaded, i- interior girder, e- represent exterior girder respectively, V=Shear Force.

70

www.manaraa.com

CHAPTER 5

PARAMETRIC STUDIES IN EVALUATION OF LLDFs

This chapter shows comparisons of LLDFs computed using the techniques described in Chapter 3 and Chapter 4. LLDFs calculated using AASHTO LRFD equations (Chapter 3) from both the single stem (SST) approach and double stem (DST) approach are compared with LLDFs determined from FEM analyses assuming simply supported and integral abutment support conditions. The variation of LLDFs depending on the assumed spacing (SST and DST) following the AASHTO LRFD specifications (2010) is first presented. This variation gives important information on which of the two methods yields more conservative results. Furthermore, the qualitative variation observed in LLDFs as other parameters are varied (skew, length) when using the AASHTO LRFD equations should be similar to the variation found when using FEM analyses. In section 5.2 LLDFs for bending moment and shear force in interior girders and exterior girders under single and multiple lanes loaded are discussed so that recommendations can be given on the assumptions to use for LLDFs of NEXT beam Bridges. Based on comparison the PCI-NE Bridge Technical Committee recommendations to determining LLDFs of NEXT beams can also be evaluated in detail.

5.1 Comparison of AASHTO LLDFs and FEM Analyses LLDFs

This section compares LLDFs obtained from AASHTO LRFD (2010) with those obtained using the detailed FEM analyses described in Chapter 4. When comparing LLDFs calculated using different methods, it was considered important that the trends observed in LLDFs obtained through FEM analyses have similarities to LLDFs obtained

71

through AASHTO LRFD (2010). To compare trends, LLDFs obtained in chapter three and four are compared when span and skew angle were varied parametrically.

5.1.1 Trends Observed for Span Variations

The trends of LLDFs as a function of span are summarized in Table5.1 and 5.2 for bending moment and shear force, respectively. Three different spans were chosen in this study (50, 66.67 and 80 ft [15.24, 20.32 and 24.38m]). LLDFs were obtained using four different approaches: (1) AASHTO LRFD equations − single stem assumption (SST); (2) AASHTO LRFD equations − double stem assumption (DST); (3) FE analysis − simple support assumption (FE$_{SS}$); and (4) FEM analysis − integral abutment assumption (FE$_{IAB}$). Because only span was varied parametrically, skew was kept constant at 0° in all these comparisons. The same information is presented graphically in Figures 5.1 through 5.4.

Table 5.1: Bending Moment LLDFs - Different Spans, (0° Skew)

Span	50 ft (15.24 m)				66.67 ft (20.32 m)				80 ft (24.38 m)			
	SST	DST	FE$_{SS}$	FE$_{IAB}$	SST	DST	FE$_{SS}$	FE$_{IAB}$	SST	DST	FE$_{SS}$	FE$_{IAB}$
gM_1^{i-}	0.66	0.53	0.51	0.31	0.63	0.50	0.42	0.33	0.61	0.49	0.40	0.33
gM_{2+}^{i-}	0.83	0.71	0.58	0.46	0.81	0.70	0.57	0.47	0.80	0.68	0.55	0.49
gM_1^{e-}	0.70	0.82	0.64	0.41	0.70	0.82	0.62	0.43	0.70	0.82	0.60	0.44
gM_2^{e-}	0.64	0.74	0.64	0.44	0.63	0.73	0.63	0.46	0.62	0.72	0.62	0.48

Notes: SST-Single Stem Approach, DST- Double Stem Approach, FE$_{SS}$ Simply Supported Approach, FE$_{IAB}$ IAB – Integral Abutment Approach, 1=one lane loaded whereas, 2+= for two or more lanes loaded, i-interior girder, e- represent exterior girder respectively, M=Bending Moment.

Table 5.2: Shear Force LLDFs - Different Spans, (0° skew)

Span	50 ft (15.24 m)				66.67 ft (20.32 m)				80 ft (24.38 m)			
	SST	DST	FE_{SS}	FE_{IAB}	SST	DST	FE_{SS}	FE_{IAB}	SST	DST	FE_{SS}	FE_{IAB}
gV_1^{i-}	1.04	0.68	0.67	0.63	1.04	0.68	0.71	0.68	1.04	0.68	0.60	0.65
gV_{2+}^{i}	1.05	0.82	0.72	0.75	1.05	0.82	0.79	0.82	1.05	0.82	0.73	0.79
gV_1^{e-}	0.70	0.82	0.75	0.79	0.70	0.82	0.82	0.85	0.70	0.82	0.79	0.74
gV_2^{e-}	0.63	0.70	0.75	0.75	0.63	0.70	0.82	0.85	0.63	0.70	0.79	0.74

Notes: SST-Single Stem Approach, DST- Double Stem Approach, SS- Simply Supported Approach, IAB – Integral Abutment Approach, 1=one lane loaded whereas, 2+= for two or more lanes loaded, i- interior girder, e- represent exterior girder respectively, M=Bending Moment.

(a)   (b)
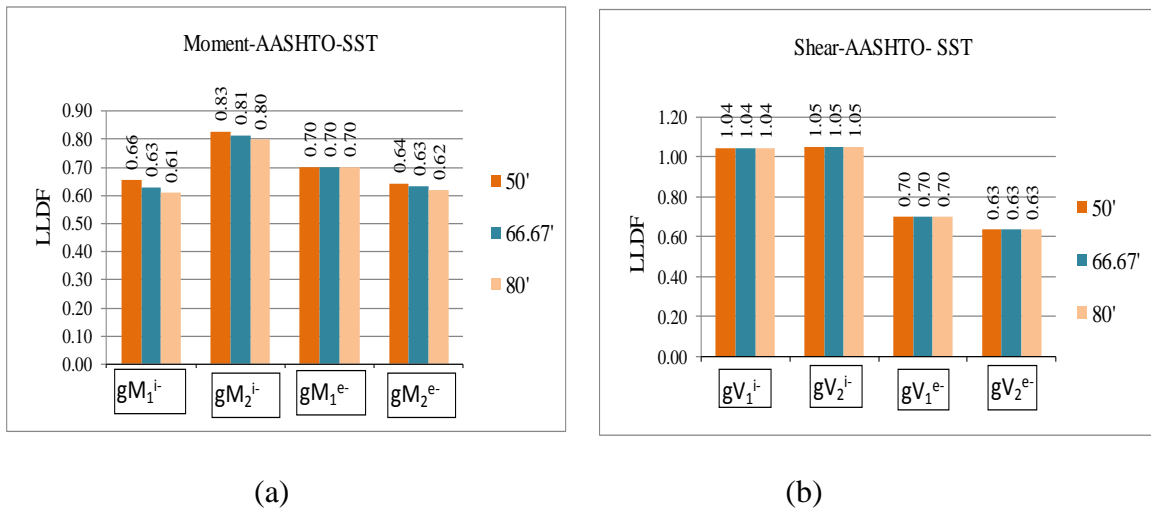
Figure 5.1(a-b) Comparisons of LLDFs – Single Stem Approach

73
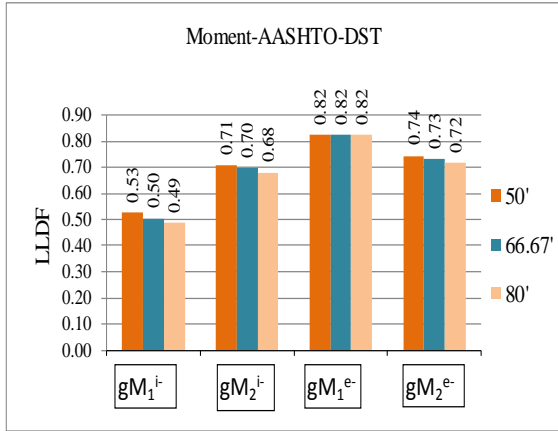
(a)
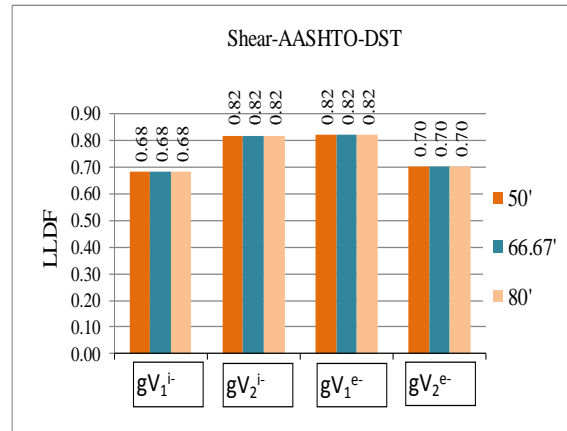
(b)

Figure 5.2(a-b) Comparisons of LLDFs – Double Stem Approach
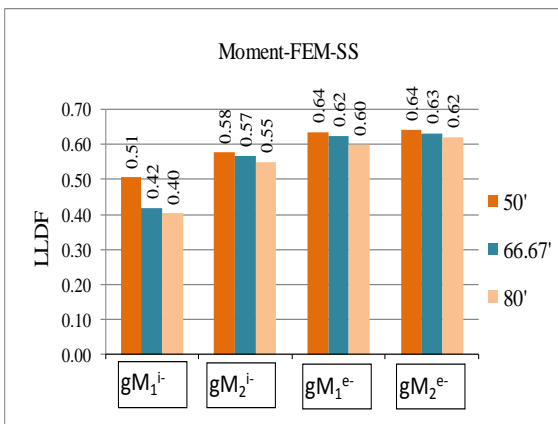
(a)
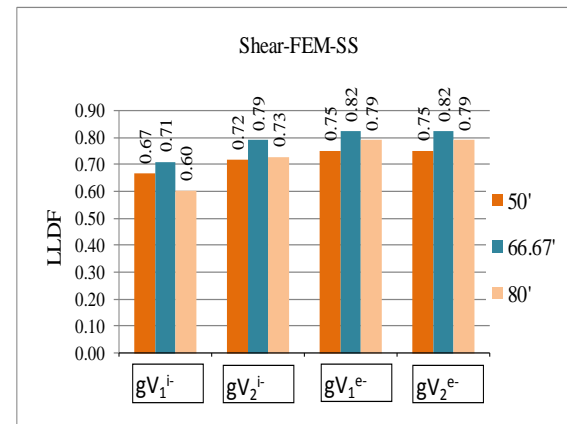
(b)

Figure 5.3(a-b) Comparisons of LLDFs –FE$_{SS}$ Approach

(a)   (b)
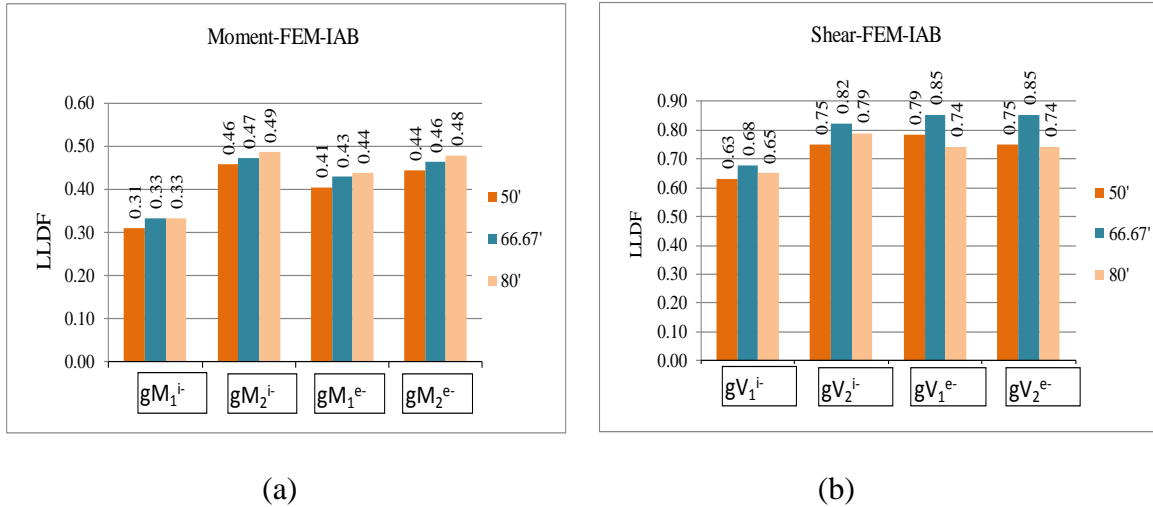
Figure 5.4(a-b) Comparisons of LLDFs –FE$_{IAB}$ Approach

Figures 5.1 and 5.2 show a comparison of LLDFs calculated using the SST and DST approaches, respectively. We can see that LLDFs for bending moment generally decrease with span, except for the case of exterior girders for a single lane loaded. LLDFs for shear force remain constant in all cases. If we compare the moment LLDFs with the results obtained from FEM analysis assuming simply supported end conditions (Figure5.3(a)), we can see that the LLDF trend is also decreasing with span as observed from AASHTO LRFD (2010). However, the results from FEM analyses assuming IAB support conditions (Figure 5.4a) show a different trend from results using AASHTO LRFD. Comparing the shear force LLDFs from FEM analyses in Figures 5.3b and 5.4b with AASTHO LRFD demonstrate that LLDFs are not constant with span as obtained from AASHTO LRFD equations.

5.1.2 Trends Observed for Skew Angle Variations

The effect of variation of skew angle on LLDFs in NEXT beam Bridges is presented in this section for a 66.67 ft (20.32m) span. This span was chosen as the middle range of spans considered to illustrate trends in variation of LLDFs. The three skew angles

considered are 0°, 30° and 45°. Tables 5.3 and 5.4summarize LLDFs calculated by the different methods described in Section 5.1.1. Figures 5.5 through 5.8 illustrate comparison of the LLDF results graphically for bending moment and shear force.

Table 5.3: Bending Moment LLDFs – Different Skew Angles (Span = 66.67 ft (20.32 m))

Skew Angle	0°				30°				45°			
	SST	DST	FE_{SS}	FE_{IAB}	SST	DST	FE_{SS}	FE_{IAB}	SST	DST	FE_{SS}	FE_{IAB}
gM_1^{i-}	0.63	0.50	0.42	0.33	0.61	0.48	0.42	0.33	0.59	0.46	0.39	0.31
gM_{2+}^{i-}	0.81	0.70	0.57	0.47	0.79	0.66	0.57	0.47	0.77	0.63	0.52	0.46
gM_1^{e-}	0.70	0.82	0.62	0.43	0.68	0.78	0.65	0.44	0.66	0.74	0.64	0.42
gM_2^{e-}	0.63	0.73	0.63	0.46	0.61	0.69	0.66	0.47	0.59	0.65	0.65	0.44

Notes: SST-Single Stem Approach, DST- Double Stem Approach, SS- Simply Supported Approach, IAB – Integral Abutment Approach, **1=**one lane loaded whereas, **2+-** for two or more lanes loaded, i- interior girder, **e-** represent exterior girder respectively, M- Bending Moment

Table5.4: Shear Force LLDFs – Different Skew Angles (66.67 ft (20.32 m) Span)

Skew Angle	0°				30°				45°			
	SST	DST	FE$_{SS}$	FE$_{IAB}$	SST	DST	FE$_{SS}$	FE$_{IAB}$	SST	DST	FE$_{SS}$	FE$_{IAB}$
gV_1^{i-}	1.04	0.68	0.71	0.68	1.17	0.75	0.82	0.66	1.27	0.80	1.21	0.68
gV_{2+}^{i-}	1.05	0.82	0.79	0.82	1.18	0.90	1.02	1.00	1.27	0.96	1.32	0.89
gV_1^{e-}	0.70	0.82	0.82	0.85	0.77	0.91	1.18	0.81	0.82	0.97	2.73	1.10
gV_2^{e-}	0.63	0.70	0.82	0.85	0.70	0.77	1.60	0.74	0.75	0.83	2.76	1.48

Notes: SST-Single Stem Approach, DST- Double Stem Approach, SS- Simply Supported Approach, IAB – Integral Abutment Approach, **1**=one lane loaded, **2**+= two or more lanes loaded, i- interior girder, **e-** exterior girder respectively, V – Shear Forces.

(a)   (b)
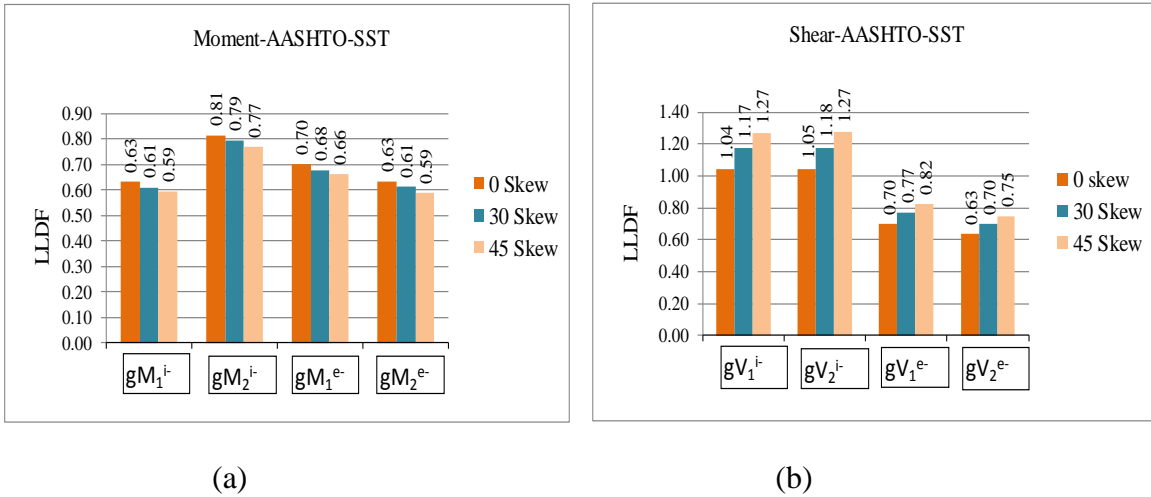
Figure5.5(a-b) LLDFs for Forces with Single Stem approach (Skew Angle Parameter)
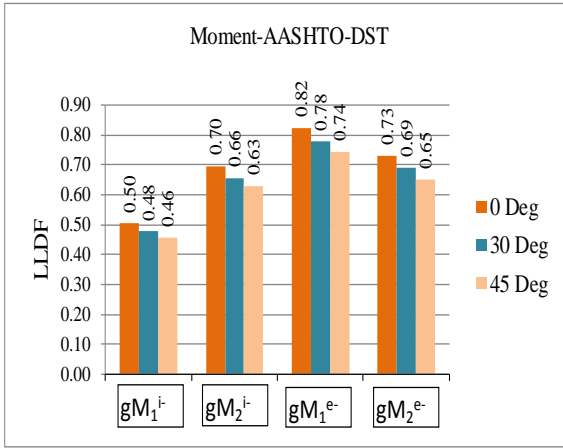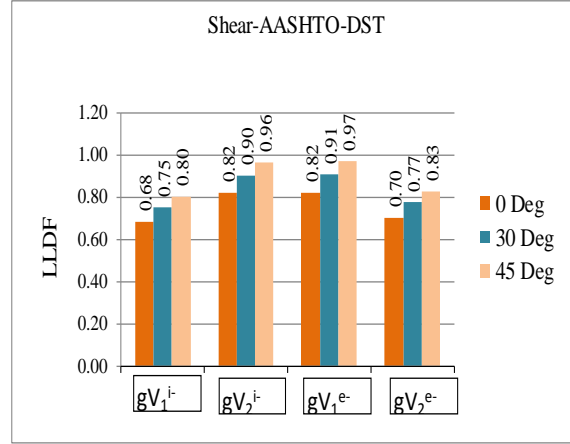
Figure 5.6(a-b) LLDFs for Forces with Double Stem approach
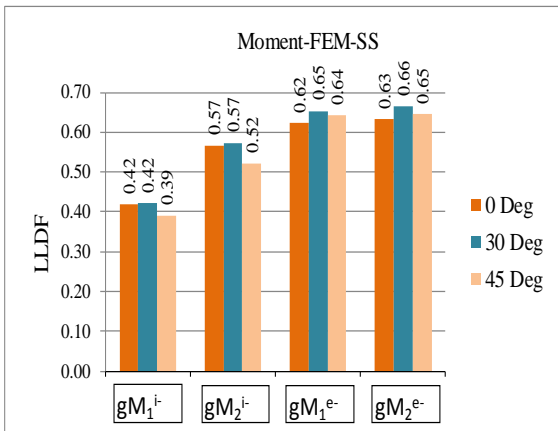
(Skew Angle Parameter)
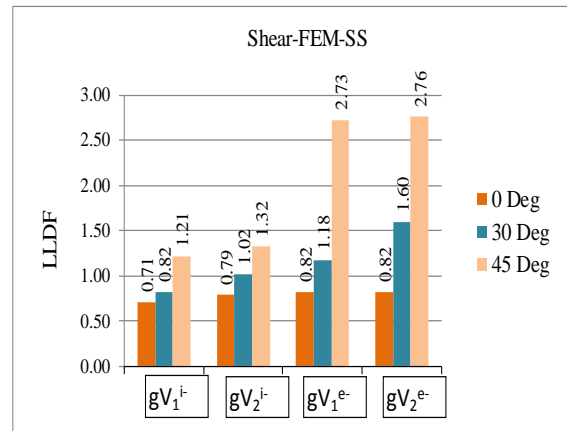
Figure 5.7(a-b) LLDFs for Forces FE_{SS} (Skew Angle Parameter)

(a)   (b)
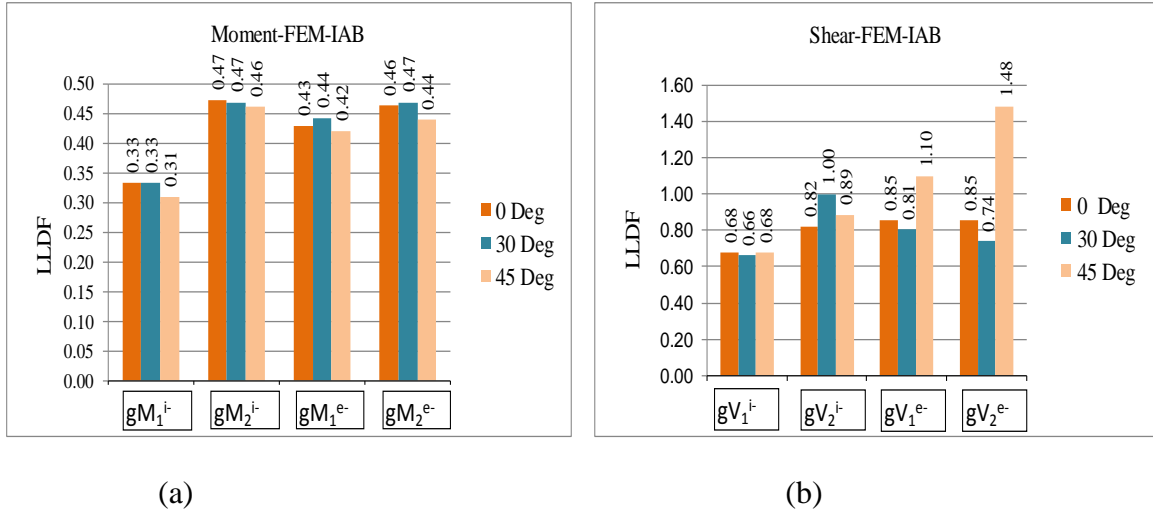
Figure 5.8(a-b) LLDFs for Forces FE$_{IAB}$ (Skew Angle Parameter)

Bending moment LLDFs obtained from AASHTO LRFD decrease with increasing skew angle, whereas shear force LLDFs increase with increasing skew angle. These general trends are not observed in the case of FEM analyses. Bending moment LLDFs obtained from FEM analyses assuming simply supported conditions remain constant for interior beams for the first two skew angles and then decrease for the highest skew angle. Moment LLDFs in exterior beams increase with increasing skew angle. When IAB support conditions are assumed, a clear trend is not apparent (higher skews cause an increase in some cases and a decrease in others). The trends in shear force LLDFs computed using FEM analyses generally increase with increasing skew angle. The increase for the largest skew angle, however, is much higher than the increase obtained when using AASHTO LRFD equations.

The reasons behind high LLDFs for shear force of exterior girder with high skew angles are attributed to the type of member considered to model the NEXT beams. The NEXT beam has been modeled as 3 dimensional frame elements at the center of gravity of the NEXT beams. The selection of this type of resulted in higher cantilever zone in

79

comparison to the actual case. This high cantilever cause higher torsion and higher torsion value cause high shear force in the exterior beam with high skew angle. The other reason is attributed to the difference in the behavior in terms of conversion of torsion force in to the shear force. The two stems of the NEXT beam will have shear forces in opposite direction due to torsion but in model the torsion results in shear force in only one direction. This phenomenon keeps higher shear force in the exterior NEXT beam for the shear force.

5.2 Comparison of LLDFs Obtained Through Different Methods

LLDFs obtained from the four different methods are further compared in this section to ascertain the one resulting in the most conservative estimates of moment and shear force. It was mentioned in Chapter 3 that the SST approach resulted in more conservative LLDF values for interior girders, but that the DST approach gave higher LLDF values for exterior girders. The results obtained FEM analyses assuming simply supported conditions (FE_{SS} approach) and integral abutment support conditions (FE_{IAB} approach) are also discussed in this section. The LLDFs from the four different approaches are summarized in Tables 5.1 to 5.4, and graphically presented in Figures 5.9 to 5.12. The comparisons are presented for the three different spans and skew angles indicated previously.

5.2.1 Comparison of LLDFs for Parametric Variations in Span

LLDFs are compared for the three spans of 50 ft (15.24m), 66.67 ft (20.32m), and 80 ft (24.38m) and a 0° skew angles. Results listed in Tables 5.1 and 5.2, and bar comparisons in Figures 5.9 to 5.11 show that LLDFs for bending moment obtained from FEM analyses are smaller in comparison with values obtained from either SST or DST

approaches, and therefore not govern the values of LLDFs. Conversely, shear force LLDFs for interior girders based on AASHTO LRFD are higher than values obtained from FEM analyses. Shear force LLDFs of exterior girders are governed by results from FEM analyses, since much higher values than AASHTO LRFD equations are obtained. These results may be attributable to high torsional stiffness of NEXT beam Bridges, not accounted by the AASHTO equations used for the two cross section types selected in this study (Type k and i).

Also based on comparison of LLDFs from two FEM analyses, we can conclude that bending moment LLDFs obtained from FE_{SS} model is conservative compared with values obtained from FE_{IAB} model. The results are consistent with anticipated values as inclusion of the sub structure and foundation increase end stiffness in the IAB model which resulted in a reduction of midspan bending moment in the beams. For shear force the LLDF values obtained from FE_{SS} model and FE_{IAB} model are marginally different. Shear force is not affected as importantly as moment when end restraint is provided by the sub structure and foundation. The comparisons between LLDFs obtained from two FEM analyses are the shown in Figure 5.9 to 5.11.
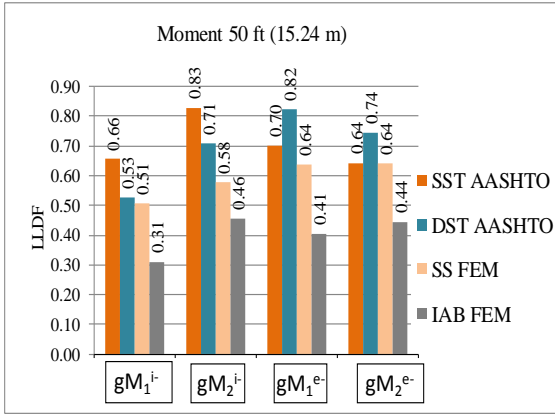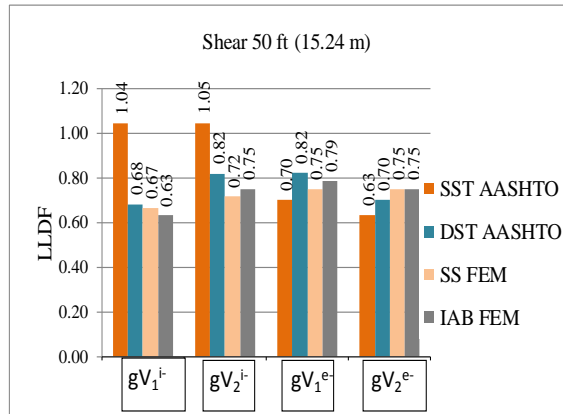
(a)   (b)

Figure 5.9(a-b) LLDF Comparisons for 50 ft Span (0° Skew Angle)
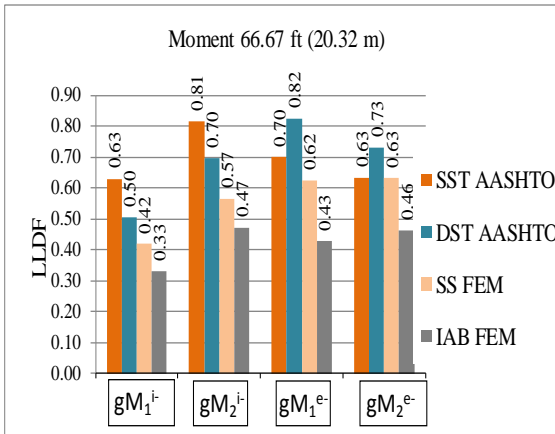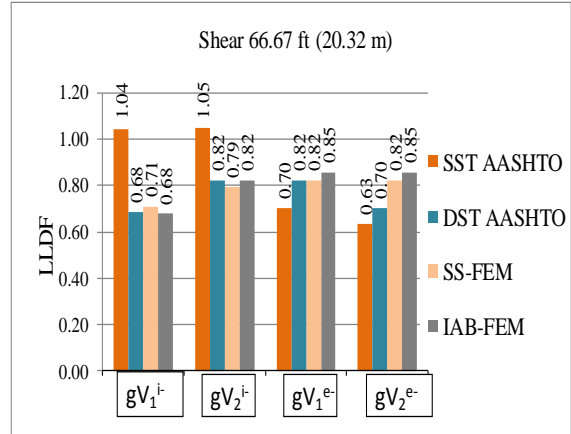
(a)   (b)

Figure 5.10 (a-b) LLDF Comparison for 66.67 ft Spans (0^oskew angle)

82
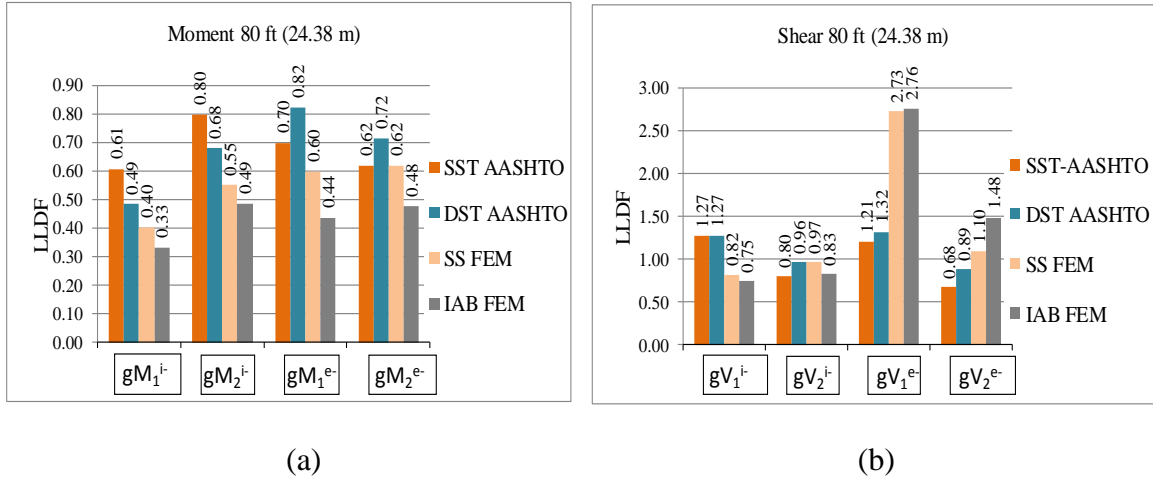
Figure 5.11(a-b) LLDF Comparison for 80 ft (24.38 m)span (0° skew Angle)

5.2.2 Comparison of LLDFs for Parametric Variations in Skew Angle

The three different skew angles of 0°, 30° and 45° degrees in combination with a 66.67 ft (20.32m) span are considered to investigate the effects of skew on LLDFs for NEXT beams. Based on results listed in Tables 5.3 and 5.4, and Figures 5.12 to 5.14, we can observed that bending moment LLDFs obtained from FEM analyses are smaller compared with values obtained from SST and DST approaches. In this case the AASHTO LRFD equations give conservative results for both cross section types considered. Shear force LLDFs for interior girders computed from AASHTO LRFD are also higher than values obtained from FEM analyses. On the other hand, the computed shear force LLDFs for exterior girders using FEM analyses are higher than LLDFs in AASTHO LRFD equations. Very high shear force LLDF values were obtained in the FEM analyses, particularly at high skews, a result that may be caused by the high torsional stiffness of NEXT beams in comparison with the two cross sections assumed when using AASHTO LRFD equations.

From the comparisons above we can conclude that bending moment LLDFs obtained from FE_{SS} model are more conservative than values obtained from an FE_{IAB} model

83

because the end restraint provided by including the sub structure and foundation. For shear force the variation in LLDFs is higher for higher skew angles (30° and 45°). This large variation in LLDFs for shear force can be attributed to the large torsion in the girder in the obtuse angle side. The comparisons between the LLDF are shown in Figure 5.12 to 5.14.

(a)

(b)
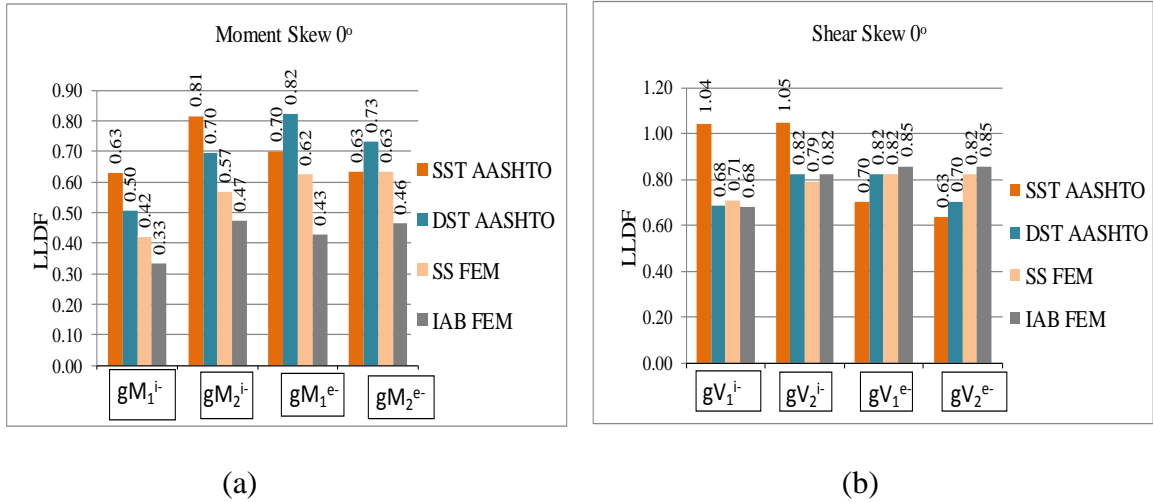
Figure 5.12(a-b) LLDF Comparison for 0o Skew angles

(a)

(b)
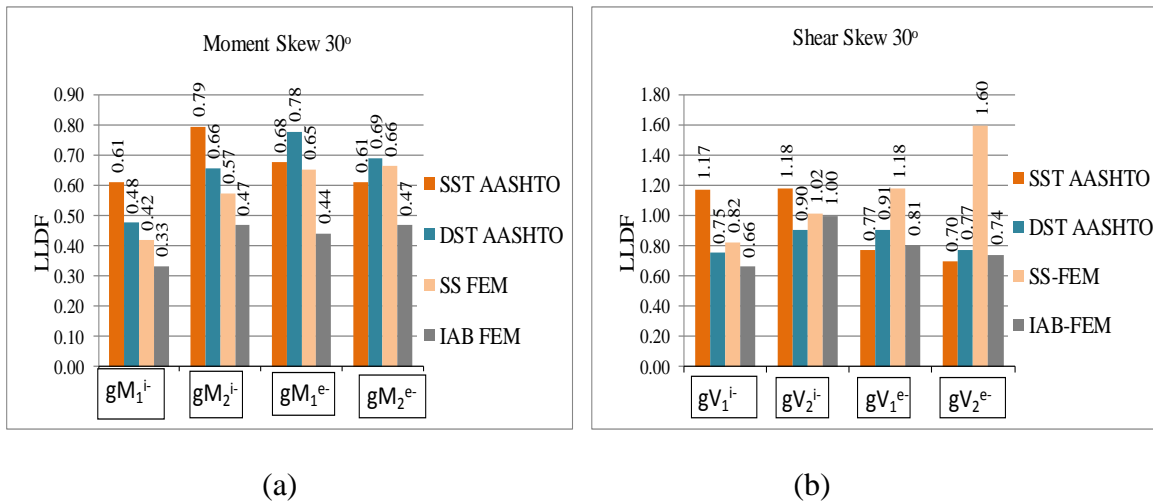
Figure 513(a-b) LLDF Comparison for 30° Skew angle

(a)   (b)
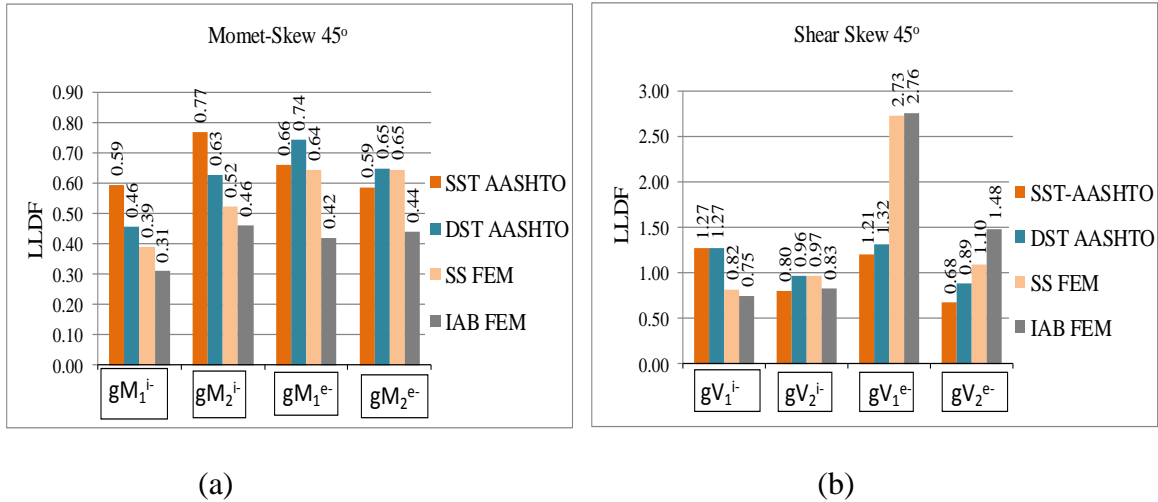
Figure 5.14(a-b): LLDF Comparison for 45° Skew angle

5.3 Summary

The results presented in this chapter can be summarized as follows:

Trend comparison span parameter

- The trend in LLDF values for bending moment (with varying span) obtained from FE_{SS} approach is similar when compared with the trend observed from AASHTO LRFD (2010).

- The trends in the LLDF values for bending moment (with varying span) obtained from FE_{IAB} approach are different when compared with trends obtained from AASHTO LRFD (2010), but AASHTO values are yielding higher values.

- The trends in LLDFs for shear force (with varying span) obtained using FE_{SS} and FE_{IAB} assumptions do not follow the trend found when applying AASHTO LRFD equations with varying span as found from latest AASHTO LRFD.

Trend comparison skew parameter

- The trends in LLDFs for bending moment (with varying skew angle) obtained from FE_{SS} and FE_{IAB} approaches are similar for interior girders but not for exterior girders when compared with trends in AASHTO LRFD equations.

85

- The trend LLDFs for shear force (with varying skew angle) obtained from the FE_{SS} approach is similar to trends in AASHTO LRFD equations.

- When using the FE_{IAB} approach, the trend in LLDFs is different from the trend observed in AASHTO LRFD equations.

Comparison for LLDFs with different end condition

- LLDFs for bending moment obtained from SS model are higher than IAB model. This trend is observed for both parameters i.e. span and skew angle of the Bridge. The trend is as per the expectation due to added stiffness of sub structure and foundations

- LLDFs for shear force for varying span (50 ft (15.24 m), 66.67 ft (20.34 m), 80 ft (24.384 m) with 0° skew angle obtained from SS model vary marginally with respect to IAB model. This result is as per the expectation as inclusion of sub structure and foundation to the model does not vary the shear force in the girder at different locations.

- LLDFs for shear force for varying skew angle (0°, 30°, 45°) with 66.67 ft span obtained from SS model attain much higher value than IAB model. The probable reason behind this could be the higher torsion force in the NEXT beam with simply supported case.

- Interior girder LLDFs for bending moment and shear forces are typically governed by the case corresponding to two or more lanes loaded case.

- Exterior girder LLDFs for bending moment and shear force are governed by one lane loaded case.

86

- In most cases LLDFs values are governed by AASHTO LRFD equations. The shear LLDFs for exterior girders is governed by FEM analyses.

CHAPTER 6

STRAIN EVALAUATION AND VERIFICATION AT DIFFERENT CONSTRUCTUION STAGES

Under the Brimfield Bridge instrumentation programme strain values are evaluated in the NEXT beam at different stages. The field strain values encompass the strain variation due to the creep and shrinkage loss in the strands. In this section the strain variations from field data are compared with the corresponding strains obtained analytically. In the analytical evaluation of strains creep and shrinkage loss as per AASHTO standards are evaluated. The nearness in the values of the strains will validate the creep and shrinkage loss equations in AASHTO standards for the newly adopted NEXT beams. The strain variation can be added to get the cumulative strain variation of NEXT beam with depth. The strain variation with depth for different duration yields clear picture of creep and shrinkage loss in the NEXT beam.

6.1 Stages for Bridge Erection and Strain Evaluation

The field values in terms of strain and temperature are recorded at different stages for the strain evaluation due to losses, lifting and transportation o NEXT beam and change in effective span at respective stages. The data are recorded at following stages. Appendix B lists the date and time for the data recorded for all the six NEXT beams. The stages selected for strain measurements are:

Stage 1- Ten minutes after after detensioning of the strands.

Stage 2-After thirty minutes in casting yard.

Stage 3-After 2 days outside the casting yard.

Stage 4-Approximately after one month outside the casting yard.

Stage 5- Approximately after three month before transferring NEXT beam.

Stage 6-After setting the NEXT beams 4 to 6 on abutments. (Approximately 3 months)

Stage 7- After pour of concrete deck on NEXT beams 4 to 6

Future strain data acquisition (Not in the scope of present thesis)

Stage 8-Strains before live-load testing.

Stage 9-Strains during live-load testing.

Strain evaluation at stages 1 to 7 is within the scope of present thesis whereas evaluation of strains for stages 8 to 9 will be conducted in the future. The Brimfield Bridge is being constructed in two phases. In phase one NEXT beam 4 to 6 are used first at the Bridge site for the erection of half of the Bridge. Once the first half of the Bridge is ready for traffic, the second phase will take place by erecting NEXT beams 1 to 3. Therefore, strains in NEXT beams 4 to 6 are measured for all the seven stages, whereas strains in beams 1 to 3 (still in the casting yard) will be measured up to stage 5 only.

6.2 Bridge Instrumentation Details

For the evaluation of strains, strain gages were installed in NEXT beams at the precasting plant. A total of 82 strain gages are used in the six NEXT beams of the Brimfield Bridge. Strain gages were placed in NEXT beam stems, NEXT beam flanges, and cast-in-place deck. All strain gages are Geokon Model 4200 vibrating wire gages typically used in concrete structures.

Strain gages were installed primarily in the midspan section of all the NEXT beams (Figure 6.2). Additional instrumented sections at one-third and two-thirds of the span were used for NEXT beams 1 and 2. The instrument locations in the NEXT beam cross-

section are shown in Figure 6.1 and 6.2. The small circles with positive sign (Figure 6.2) are used to represent the instruments. Instrument locations vary for different NEXT beams. Table 6.1 lists the instrument depths (d_B, d_M and d_T) within the NEXT beam cross section with respect to the bottom. Instruments (1 to 3 and 5 to 7) are aligned with the stem of NEXT beams are used to measure the longitudinal strains whereas instruments (4 and 8) installed in the flange between stems are intended to measure deck strains in the transverse direction. Strain gages within the depth of the cast-in-place deck were placed (9 to 15) at different locations to measure strains in the transverse direction to assess live-load distribution among NEXT beams in service. In the present scope of thesis the strain gauge data for instruments installed in the stem of NEXT beams are used to record and interpret the data.
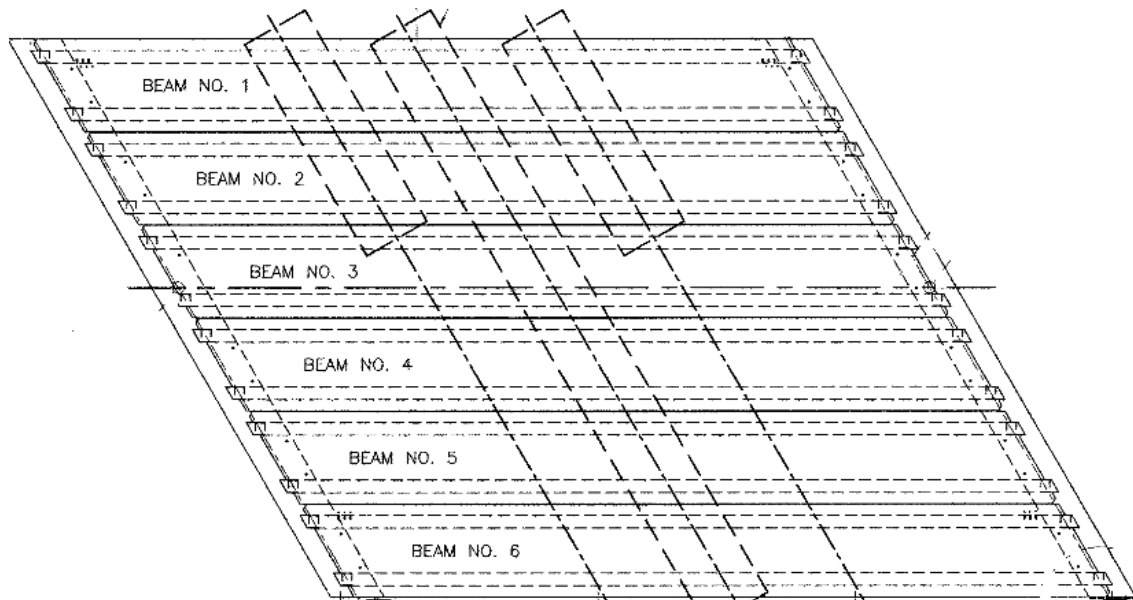
Figure 6.1 Instrumentation Plan

Figure 6.2 Instrumentation in the NEXT Beam

6.3 Evaluation of Longitudinal Strain

In this section longitudinal strain variation are evaluated using two methods. Longitudinal strains are first computed analytically and in second method the values are evaluated based on the field data. Only the section at midspan of NEXT beam is used in both cases. The longitudinal strains from field measurements are determined at three depths (d_B,d_M,d_T-Table 6.1) in the NEXT beams. AASHTO equations are written to evaluate elastic shortening, creep and shrinkage losses at the level of the center of prestressing force. Therefore, comparisons are done at the center of prestressing force of the strands. Strains measured at the center of the prestressing force are compared through interpolation based on the three strains values at different locations (d_B,d_M,d_T-Table 6.1) in both methods(strains obtained from field data and strains obtained from analytical method).

6.3.1 Strain Variation due to Prestress Losses – Analytical Evaluation

Out of different stages (Stage 1 to 6) there is no exterior load applied in the NEXT beams. But based on instrument data strains were noted to be changed. These strain changes were attributed to the losses in strands. So for stages 1 to 6 it is the losses causing strain variation in the NEXT beam whereas in the last stage 7 the strain variation is caused by loses and weight of fresh concrete.

The analytical values of strain are evaluated in two stages. At first the stress variations at different instrument locations between different fabrication or construction stages are calculated. After calculating stress it is divided by the modulus of elasticity of concrete to determine the strains at those depths. The evaluations of strains by this method are done only among the seven stages (section 6.1) in which the respective field data are available so that comparison can be established. For stages 1 to 7 the NEXT beam resists all the actions. After stage 7 when fresh concrete solidifies, the composite section (future scope) will be subjected to future actions.

Table 6.1 lists the cross-section properties of the NEXT beam used in the Brimfield Bridge. The section modulus Z_s at a given depth can be obtained by dividing moment of inertia of the section by the respective depth measured from the elastic centroid of the NEXT beam cross section.

Table 6.1: Brimfield Bridge-Section Property

Section Property	unit	NEXT1	NEXT2	NEXT3	NEXT4	NEXT5	NEXT6
A	in^2	1166	1166	1166	1166	1166	1166
d	in	32	32	32	32	32	32
c.g	in	19.35	19.35	19.35	19.35	19.35	19.35
I	in^4	116100	116100	116100	116100	116100	116100
d_B	in	3.75	3.75	3.5	4	4	4.25
d_M	in	8.25	8.125	8.25	8	8.125	8
d_T	in	29.5	29.5	29.5	29.5	29.5	29.5
$Z_{SB} = I/(c.g - d_B)$	in^3	7442	7442	7325	7564	7564	7689
$Z_{SI} = I/(c.g - d_M)$	in^3	10459	10343	10459	10229	10343	10229
$Z_{ST} = I/(d_T - c.g)$	in^3	11438	11438	11438	11438	11438	11438

Notes :A= Area of NEXT 32 Beam Cross Section; d=Depth of the NEXT beam, c.g =Centre of gravity of NEXT beam from bottom fiber; I =Moment of Inertia of NEXT 32 beam; d_b= Depth of Bottom instrument from bottom fiber; d_M= Depth of Middle Instrument From Bottom Fiber; d_T= Depth of Top instrument from Bottom fiber , Z_{SB}=Section Modulus at bottom instrument level; Z_{SI}=Section Modulus at intermediate Instrument location; Z_{ST} =Section Modulus at Top instrument location.

6.3.1.1 Strain due to Prestressing Forces

In order to compare measured with calculated strains, the stresses induced in the NEXT beam cross section at different stages were first determined by calculation. Subsequently these values were divided by modulus of elasticity of concrete to calculate strains in the prestressed cross section.

6.3.1.2 Calculation of Stresses Induced due to Prestressing Force

Thirty-six uncoated, low relaxation 0.6-in. prestressing strands (satisfying AASHTO M203 specifications) were used in each NEXT beam of the Brimfield Bridge to apply the required prestressing force. The minimum guaranteed ultimate tensile strength of

prestressing strand was 270 ksi. An initial tension of 44 kips per strand was applied to all NEXT beams.

The strand pattern is summarized in Table 6.2 and illustrated graphically in Figure 6.3. Given this strand pattern, the centroid of the prestressing force is located 8.16 in. (207 mm) from the bottom of the NEXT beams.

Table 6.2: Details of Strand Layer used in NEXT beams

Layers (from bottom)	Number of strands	Distance From Bottom Fiber
		in. (mm)
1st Layer	6	2.5 (64)
2nd Layer	10	4.50 (114)
3rd Layer	10	6.50 (165)
4th Layer	6	8.5 (216)
5th Layer	4	29.5 (749)
Center of prestressing force		8.16 (207)
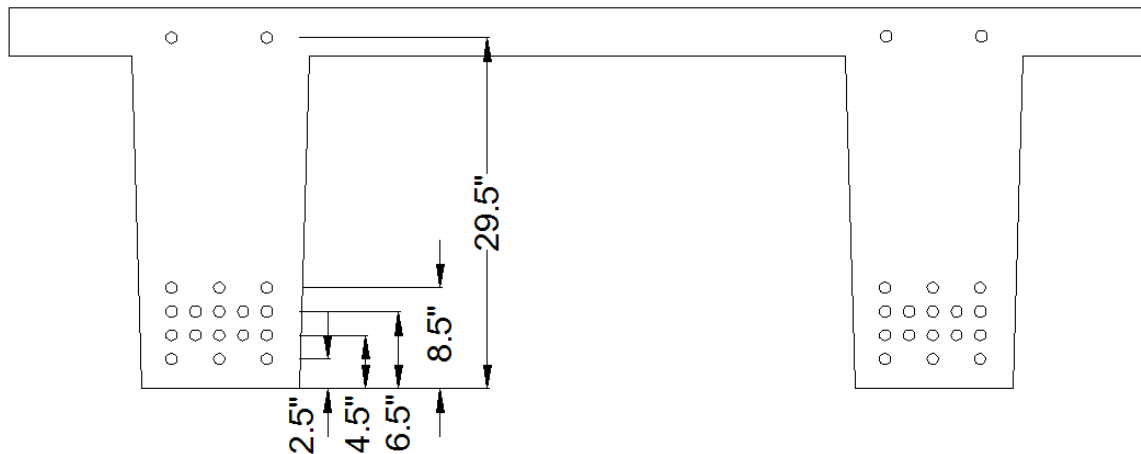
Figure 6.3 Strand Location in the NEXT Beam

Table 6.3 lists the details of prestressing force and stress factor calculation (at d_B, d_M, d_T- Table 6.1). This stress factor is used for the evaluation of stress at instrument locations by multiplying the factor times the prestressing force. The stress factors at the different

94

www.manaraa.com

instrument depths are calculated using Equation 6.1 to 6.3, where positive values are indicative of compressive stresses.

$$Z_{BI}=1/A+e/Z_{SB} \qquad ….. \text{ Equation 6.1}$$

$$Z_{MI}=1/A+e/Z_{SI} \qquad …..\text{Equation 6.2}$$

$$Z_{TI}=1/A-e/Z_{ST} \qquad …..\text{Equation 6.3}$$

Where,

Z_{BI} =Stress factor at bottom instrument location.

Z_{MI} =Stress factor at bottom instrument location.

Z_{TI} =Stress factor at Top instrument location.

e = eccentricity of center of gravity of tendons from cg of NEXT beam.

Z_{SB}=Section modulus at bottom instrument level.

Z_{SI}=Section modulus at intermediate Instrument location.

Z_{ST} =Section modulus at top instrument location.

Table6.3: Prestressing force and Stress Factor

Number of Strands	-	36	36	36	36	36	36
P	kips	1584	1584	1584	1584	1584	1584
c.g	in	19.4	19.4	19.4	19.4	19.4	19.4
y	in	8.167	8.167	8.167	8.167	8.167	8.167
e	in	11.18	11.18	11.18	11.18	11.18	11.18
y	in	0.00236	0.00236	0.00238	0.00234	0.00234	0.00231
Z_{BI}	/in^2	0.00193	0.00194	0.00184	0.00195	0.00194	0.00195
Z_{MI}	/in2	-0.00012	-0.00012	-0.00012	-0.00012	-0.00012	-0.00012
Z_{TI}	/in2	1584	1584	1584	1584	1584	1584

Notes : P = Total Prestressing force; e = eccentricity of c.g. of tendons from cg of NEXT beam; y = Distance of c.g. of tendons from soffit; Z_{BI} = Section factor at bottom instrument location; Z_{MI} = Section factor at bottom instrument location; Z_{TI} = Section factor at Top instrument location.

95

Table 6.4 lists the stresses due to prestressing force at the three instrument depths within the NEXT beam cross section (see Figure 6.2).

Table 6.4 : Stress and Strain due to Prestressing

NEXT BEAM		NEXT 1	NEXT 2	NEXT 3	NEXT 4	NEXT 5	NEXT 6
Duration	Unit	At Release	At Release	At Release	At Release	At Release	At Release
$\sigma_{BI} = PxZ_{BI}$	ksi	3.74	3.74	3.78	3.70	3.70	3.66
$\sigma_{MI} = PxZ_{MI}$	ksi	3.05	3.07	3.05	3.09	3.07	3.09
$\sigma_{TI} = PxZ_{TI}$	ksi	-0.19	-0.19	-0.19	-0.19	-0.19	-0.19
$\varepsilon_{BI} = \sigma_{BI}/E$	με	690.16	690.16	697.20	683.11	683.11	676.07
$\varepsilon_{MI} = \sigma_{MI}/E$	με	563.41	566.93	563.41	570.45	566.93	570.45
$\varepsilon_{TI} = \sigma_{TI}/E$	με	-35.11	-35.11	-35.11	-35.11	-35.11	-35.11

6.3.1.3 Stress Variation due to Losses and Self Weight

6.3.1.4 Short-Term Loss with Relaxation Loss

After releasing the prestressing force onto the beams the following day after casting, elastic shortening takes place. This loss was estimated as 6.57 % (Appendix C.1.1 for details). Strand relaxation loss between transfer and deck pour is 0.94 % evaluated in Appendix C.2.3.Although relaxation loss is long term loss, it is considered with short term loss to simplify the evaluation of strain. The prestressing force loss is used when evaluating the effective stress and strain on the cross section after release of the strand. The only other effect that generates stress in the cross section at this time is caused by beam self-weight (dead load), which will generate stresses of opposite sign to the prestressing force at a section at midspan. The effective span to calculate self-weight

stresses in the NEXT beams is 66.67 ft (20.32m), assuming that the beam rotates on the casting bed about its ends. The bending moment at mid span is calculated as 8070 kip-in (911.78 kN-m). The dead load stresses at different depths for the different NEXT beams are listed in Table 6.5. The stress is evaluated using the flexure formula (Equation 6.4), and strains are evaluated by dividing stress by the concrete modulus of elasticity E for each beam.

$$\sigma = M/Z \qquad\qquad …..Equation 6.4$$

$$\varepsilon = \sigma/E \qquad\qquad …..Equation 6.5$$

Where,

σ = Longitudinal Bending Stress in the NEXT beam.

M = Bending Moment at the mid Spam

Z = Section modulus at instrument depths.

E=5417.2 ksi (For stage 1 to 3)

E=5795 ksi (For stage 4 to 7)

Table6.5: Stress due to Self Weight

NEXT BEAM		NEXT 1	NEXT 2	NEXT 3	NEXT 4	NEXT 5	NEXT 6
	Unit	At Release	At Release	At Release	At Release	At Release	At Release
$\sigma_{DB}=8070/Z_{SB}$	ksi	-1.08	-1.08	-1.10	-1.07	-1.07	-1.05
$\sigma_{DM}=8070/Z_{SM}$	ksi	-0.77	-0.78	-0.71	-0.79	-0.78	-0.79
$\sigma_{DT}=8070/Z_{ST}$	ksi	0.71	0.71	0.71	0.71	0.71	0.71
$\varepsilon_{DB}=\sigma_{DB}/E$	$\mu\varepsilon$	-199.4	-199.4	-203.1	-197.5	-197.5	-193.8
$\varepsilon_{DM}=\sigma_{DM}/E$	$\mu\varepsilon$	-142.1	-144.0	-131.1	-145.8	-144.0	-145.8
$\varepsilon_{TT}=\sigma_{DT}/E$	$\mu\varepsilon$	131.1	131.1	131.1	131.1	131.1	131.1

Considering the total short term losses TL=6.58+0.94=7.52% , The effective calculated stress in the NEXT beam considering the elastic shortening and beam self-weight at instrument depths are listed in Table 6.6. This stress condition corresponds to stage 1 as presented in Table 6.6.

Table6.6: Stress and Strain at Stage 1

NEXT BEAM		NEXT 1	NEXT 2	NEXT 3	NEXT 4	NEXT 5	NEXT 6
Duration	Unit	10 Minutes	10 Minutes	10 Minutes	10 Minutes	10 Minutes	10 Minutes
$\sigma_{BI} = \sigma_{DB} + P(1-L/100)xZ_{BI}$	ksi	2.37	.37	2.39	2.35	2.35	2.34
$\sigma_{MI} = \sigma_{DM} + P(1-TL/100)xZ_{MI}$	ksi	2.05	2.06	2.05	2.07	2.06	2.07
$\sigma_{TI} = \sigma_{DT} + P(1-TL/100)xZ_{TI}$	ksi	0.53	0.53	0.53	0.53	0.53	0.53
$\varepsilon_{BI} = \sigma_{BI}/E$	$\mu\varepsilon$	437.69	437.69	440.99	434.39	434.39	431.09
$\varepsilon_{MI} = \sigma_{MI}/E$	$\mu\varepsilon$	378.29	379.94	378.29	381.59	379.94	381.59
$\varepsilon_{TI} = \sigma_{TI}/E$	$\mu\varepsilon$	97.79	97.79	97.79	97.79	97.79	97.79

6.3.1.5 Time Dependent (Long-term) Losses

Time-dependent deformation of concrete (creep) is a well known effect that must be considered in elements subjected to sustained compressive forces (such as prestressing). Concrete also contracts due to loss of water that migrates to the surface (shrinkage). These volumetric changes in the concrete induce prestressing force losses that must be accounted. The prestressing strand also suffers from relaxation with time that generates a loss of prestressing force. Although the strands used in the Brimfield Bridge are low relaxation, some loss of prestressing force will occur in the long-term. These three sources of prestressing force loss are time dependent and will continue with time. In Appendix C creep (Appendix C.2.2) and shrinkage (Appendix C.2.1) losses are calculated after 30.16 days. In the present thesis time dependent losses were also calculated at other times in the same way as it is presented for 30.16 days. At each stage loss will be used in reducing the prestressing force to evaluate the stress in similar way as it is done for elastic shortening. Table 6.7 (a to f) list the time dependent losses in percentage of the initial prestressing stress for all the six NEXT beams at different stages. The "C+S" is representing the sum of creep and shrinkage loss. The detailed evaluations of creep and shrinkage losses along with corresponding strains are listed in all tables of Appendix C.

100

Table 6.7(a-f): Stage wise Creep and Shrinkage Losses

(a) Time Dependent Loss for NEXT beam 1

NEXT Beam 1 Stage	Date	Time	Days	(C+S) %Age Loss
After detensioning	4-26	8:00	0.00	0.000
After set on temporary support	4-26	8:30	0.02	0.010
NEXT Beam outside plant	4-28	8:30	2.02	0.893
NEXT Beam outside plant	5-26	12:15	30.16	6.469
NEXT Beam outside plant	8-05	11:35	101.15	9.440
NEXT Beam on abutment	8-11	8:00	107.00	9.54

NOTES: C+S Creep and Shrinkage Loss at the Prestressing Force

(b) Time Dependent Loss for NEXT beam 2

NEXT Beam 2 Stage	Date	Time	Days	(C+S) %Age Loss
After detensioning	4-22	8:00	0.00	0.00
After set on temporary support	4-22	8:30	0.02	0.01
NEXT Beam outside plant	4-26	10:00	4.08	1.68
NEXT Beam outside plant	4-28	7:15	5.97	2.27
NEXT Beam outside plant	5-26	12:15	34.16	6.74
NEXT Beam outside plant	8-05	11:50	105.15	9.39

(c) Time Dependent Loss for NEXT beam 3

NEXT Beam 3 Stage	Date	Time	Days	(C+S) % Age Loss
After detensioning	4-22	8:00	0.00	0.00
After set on temporary support	4-22	8:30	0.02	0.01
NEXT Beam outside plant	4-26	8:30	4.08	1.68
NEXT Beam outside plant	4-28	12:15	5.97	2.27
NEXT Beam outside plant	5-26	11:35	34.16	6.74
NEXT Beam outside plant	8-05	08:00	105.15	9.39

101

(d) Time Dependent Loss for NEXT beam 4

NEXT Beam 4 Stage	Date	Time	Days	(C+S) % Age Loss
After detensioning	4-26	8:00	0.00	0.00
After set on temporary support	4-26	8:30	0.02	0.01
NEXT Beam outside plant	4-28	8:30	2.02	0.89
NEXT Beam outside plant	5-26	12:15	30.11	6.47
NEXT Beam outside plant	8-05	11:35	101.17	9.44
NEXT Beam on Abutment	8-11	8:00	107.00	9.54
After Pour of Fresh Concrete	9-13	9:50	140.08	9.98

(e) Time Dependent Loss for NEXT beam 5

NEXT Beam 5 Stage	Date	Time	Days	(C+S) % Age Loss
After detensioning	4-28	8:00	0.00	0.00
After set on temporary support	4-28	8:30	0.02	0.01
NEXT Beam Outside plant	5-26	8:30	28.13	6.26
NEXT Beam Outside plant	8-5	12:15	98.17	9.38
NEXT Beam on Abutment	8-11	11:35	104.00	9.49
After Pour of Fresh Concrete	9-13	10:15	136.94	9.95

(f) Time Dependent Loss for NEXT beam 6

NEXT Beam 6 Stage	Date	Time	Days	(C+S)% Age Loss
After detensioning	4-28	8:00	0.00	0.00
After set on temporary support	4-28	8:30	0.02	0.01
NEXT Beam Outside plant	5-26	8:30	28.13	6.26
NEXT Beam Outside plant	8-5	12:15	98.17	9.38
NEXT Beam on Abutment	8-11	11:35	104.00	9.49
After Pour of Fresh Concrete	9-13	10:15	136.38	9.94

102

During the different stages presented in Table 6.7, the support condition of the beams changed during handling, which resulted in different magnitudes of dead load bending moment at midspan. As discussed earlier at the time of prestressing force release the NEXT beams are assumed to rotate about its ends with an effective span of 66.67ft (20.32m). Beam handling and positioning inside the precasting plant because changes in the stresses throughout the NEXT beam depth. Temporary beam supports (inside and outside casting yard) were placed approximately 36in. (0.91m) from each end shortening the span by 72in. (1.82m). The effective span for the NEXT beams under self-weight decreased to 60.72ft (18.50 m) for these two stages.

The self-weight bending moment at midspan for this effective span is 6683 kip-in (755 kN-m). As we are concerned with change in strains between stages, the net bending moment induced by self-weight considered to evaluate stress and strain at stages between detensioning and placement of beams on abutments is calculated as 6683-8070 = -1387.06 kip-in (-156.46 kN-m). Table 6.8 lists the stress and strain variations due to change in effective span.

Table 6.8: Stress due to Change in Effective Span

NEXT BEAM		NEXT 1	NEXT 2	NEXT 3	NEXT 4	NEXT 5	NEXT 6
Duration	Unit	30 Minutes	30 Minutes	30 Minutes	30 Minutes	30 Minutes	30 minutes
$\sigma_{DBV}=-1387/Z_{SB}$	ksi	0.19	0.19	0.19	0.18	0.18	0.18
$\sigma_{DMV}=-1387/Z_{SM}$	ksi	0.13	0.13	0.13	0.14	0.13	0.14
$\sigma_{DTV}=-1387/Z_{ST}$	ksi	-0.12	-0.12	-0.12	-0.12	-0.12	-0.12
$\varepsilon_{DB}=\sigma_{DB}/E$	$\mu\varepsilon$	35.1	35.1	35.1	33.2	33.2	33.2
$\varepsilon_{DM}=\sigma_{DM}/E$	$\mu\varepsilon$	24.0	24.0	24.0	25.8	24.0	25.8
$\varepsilon_{TT}=\sigma_{DT}/E$	$\mu\varepsilon$	-22.2	-22.2	-22.2	-22.2	-22.2	-22.2

These stresses are considered in addition to the variation in stress due to creep and shrinkage losses. For stage 2 the elapsed time is 30 minutes so time dependent loss (creep + shrinkage loss, in percent) is L=0.01.

104

Table 6.9: Stress and Strain between Stage 1 and Stage 2

NEXT BEAM	Unit	NEXT 1	NEXT 2	NEXT 3	NEXT 4	NEXT 5	NEXT 6
Duration		30 Minutes	30 Minutes	30 Minutes	30 Minutes	30 Minutes	30 Minutes
$\sigma_{BI2} = \sigma_{DBV} + P(-L/100) x Z_{BI}$	ksi	0.19	0.19	0.19	0.18	0.18	0.18
$\sigma_{MI2} = \sigma_{DMV} + P(-L/100) x Z_{MI}$	ksi	0.13	0.13	0.13	0.14	0.13	0.14
$\sigma_{TI2} = \sigma_{DTV} + P(-L/100) x Z_{TI}$	ksi	-0.12	-0.12	-0.12	-0.12	-0.12	-0.12
$\varepsilon_{BI} = \sigma_{BI} / E$	$\mu\varepsilon$	34.32	34.34	34.89	33.77	33.77	33.22
$\varepsilon_{MI} = \sigma_{MI} / E$	$\mu\varepsilon$	24.41	24.70	24.43	24.96	24.69	24.96
$\varepsilon_{TI} = \sigma_{TI} / E$	$\mu\varepsilon$	-22.38	-22.38	-22.38	-22.38	-22.38	-22.38

In a similar way, for other stages before transfer the NEXT beam to the site the stress and strain variations between stages are calculated and results are summarized in Appendices G and H, respectively.

At the Bridge site, the NEXT beams were supported on blocks located 7 in. from the end of each beam so the span changed to 65.56 ft (19.98 m). The corresponding bending moment at midspan is 7790 kip-in (880 kN-m).The self-weight stress and strain changed because of beam positioning on abutments due to a net bending moment change at midspan of 7790-8070=-280.06 kip-in (-31.5 kN-m).

Table 6.10 lists the stress and strain variations due to change in effective span at this stage. Only NEXT beams 4 to 6 were transferred to the site.

Table 6.10: Stress Change due to Change in Effective Span

NEXT BEAM		NEXT 4	NEXT 5	NEXT 6
Duration	Unit	107 Days	104 Days	104 Days
$\sigma_{DBV}=-280.6/Z_{SB}$	ksi	-1.03	0.04	0.04
$\sigma_{DMV}=-280.6/Z_{SM}$	ksi	-0.76	0.03	0.03
$\sigma_{DTV}=-280.6/Z_{ST}$	ksi	-0.02	-0.02	-0.02
$\varepsilon_{DBV}=\sigma_{DBV}/E$	$\mu\varepsilon$	-177.7	6.9	6.9
$\varepsilon_{DMV}=\sigma_{DMV}/E$	$\mu\varepsilon$	-131.1	5.2	5.2
$\varepsilon_{DTV}=\sigma_{DTV}/E$	$\mu\varepsilon$	-3.5	-3.5	-3.5

At the site, the deck is poured onto the NEXT beam flanges; therefore NEXT beams support the weight of wet concrete in addition to self-weight prior to development of composite action. The bending moment calculated at midspan from the weight of wet

concrete is 4992 kip-in (563.86 kN-m). Only the beams erected during phase I NEXT

beams 4 to 6) are included in these calculations.

Table 6.11: Stress Change Induced by Weight of Wet Concrete

NEXT BEAM		NEXT 4	NEXT 5	NEXT 6
Duration	Unit	140 Days	136 Days	136 Days
$\sigma_{DB}=4992/Z_{SB}$	ksi	-0.66	-0.66	-0.65
$\sigma_{DI}=4992/Z_{SM}$	ksi	-0.49	-0.48	-0.49
$\sigma_{DT}=4992/Z_{ST}$	ksi	0.44	0.44	0.44
$\varepsilon_{DB}=\sigma_{DB}/E$	$\mu\varepsilon$	-113.9	-113.9	-112.2
$\varepsilon_{DI}=\sigma_{DI}/E$	$\mu\varepsilon$	-84.6	-82.8	-84.6
$\varepsilon_{DT}=\sigma_{DT}/E$	$\mu\varepsilon$	75.9	75.9	75.9

The stage wise strain variations induced by long term effects, weight of wet concrete, and change in effective span were used to determine the stress and strains presented in Appendix D and Appendix E, respectively.

6.3.2 Longitudinal Strains Determined from Field Data

Strain data were collected periodically over 5 months (between 22 April 2011 and 22 September 2011) to determine the long-term field behavior of NEXT beams in the Brimfield Bridge. Data were collected for all the strain gages cast in the six NEXT beams of the Brimfield Bridge at different locations. The dates of data collection are listed in Appendix B under Table B.1.The tables of Appendix F list all the field data for strain and temperature for the six NEXT beams in the Brimfield Bridge. Strains between different stages are evaluated by using temperature correction equation in all the tables of

107

Appendix G. After temperature correction, the true load related strains were used to get the cumulative strains at different stages and be able to generate strain profiles along NEXT beam depth. The evaluated cumulative strains are listed in the tables of Appendix H.

6.3.2.1 Evaluation of Stage Wise Strain variation due to losses

The stage wise measured strains are presented in Appendix G with the help of Equation 6.6 As an example, Table 6.12 presents the field data collected for NEXT beam 1. Full data are available in the appendix.

$$\mu_{True} = (R1-R0)\ B + (T1-T0)\ (C1-C2) \qquad \text{.....Equation 6.6}$$

Where,

μ_{True} = true load related strain.

R_1 = measured strains at present stage.

R_0 = measured strains at previous stage.

B = 0.975 is calibration factor

T_1 = measured temperature at present stage.

T_0 = measured temperature at previous stage

C_1 = 12.2 micro strain/^{o}C Thermal coefficient of expansion for wire

C_2 = 10.0 micro strain/^{o}C Thermal coefficient of expansion for wire

Table 6.12: Field Data for NEXT Beam 1

Date (Time)		Date: 04/26/2011 (08.10)		Date: 04/26/2011 (08.30)		Date: 04/28/2011 (08.30)		Date: 05/26/2011 (12:15)	
GEOKON 4200		After De Tensioning		Temporary Support (OY)		Temporary Support (OY)		Temporary Support (OY)	
Gage Location	GL	Strain ($\mu\varepsilon$)	T (°C)	Strain ($\mu\varepsilon$)	T (°C)	Strain ($\mu\varepsilon$)	T (°C)	Strain ($\mu\varepsilon$)	T (°C)
Midspan	1-9	2018.9	66.0	1901.7	64.9	1712.3	22.7	1645.6	20.7
Midspan	1-10	1984.1	67.2	1891.0	66.2	1753.4	22.9	1725.0	20.5
Midspan	1-11	2008.1	64.6	1864.0	63.0	1674.8	22.7	1584.2	22.8
Midspan	1-12	2028.1	65.0	1915.9	63.7	1781.0	22.9	1727.1	22.8
Midspan	1-13	2213.8	62.4	2249.7	60.4	2204.7	22.3	2211.4	27.2
Midspan	1-14	2501.1	51.4	2493.6	47.2	2410.7	21.6	2400.7	34.2
Midspan	1-15	2398.5	63.5	2430.2	60.9	2405.1	22.4	2394.7	30.0
Midspan	1-16	2470.4	47.0	2520.8	60.0	2408.9	21.8	2416.6	35.7

Notes: GL: Gage Label; OY: Outside Yard

Based on field data (Table 6.12) individual load related strains between two stages are evaluated with the help of Equation 6.6. In all the stages listed in Table 6.12, no exterior load was applied, but changes in strains were observed. These changes were attributed to long term losses (creep and shrinkage loss) and beam handling during lifting and transportation. Table 6.13 lists the individual load related strains between data taken on four different dates. These values are calculated by using Equation 6.6. The comprehensive calculation of individual load related strains are listed in Appendix G for all six NEXT beams.

Table 6.13: Strain Variation due to Creep and Shrinkage

GEOKON 4200	Duration	30 Minutes	2 Days	1 months
	Instrument Depth from BF	C+S	C+S	C+S
Gage Label	y	Strain($\mu\epsilon$)	Strain($\mu\epsilon$)	Strain($\mu\epsilon$)
1-9	3.75	-117	-278	-69
1-10	8.25	-93	-229	-33
1-13	29.50	31	-128	17
1-11	3.75	-144	-273	-88
1-12	8.00	-112	-221	-53
1-15	29.50	25	-109	7

Notes : C: Creep Loss; S: Shrinkage Loss, BF : Bottom Fiber

6.3.2.2 Cumulative Strains by Construction Stage

The individual strain changes by stage are used to compute the cumulative strain value. The cumulative strains are necessary to determine the total strains at any given stage including time dependent phenomena related to long term losses from creep, shrinkage and relaxation for the NEXT beams. Cumulative strains are obtained by adding the individual strain change at a given stage with the cumulative strain calculated at the previous stage. Table 6.13 lists cumulative strains for NEXT beam 1. In each evaluation cumulative strain of last stage is added to the individual true load related strain of that stage. Cumulative strains for other NEXT beams (beams 1 to 6) are presented in Appendix H.

110

Table 6.14: Stage Wise Cumulative Strain

GEOKON 4200	Duration Instrument Depth from BF	30 Minutes C+S	2 Days C+S	1 Months C+S
Gage Label	y(in)	Strain(με)	Strain(με)	Strain(με)
1-9	3.75	-715-117=-832	-832-278=-1109	-69-1109=-1256
1-10	8.25	-674-93=-767	-229-767=-997	-33-997=-1029
1-13	29.50	-414+31=-383	-128-383=-511	17-511=-494
1-11	3.75	-729-144=-873	-273-873=-1146	-88-1146=-1234
1-12	8.00	-704-112=-816	-221-816=-1037	-53-1037=-1090
1-15	29.50	-437+25=-412	-109-412=-521	7-521=-514

Notes : C: Creep Loss; S: Shrinkage Loss, BF: Bottom Fiber

6.4 Comparison of Measured and Calculated Strains

Strains presented in section 6.3 were obtained in the field from the instrumentation used in the NEXT beams. These strains are compared with strains calculated analytically that include short term and long-term effects of prestressed NEXT beams in this section. The strains obtained at the three different instrumented heights in the stem of the NEXT beams were used to determine the strains at the center of the prestressing force using interpolation. Figure 6.4 shows the location of center of the prestressing force in the NEXT beams of the Brimfield Bridge, where the strain comparison is carried out. Table 6.15 list and compare the strain values obtained from field data and those obtained analytically.

Figure 6.5 (a to f) presents the graphical presentation of strain comparison for all the six NEXT beams. The comparison for NEXT beams 1 to 3 has been done for first five stages

111

whereas for NEXT beams 4 to 6 has been done for all the seven stages due to the

different construction phases. We can see that the strain at stages beyond 30 days and 105

days are closer whereas immediately after transfer of prestrees load the variation is

higher. This large variation can be attributed to lifting and transportation of the NEXT
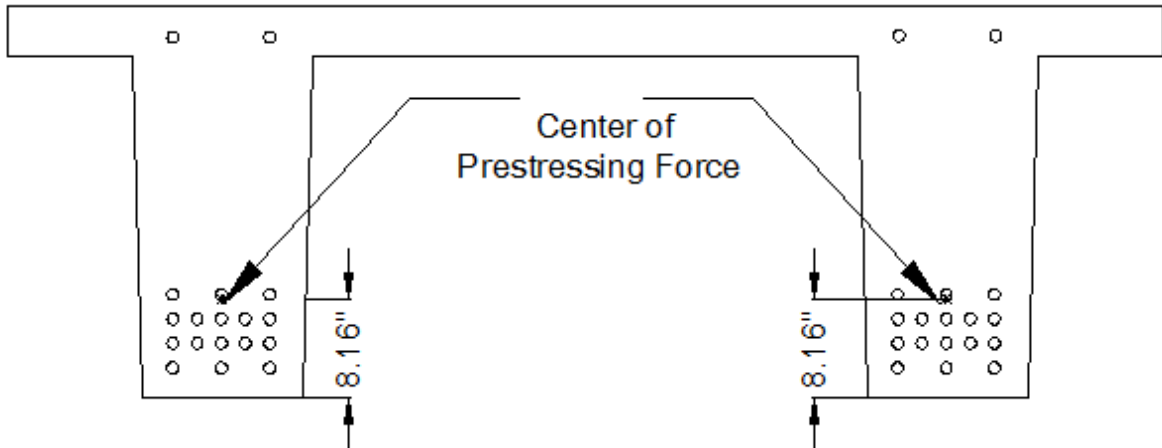
beam.

Figure 6.4 NEXT Beam with Center of Prestressing Force

Table 6.15 Long Term Loss Comparison for All Six NEXT Beams

Days	Strains (με)											
	NEXT 1		NEXT 2		NEXT 3		NEXT 4		NEXT 5		NEXT 6	
	M	A	M	A	M	A	M	A	M	A	M	A
0	456	379	399	381	442	379	496	379	430	381	-414	-383
0.02	102	25	94	25	85	25	99	25	105	25	-136	-25
2	225	-5	185	-9	192	-9	229	-5			-255	33
28									226	-33		
30	43	-30	-13	-3	-12	-3	49	-29				
98									89	-17	-88	17
101	92	-16	40	-24	49	-24	99	-16				
104							-14	4	-12	4	17	-4
107			65	-14	49	-14						
136									-60	-86	109	87
140							-70	-85				

Notes: M: Measured Strain based on Field Data; A: Analytically alculated Strain
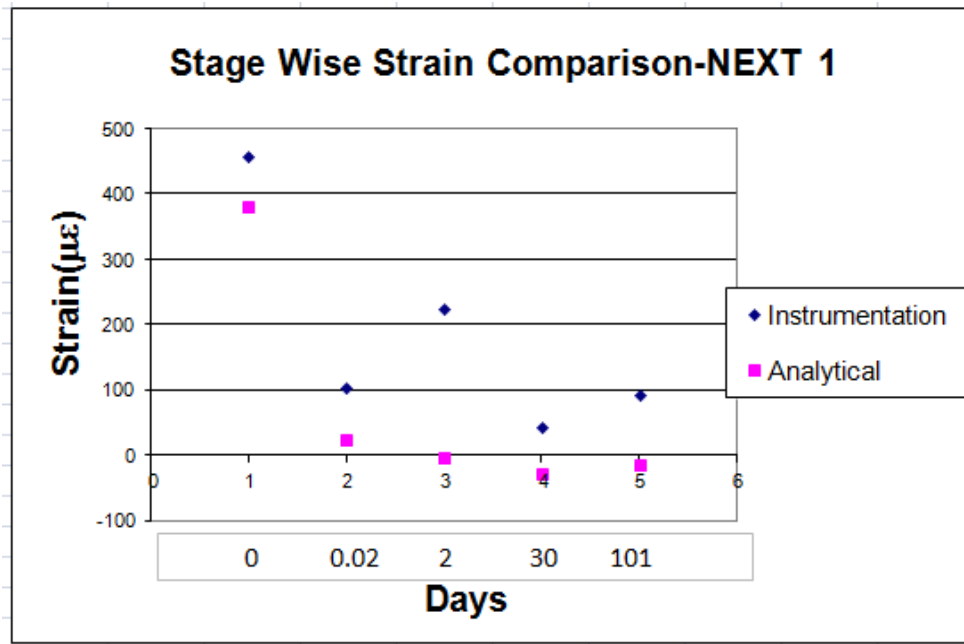
(a) Stage Wise Strain Comparison - NEXT Beam 1
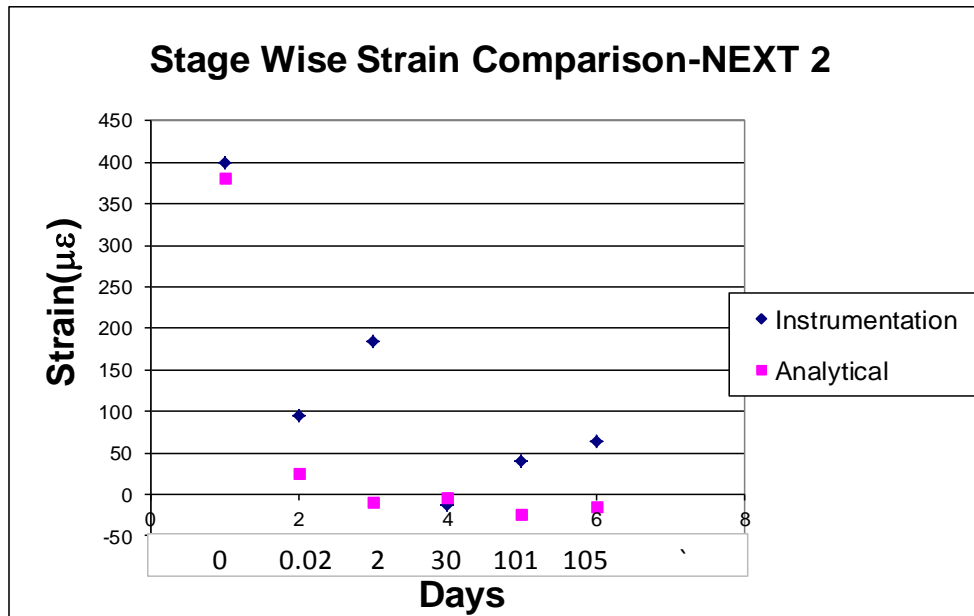
(b) Stage Wise Strain Comparison - NEXT Beam 2
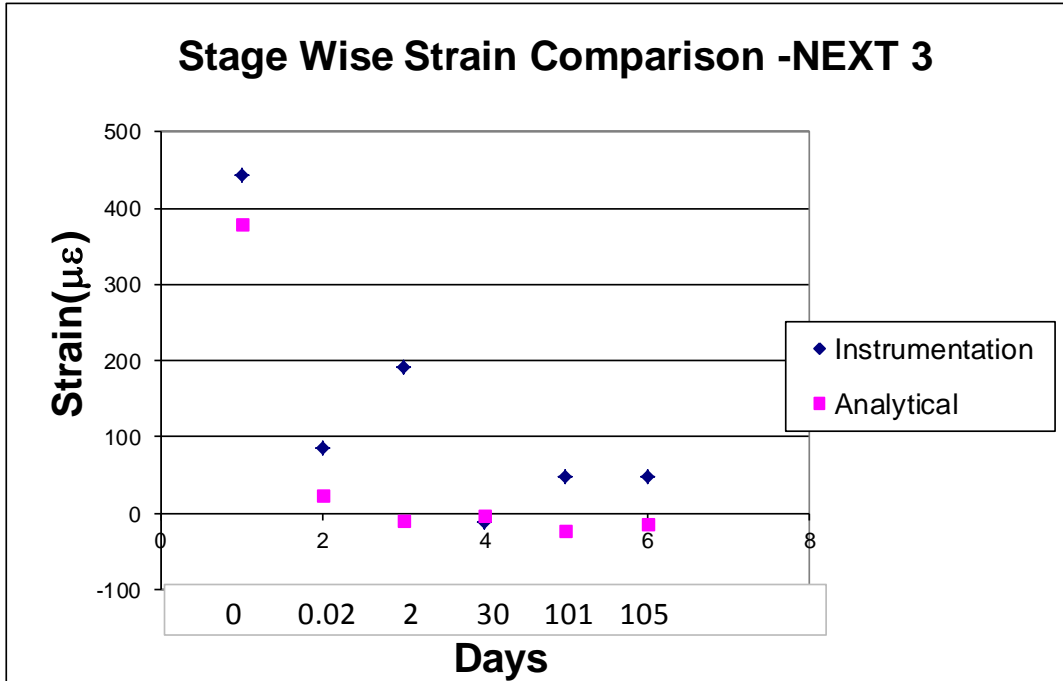
(c) Stage Wise Strain Comparison - NEXT Beam 3
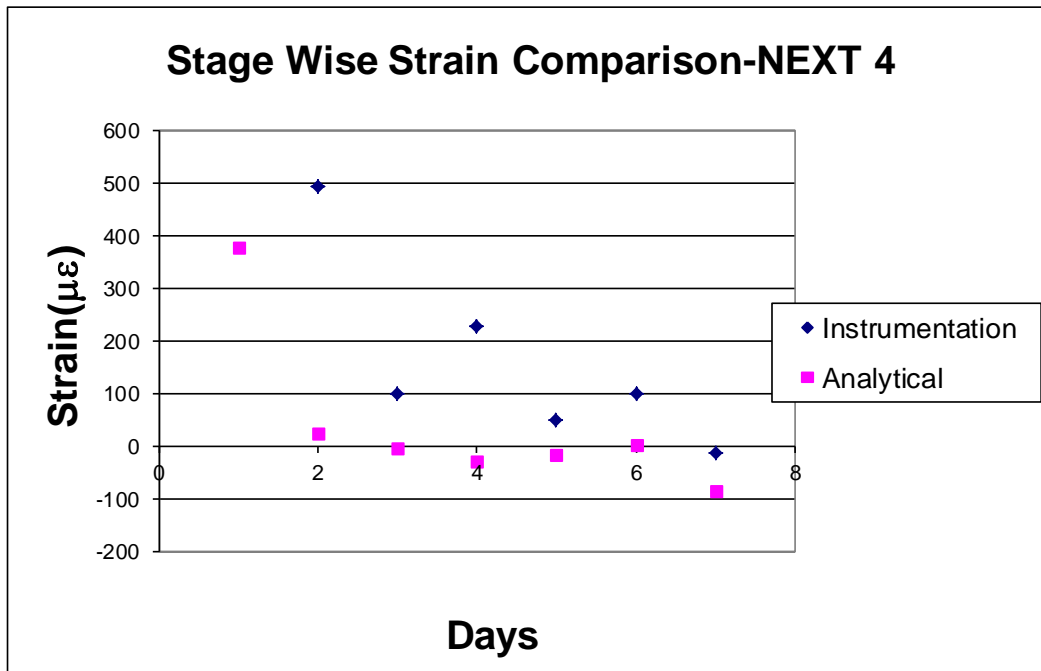
(d) Stage Wise Strain Comparison - NEXT Beam 4
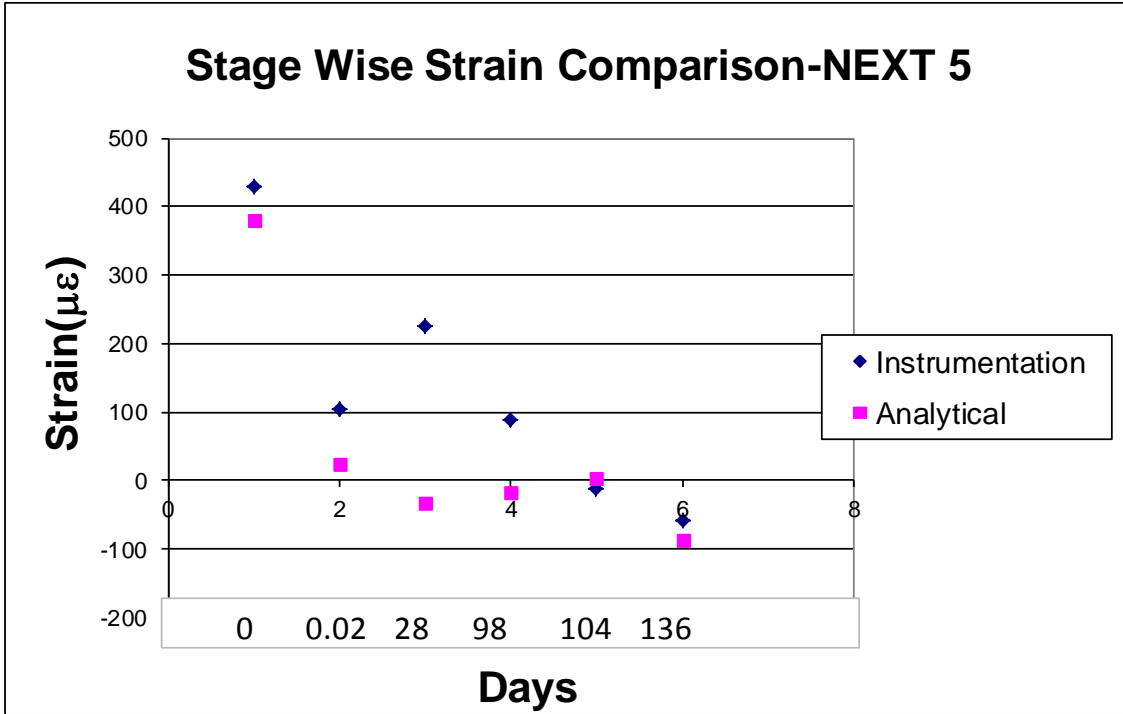
(e) Stage Wise Strain Comparison - NEXT Beam 5
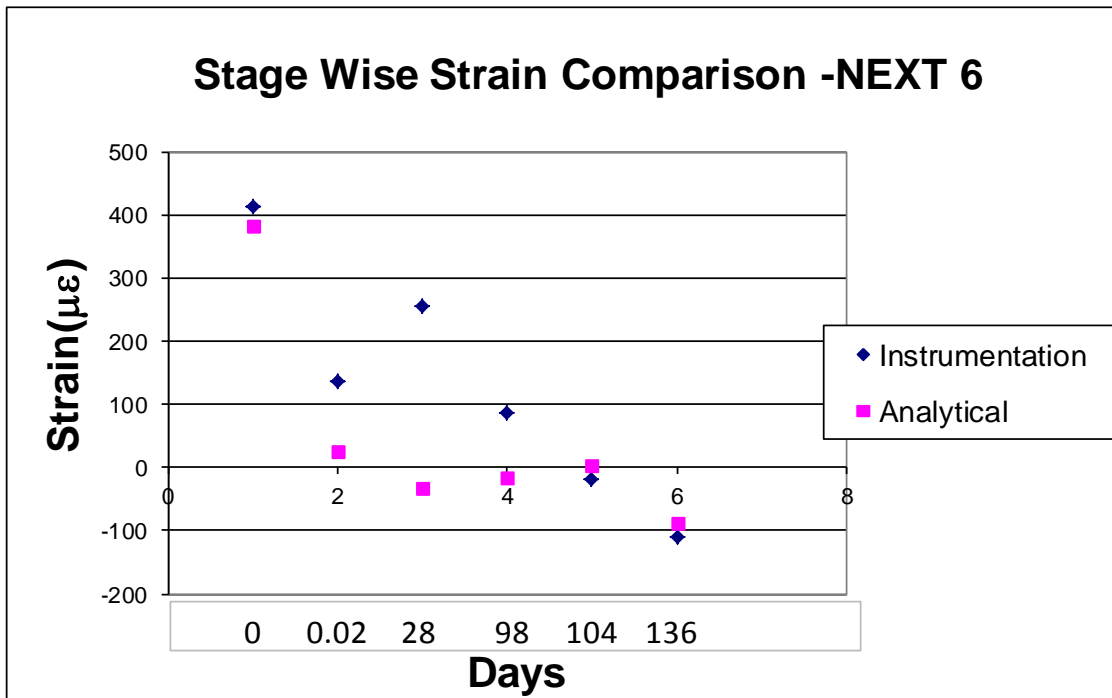
(f) Stage Wise Strain Comparison - NEXT Beam 6

Figure 6.5: (a-f) Stage Wise Strain Comparison – All Six NEXT Beam

6.5 NEXT Beam Strain Profiles at Various Construction Stages

Cumulative strain components are useful to get the variation pattern of strain with beam depth. The three measured strain values in each stem were used to get the strain pattern with NEXT beam depth at different stages. Proximity of measured strain profiles to a linear variation with depth can also be determined using the three strain values measured at each stage to assess data reliability. The following sections discuss the measured strain profiles in detail.

6.5.1 Evaluation of Creep and Shrinkage Strains

Strains vary for each construction stage as discussed above. Some of these changes were caused, in the short term, by elastic shortening, beam handling between stages, and changes in the effective beam span. Other variations are induced by long-term effects such as creep, shrinkage and strand relaxation. For the first measurement taking place 10 minutes after strand detensioning, the measured strains are solely caused by elastic shortening of the NEXT beams due to transfer of the prestressing force. Strain changes after detensioning are induced by beam handling (short term) or creep, shrinkage and relaxation (long term). In the long-term, prestressing force losses cause strain variations to take place with time. The long-term measured strain variation results from the combined effect of creep, shrinkage and relaxation since the instrumentation did not allow separation of these effects. These long-term measured strains are compared with results obtained from long-term loss equations latest AASHTO LRFD Specifications (2010). To facilitate the comparisons, strains are computed the center of prestressing force and compared with interpolated values from the instrumentation.

117

Because of unequal top and bottom creep and shrinkage strains, the strain variation with depth of NEXT beams will likely follow the pattern shown in Figure 6.6. This distribution assumes that creep strains are going to be larger than shrinkage strains that would typically be maximum at the top surface of the NEXT beams. Strand relaxation would tend to have an offsetting effect to the strain distribution shown, but the change in strain caused by strand relaxation will be smaller than the change induced by creep and shrinkage.
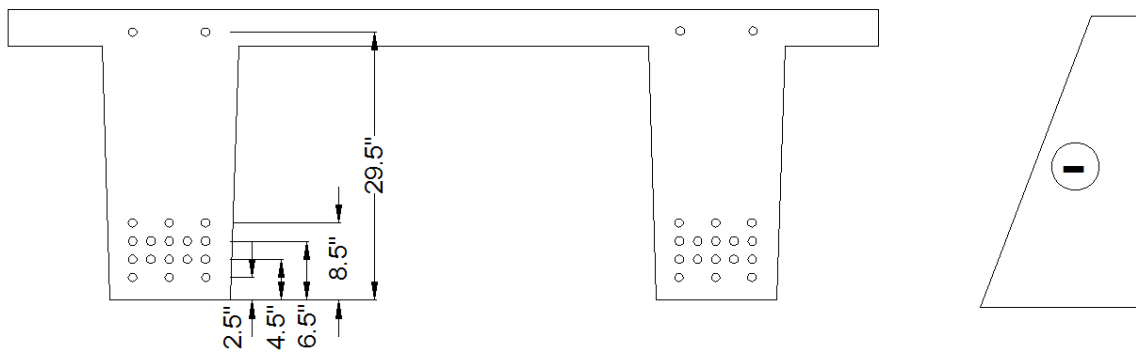
Figure6.6 Trapezoidal Stress Variation due to Creep

Therefore, the time dependent variation of strain and stress due to creep, shrinkage and relaxation loss of the NEXT beams should be trapezoidal. Figure 6.7 (a to f) show the strains measured at the first, third (approximately after 1 month), and fifth stages (approximately after 105 days) for all NEXT beams at midspan. The measured strain profiles are approximately linear, with the highest compressive strain near the bottom of the NEXT beams as would be expected. Furthermore, the changes in strain between the first stage (30 minutes after detensioning) and the second stage are primarily induced by beam handling, but some changes induced by creep, shrinkage and relaxation are also

apparent. The decreased effect of long-term strains with time is evidenced by the small variation observed between 30 days and 100 days.
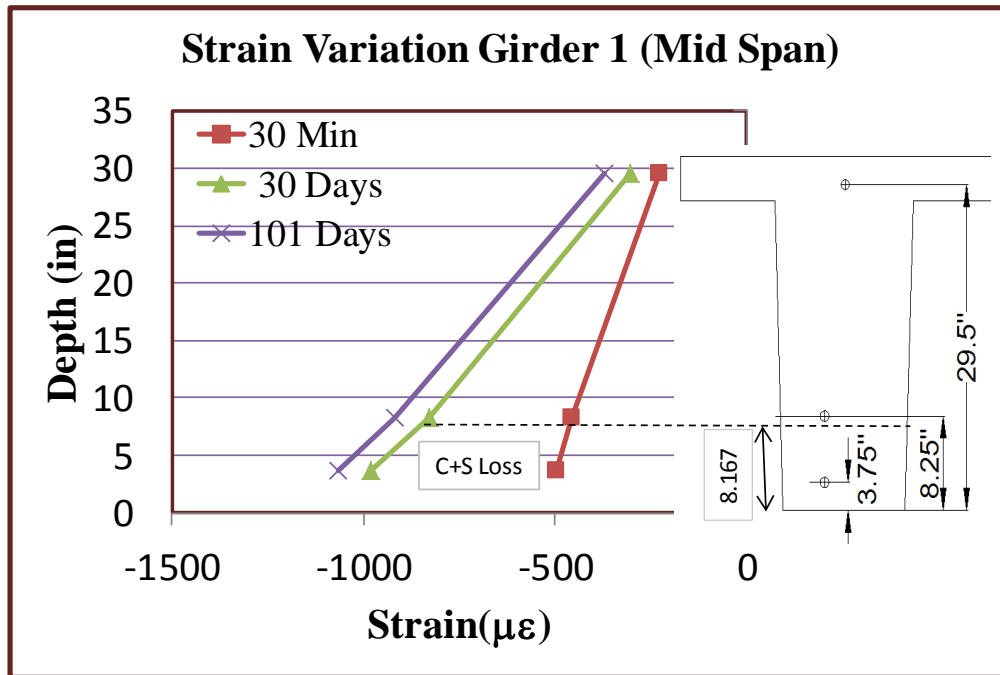
(a) Strain Variation-NEXT Beam 1
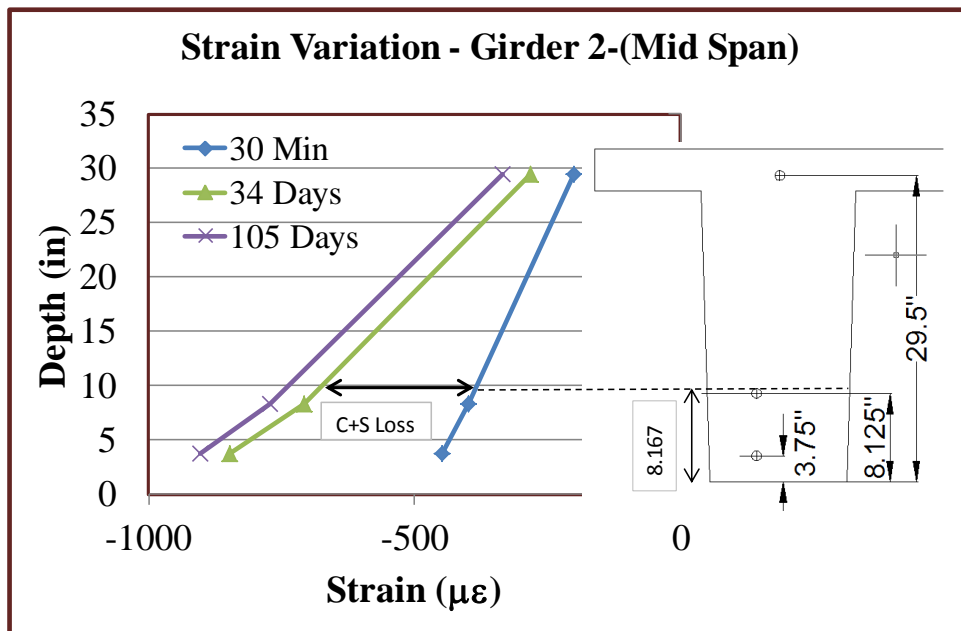
(b) Strain Variation-NEXT Beam 2

119
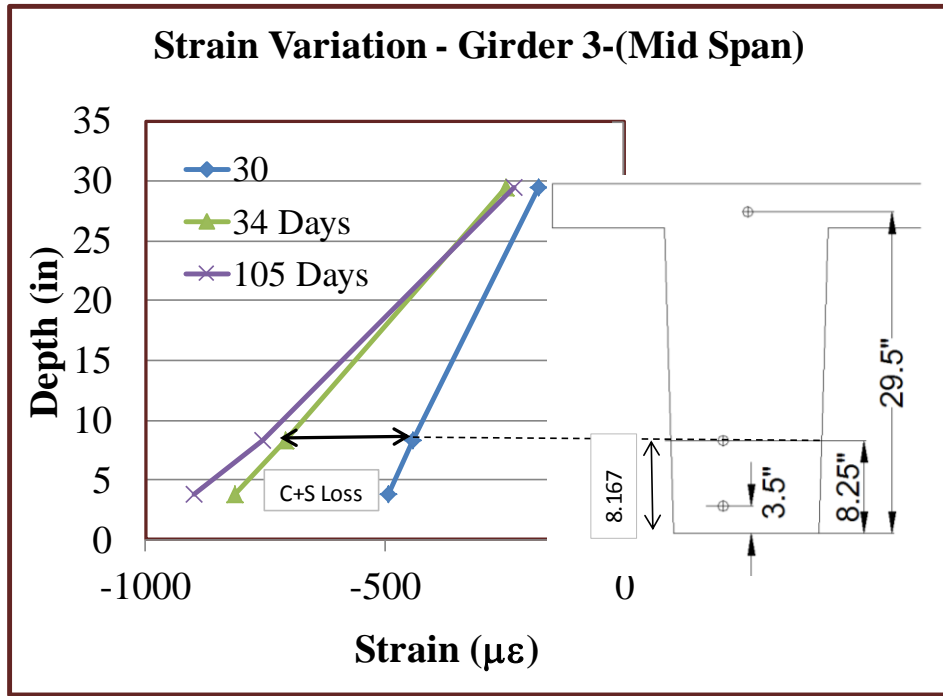
(c) Strain Variation-NEXT Beam 3
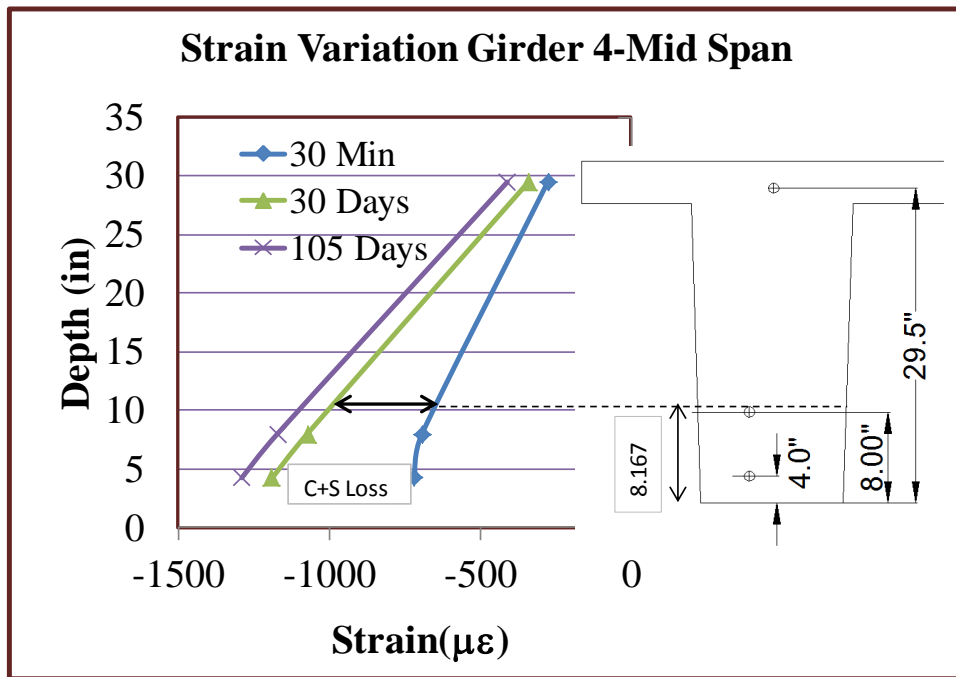
(d) Strain Variation-NEXT Beam 4

120
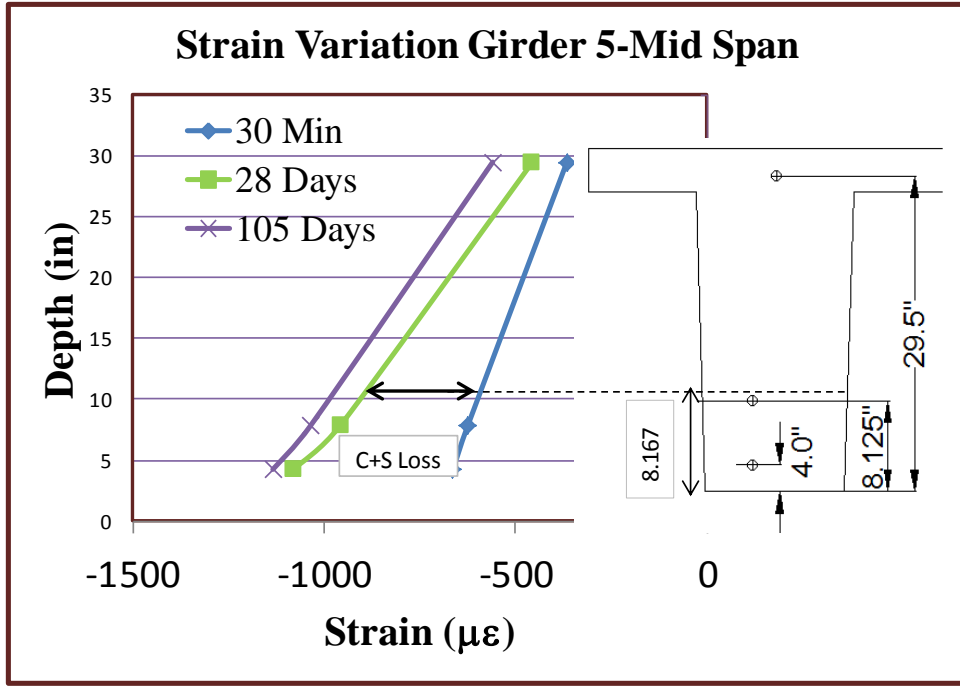
(e) Strain Variation-NEXT Beam 5
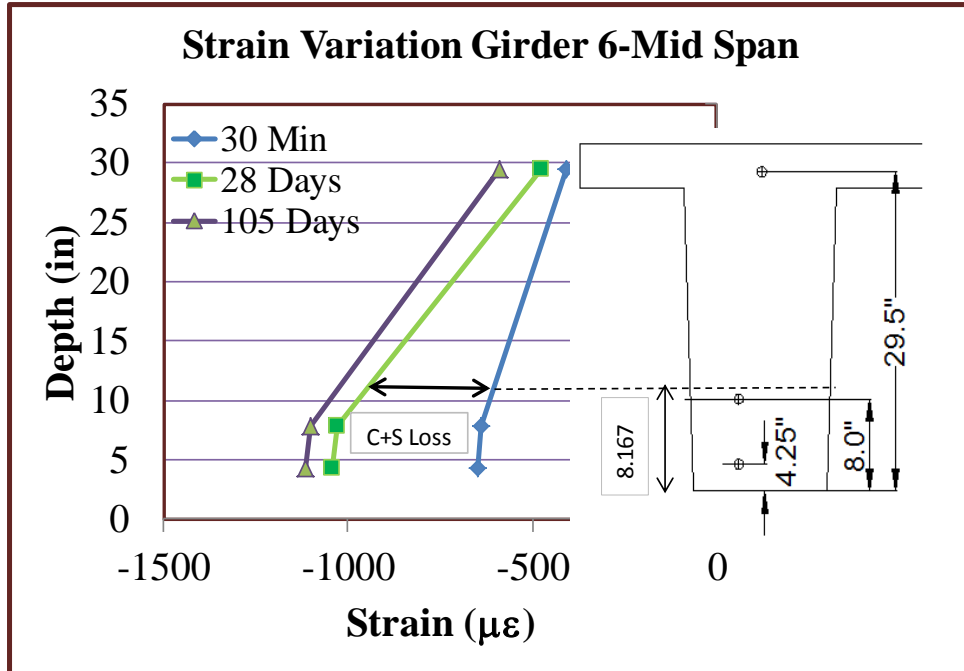
(f) Strain Variation-NEXT Beam 6

Figure 6.7 (a-f): Strain Vs Depth NEXT Beam 1to 6

121

The strain values at the center of the prestressing force located 8.16in (207.44mm) above the bottom flange were calculated based on values measured at the three instrument locations . The black arrows (at the level of center of prestressing force) in Figure 6.7 represent primarily the strain due to creep and shrinkage that occurred approximately after one. However, because the beams were handled during this period, there is also a small strain change induced by repositioning of the supports near the ends of the beams as mentioned before. Similarly the strain change approximately 100 days after casting is shown not to differ much from the values obtained at 30 days. The obtained strain variation due to creep (Appendix C.2.2.1) and shrinkage (Appendix C2.2.2.2) loss is compared to the strain variation obtained from AASHTO LRFD equations. This comparison is listed in Table 6.15. The comparison is done for the approximate duration of 30 and 105 days.

Table 6.16: comparison of Strain Variation due to Time Dependent Loss

BEAM	Days	Time Dependent Loss		% Age Difference	Days	Time Dependent Loss		% Age Difference
		A	M			A	M	
NEXT 1	30	452	373	17	105	573	465	19
NEXT 2	34	470	309	34	105	655	374	43
NEXT 3	34	470	315	33	105	655	265	59
NEXT 4	30	452	378	16	105	659	477	28
NEXT 5	28	438	332	24	105	567	422	26
NEXT 6	28	438	393	10	105	567	481	15

Notes: M: Measured Strain based on Field Data; A: Analytically alculated Strain

Based on comparison we can see that results are relatively near to the NEXT beam 1, 2, 5 and 6. The large difference for the strain in the NEXT beam 3 and 4 could be attributed to

the condition inside and outside the casting yard. Both beams were cast at the same time and went through similar construction conditions.

The differences for the other four NEXT beams are varying in the range of 10 to 15 percent. Based on the results so far we can conclude that time dependent equations to evaluate creep and shrinkage losses in AASHTO LRFD (2010) can be applied to NEXT beams.

6.6 Conclusion

- Based on the field data, strain variation in the NEXT beams due to prestress loss are calculated between different stages. The evaluated strains from filed data were compared with the strain obtained from AASHTO equation. The strains after large duration are found to be closer which asserts the accuracy of AASHTO equation of losses for the NEXT beam. The variation in strains immediately after stressing found to be higher. The high variation in strains can be attributed lifting and transportation of the NEXT beam. The support conditions which were changed for different stages at also causes strain variation obtained from field data and analytical method.

- The strain variation of NEXT beams with depth at different stages is calculated. Based on the variation it was found that the strain profile with the depth is linear. It was also revealed that deformation is higher in concentrated zone of prestressing. The higher deformation in the zone of prestressing forces is the creep deformation under sustained loads (prestressing forces).

123

CHAPTER 7

SUMMARY AND CONCLUSION

The complex shape of NEXT beam in terms of spacing between the girders and calculation of live load distribution factors (LLDFs) has originated this thesis. Also in the past bridge with NEXT beam type girder were not verified with any of the advanced form of analysis.

Based on these reasons following points were considered in this thesis.

-Verification of outcome of PCI technical committee for span and skew parameter, whether single stem approach results in higher LLDFs for NEXT beams or not.

-Verification of trends of AASHTO LLDFs for span and skew parameter with the help of FEM model with different end conditions.

-Four methods are used to evaluate the LLDFs were compared to check which method is yielding the higher value of LLDFs.

All evaluation and verification of LLDFs for different parameters are done with the help of different models which are created in SAP 200014.2 based on the Brimfield Bridge model. UMASS is associated with instrumentation of the Brimfield Bridge model. The readings at the instrumentation at different stages were further used in the verification of prestress loss equation of the NEXT beam. The strain variation along the depth of the NEXT beam also helped in appreciating the behavior of NEXT beam in terms of creep and shrinkage.

124

7.1 Outcome and Suggestions

7.1.1 Verification of outcome of PCI technical committee.

Based on the result it was concluded that single stem (SST) approach gives higher values of LLDF (for both bending moment and shear force) for the interior girder for span and skew parameter and agrees the outcome of PCI technical committee of the particular case. On the contrary the double stem approach is yielding higher value of LLDFs. As LLDFs for exterior girders depends on the configuration of the footpath and kerb, it is difficult to generalize that which method will give higher value of LLDFs. So for interior girder SST approach can be used and for exterior girder the LLDF has to be taken the maximum of the two obtained from SST and DST approach.

The LLDFs (for both bending moment and shear forces) for the interior girders are governed by two or more lanes loaded case whereas for exterior girders case it is governed by one lane loaded case.

7.1.2 Trend Comparison Span Parameter

As per AASHTO equations the LLDFs for bending moment decrease as we increase the span whereas LLDFs for shear force remain constant, Based on verification with FEM model with simply support (FE_{SS}) condition similar trend was observed for the LLDFs for the bending moment. The LLDFs for shear force were not constant for the FEM model (FE_{SS} case) but the variation was in the range of 1 to 5%, which can be treated as constant. The verification of LLDFs with FEM model with integral abutment case (FE_{IAB}) was not in the agreement of AASHTO variation for the bending moment, but the LLDFs are values were lesser for FE_{IAB} case. The LLDF variation was similar to the FE_{SS} case.

7.1.3 Trend comparison Skew Parameter

As per AASHTO equations the LLDFs for bending moment decrease as we increase the skew whereas LLDFs for shear force increases. The trends were in agreement to the FEM model with different end condition. However the value for LLDFs for shear force for the exterior girder for FEM model was found to be higher. The reason behind high value of LLDFs for the exterior girder is the type of member considered (3D frame element).

The 3D frame element resulted in higher value of cantilever zone which further resulted in torsion. This torsion transferred to support in from of one way shear which is opposite to the two way shear caused in the NEXT beam.

7.1.4 Comparison for LLDFs with different end condition

LLDFs for bending moment obtained from SS model are higher than IAB model. This trend is observed for both parameters i.e. span and skew angle of the Bridge. The trend is as per the expectation due to added stiffness of sub structure and foundations. For shear force LLDFs for shear force for varying span (50 ft (15.24 m), 66.67 ft (20.34 m), 80 ft (24.384 m) with 0° skew angle obtained from SS model vary marginally with respect to IAB model. This result is as per the expectation as inclusion of sub structure and foundation to the model does not vary the shear force in the girder at different locations.

LLDFs for shear force for varying skew angle (0°, 30°, 45°) with 66.67 ft span obtained from SS model attain much higher value than IAB model. The reason behind the high value of LLDFs of shear force for high skew angle is discussed in the section 7.1.2.

The LLDFs (for both bending moment and shear forces) for the interior girders are governed by two or more lanes loaded case whereas for exterior girders case it is governed by one lane loaded case.

126

7.1.5 Verification of Prestress Loss Equation of AASHTO

The strain variation caused by the losses are calculated by two different methods and compared to verify the different loss equations mentioned in AASHTO. The strain variations between stages for larger duration were found to be closer and assert the accuracy of loss equations for the NEXT beams. The variation in strain value after the release was attributed to the lifting, transportation of the NEXT beams. The change in span of the support condition was the other reasons resulted in strain variation.

127

APPENDICES

APPENDIX A

CURVE EVALUATION FOR SOIL STRUCTURE INTERACTION

Equation A.1 gives us the nonlinear force displacement curve for the soil at a particular depth Z. For a fixed value of Z we can obtain the relationship between force P (soil resistance at varying depth as function of Y) and displacement Y (lateral displacement of pile due to load application on Bridge). The P-Y curve has been evaluated at each 1 ft distance of the pile. The other curves at different depths are not shown for sake of clarity. Equation A.2 is an empirical factor that fits analytical data to experimental results. It is further dependent on depth of the soil modeled and equivalent diameter of pile which will be obtained by converting the area of pile in to an equivalent circle.

$$F = AP_U \tanh (K_1 ZY/AP_U) L_P \qquad \text{.....Equation A.1}$$

$$A = 3 - 0.8[Z/D] >= 0 \qquad \text{.....Equation A.2}$$

P_U is used in Equation A.1 is estimating ultimate lateral soil resistance which will be taken as minimum of P_{US} and P_{UD} obtained through equation A.3 and A.4 respectively.

$$P_{US} = [C_1 Z + C_2 D]\gamma Z \qquad \text{.....Equation A.3}$$

$$P_{UD} = C_3 \gamma Z \qquad \text{.....Equation A.4}$$

128

C_1, C_2 and C_3 are different soil parameters which are further dependent on the factors defined through equation A.8 to equation A.11. The obtained value of C_1, C_2 and C_3 are 3.02, 3.42 and 54.04 respectively.

$$C_1 = K_0 \tan\phi \sin\beta / \tan(\beta-\phi) \cos\alpha + \tan^2\beta \tan\alpha / \tan(\beta-\phi) \, K_0 \tan\beta (\tan\phi\sin\beta - \tan\alpha) \qquad \text{.....Equation A.5}$$

$$C_2 = \tan\beta / \tan(\beta-\phi) - \tan^2(45-\phi/2) \qquad \text{.....Equation A.6}$$

$$C_3 = K_0 \tan\phi \tan^4(\beta-\phi) + K_a - \tan^8\beta - 1 \qquad \text{.....Equation A.7}$$

Equation 4.8 and equation 4.9 represent active earth pressure coefficient and pressure coefficient at rest. As evident these pressure coefficients are used to evaluate parameter C_1 C_2 and C_3 represented by equation 4.5, equation 4.6 and equation 4.7 respectively.

$$K_a = \tan[\pi/4 - \phi/2]^2 \qquad \text{.....Equation A.8}$$

$$K_0 = [1 - \sin\phi] \qquad \text{.....Equation A.9}$$

α and β are soil parameters which are dependent on ϕ. ϕ is representing angle of repose or soil friction angle. For the IAB modeling sandy soil is considered and the value of ϕ taken in modeling the soil is 35° at all the depths. The values obtained for α and β are 17.5 degree and 62.5 degree respectively. β is representing the plane of maximum shear stress in the soil.

$$\alpha = \phi/2 \qquad \text{....Equation A.10}$$

$$\beta = 45 + \phi/2 \qquad \text{....Equation A.11}$$

APPENDIX B

DATE AND TIME OF RECORDED FIELD DATA

Table B 1: Date of Field Data

NEXT1		NEXT2		NEXT3		NEXT4		NEXT5		NEXT6	
Date	Time	Date	Time	Date	Time	Date	Time	Date	Time	Date	Time
4/26/2011	8:00	4/22/2011	8:00	4/22/2011	8:00	4/26/2011	8:00	4/28/2011	8:00	4/28/2011	8:00
4/26/2011	8:30	4/22/2011	8:30	4/22/2011	8:30	4/26/2011	8:30	4/28/2011	8:30	4/28/2011	8:30
4/28/2011	8:30	4/26/2011	8:30	4/26/2011	8:30	4/28/2011	8:30	5/26/2011	8:30	5/26/2011	8:30
5/26/2011	12:15	4/28/2011	12:15	4/28/2011	12:15	5/26/2011	12:15	8/5/2011	12:15	8/5/2011	12:15
8/5/2011	11:35	5/26/2011	11:35	5/26/2011	11:35	8/5/2011	11:35	8/11/2011	11:35	8/11/2011	11:35
		8/05/2011	11:50	8/5/2011	8:00	8/11/2011	8:00	9/13/2011	10:15	9/13/2011	10:15
						9/13/2011	9:50	9/22/2011	4:15	9/22/2011	4:00
						9/22/2011	4:30				

APPENDIX C

LOSS EVALUAION

In pretentioned Members

$\Delta f_{pT} = \Delta f_{pS} + \Delta f_{pLT}$

Where,

$\Delta f_{pT} =$ Total Loss

$\Delta f_{pS} =$ Short term Loss

$\Delta f_{pLT} =$ Losses due to long terms Shrinkage and creep of concrete, and Relaxation of the steel (ksi)

C.1 Short Term Loss

$\Delta f_{pS} = \Delta f_{pES} + \Delta f_{pR1}$

Where

$\Delta f_{pES} =$ Prestress Loss due to Elastic Shortening (ksi).

C.1.1 Evaluation of Δf_{PES}.

Δf_{PES}	=	$E_P/E_{CI} * f_{cgp}$	=	13.32 ksi
E_P	=	Modulus of Elasticity of Prestress Tendons	=	29000 ksi
E_{CI}	=	Modulus of Elasticity of Concrete at Transfer	=	5297 ksi
fci'	=	Specified concrete strength at the time of transfer.	=	8.63 ksi
f_{cgp}	=	Stress at the CG of strands.	=	2.432 ksi
% Age Loss	= 13.31/202*100		=	6.57 %

C.2 Long Term Loss

$\Delta f_{pLT=} (\Delta f_{pSR} + \Delta f_{pCR} + \Delta f_{pR1})_{id} + (\Delta f_{pSD} + \Delta f_{pCD} + \Delta f_{pR2} - \Delta f_{pSS})_{DF}$

Where

$\Delta f_{pSR} =$ Prestress Loss due to Shrinkage of Girder Concrete between transfer and deck placement (ksi).

$\Delta f_{pCR} =$ Prestress Loss due to Creep of Girder Concrete between transfer and deck placement (ksi).

$\Delta f_{pR1} =$ Prestress Loss due to Relaxation of Prestressing Strand between transfer and deck placement (ksi).

$\Delta f_{pSD} =$ Prestress Loss due to Shrinkage of Girder Concrete between time of deck placement and final time (ksi). (Future Scope)

131

Δf_{pCD} = Prestress Loss due to Creep of Girder Concrete between time of deck placement and final time (ksi). (Future Scope)

Δf_{pR2} = Prestress Loss due to relaxation of strands in composite section between time of deck placement and final time (ksi). (Future Scope)

Δf_{pSS} = Prestress Gain due to Shrinkage of deck in Composite Section (ksi). (Future Scope)

C.2.1 Evaluation of Δf_{pSR}

Δf_{PSR}	Stress loss in Strands due to shrinkage for the mentioned case=ε_{bid}*E_P*K_{ID}	=	3.72	ksi
ε_{SR}	Strain loss in the strands due to mentioned Shrinkage=ε_{bid}*K_{ID}	=	128.21	μ
K_{ID}	=1/[1+(E_P/E_{CI})*(A_{PS}/A_G)*(1+A_G*e^2_{PG}/I_G){1+0.7$\varphi_b(t_f,t_i)$}] Transformed Section Coefficient that account for time-dependent interaction between concrete and bonded steel in the section being considered for time between transfer and deck placement.	=	0.89	
ε_{bid}	Shrinkage Strain between transfer and Deck Placement=K_s*K_{hs}*K_f*K_{td}*0.48*10^{-3}	=	0.00014	
$\varphi_b(t_f,t_i)$	Creep Coefficient between transfer and deck placement =1.9*K_s*K_{hc}*K_f*K_{td}*$t_i^{-0.118}$	=	0.79	
K_s	Effect for the volume to Surface Ration =1.45-0.13(V/S)>=1.0	=	1.00	
K_{hs}	Humidity Factor for the Shrinakge =2.00-0.014H	=	1.09	
K_{hc}	humidity Factor for the Creep=1.56-0.008H	=	1.04	
K_f	Factor for the effect of Concrete Strength =5/(1+f_{ci}')	=	0.52	
K_{td}	Time Development Factor=t/(61-4f_{ci}'+t)	=	0.53	
V	Volume/Length of Double T Section	=	1182	in^2
S	Surface Area/Length of Double T Section	=	311	in
H	Average Annual Ambient mean Relative Humidity.	=	65	
t_i	Final age (Days)	=	30.16	days
t_f	Age at Transfer (Days)	=	0.042	days

132

Matereial Properties

f_{ci}'	specified concrete strength at the time of transfer.	=	8.64	ksi
E_P	Modulus of Elasticity of Prestress Tendons	=	29000	ksi
E_{CI}	Modulus of Elasticity of Concrete at Transfer	=	5297	ksi

Section Property

A_{PS}	Area of Prestressing Steel	=	7.81	in^2
A_G	Gross Area of Section	=	1182	in^2
I_G	Moment ofInertia of Gross concrete Section about Centroidal Axis	=	116100	in^4

Eccentricities

e_{PG}	eccentricity of Strand with respect to centroid of Girder	=	11.18	in

C.2.2 Evaluation of Δf_{pSD}

Δf_{PCR}	Stress loss in strand due to creep between transfer and deck placement=$f_{cgp}*E_P/E_{ci}*K_{id*}\varphi_b(t_d,t_i)$	=	9.38	ksi
ε_{CR}	Strain Loss in Strands due to creep loss=$f_{cgp}/E_{ci}*K_{id*}\varphi_b(t_d,t_i)$	=	323.47	μ
K_{id}	=$1/[1+(E_P/E_{CI})*(A_{PS}/A_G)*(1+A_G*e^2_{PG}/I_G)\{1+0.7\varphi_b(t_f,t_i)\}]$	=	0.89	
	Transformed Section Coefficient that account for time-dependent interaction between Concrete and bonded steel in the section being considered for time between transfer and deck placement.			
$\varphi_b(t_d,t_i)$	Girder Creep coefficient between transfer and deck placement =$1.9*K_s*K_{hc}*K_f*K_{td}*t_i^{-0.118}$	=	0.79	
K_s	Effect for the volume to Surface Ration =$1.45-0.13(V/S)>=1.0$	=	1	

133

K_{hc}	humidity Factor for the Creep=1.56-0.008H	=	1.04	
K_f	Factor for the effect of Concrete Strength $=5/(1+f_{ci}')$	=	0.52	
K_{td}	Time Development Factor$=t/(61-4f_{ci}'+t)$	=	0.53	
V	Volume/Length of Double T Section	=	1182	in^2
S	Surface Area/Length of Double T Section	=	311	in
H	Average Annual Ambient mean Relative Humidity.	=	65	%
t_i	Age at Transfer (Days)	=	0.042	days
t_d	Age at Deck Placement (Days)	=	30.16	days
f_{cgp}	Stress at the CG of strands.	=	2.43	ksi

Material Properties

E_P	Modulus of Elasticity of Prestress Tendons	=	29000	ksi
E_{CI}	Modulus of Elasticity of Concrete at Transfer	=	5297.01	ksi
f_{ci}'	specified concrete strength at the time of transfer.	=	8.64	ksi

Section Properties

A_{PS}	Area of Prestressing Steel	=	7.81	in^2
A_G	Gross Area of Composite Section	=	1182	in^2
I_G	Moment of Inertia of Gross concrete Section of Girder about Centriodal Axis	=	116100	in^4

Eccentricity

| e_{PG} | Eccentricity of Strand with respect to centroid of | = | 11.18 | in |

134

C.2.3 Evaluation of Δf_{pR2}

Δf_{pR1} = Stress Loss Due to relaxation of Strands = $f_{pt}/K_L*(f_{pt}/f_{py}-0.55)$ =   1.89   ksi

ϵf_{pR2} = Loss of Strain due to relaxation of Strand   =   65.31   mm

f_{pt} Stress in prestressing strands immediately after transfer, taken not less than $0.55 f_{py}$.   =   202   ksi

K_L a constant 30 for low relaxation strand   =   30

f_{py} $0.9*fpu$ =   243   ksi

f_{pu} Tensile Strength of Low Relaxation Strand   =   270   ksi

Δf_{pr2} in % Age   =   0.94   %

Table C 1 *(a-f): Details of Time Dependent Loss for NEXT Beams*

(a): Details of Time Dependent Loss for NEXT Beam 1

NEXT Beam 1				Cumulative Strain		Cumulative Stress		Stage-wise Strain		Stage Wise Stress		
				CS	SS	CL	SL	CS	SS	CL	SL	(C+S)%
Stage	Date	Time	Days	με	με	ksi	ksi	με	με	ksi	ksi	Age Loss
After Detentioning	4-26	8:00	0.00	0.00	0.00	0.00	0.00	0.00	0.00	0.00	0.00	0.000
On temporary support	4-26	8:30	0.02	0.48	0.19	0.01	0.01	0.48	0.19	0.01	0.01	0.01
Outside plant	4-28	8:30	2.02	44.64	17.69	1.30	0.51	44.16	17.50	1.29	0.50	0.89
Outside plant	5-26	12:15	30.16	323.47	128.20	9.38	3.72	278.83	110.51	8.08	3.21	6.47
Outside plant	8-05	11:35	101.15	471.98	187.07	13.69	5.43	148.51	58.87	4.31	1.71	9.44

NOTES: CS=Creep Strain; SS=Shrinkage Strain; CL=Creep Loss;SL=Shrinkage Loss; C=Creep;S=Shrinkage

135

(b): Details of Time Dependent Loss for NEXT Beam 2

NEXT Beam 2				Cumulative Strain		Cumulative Stress		Stage-wise Strain		Stage Wise Stress		
				CS	SS	CL	SL	CS	SS	CL	SL	(C+S)%
Stage	Date	Time	Days	με	με	ksi	ksi	με	με	ksi	ksi	Age Loss
After Detentioning	4-22	8:00	0.00	0.00	0.00	0.00	0.00	0.00	0.00	0.00	0.00	0.00
On temporary support	4-22	8:30	0.02	0.48	0.19	0.01	0.01	0.48	0.19	0.01	0.01	0.01
Outside plant	4-26	10:00	4.08	83.67	31.67	2.48	0.92	83.19	31.48	2.47	0.91	1.68
Outside plant	4-28	7:15	5.97	114.84	43.42	3.33	1.26	31.17	11.75	0.85	0.34	2.27
Outside plant	5-26	12:15	34.16	341.39	129.10	9.90	3.74	226.55	85.68	6.57	2.48	6.74
Outside plant	8-05	11:50	105.15	475.51	179.82	13.79	5.21	134.12	50.72	3.89	1.47	9.39

NOTES: CS=Creep Strain; SS=Shrinkage Strain; CL=Creep Loss;SL=Shrinkage Loss; C=Creep;S=Shrinkage

136

(c): Details of Time Dependent Loss for NEXT Beam 3

NEXT Beam 3				Cumulative Strain		Cumulative Stress		Stage-wise Strain		Stage Wise Stress		
				CS	SS	CL	SL	CS	SS	CL	SL	
Stage	Date	Time	Days	με	με	ksi	ksi	με	με	ksi	ksi	(C+S)%AgeLoss
After detentioning	4-22	8:00	0.00	0.00	0.00	0.00	0.00	0.00	0.00	0.00	0.00	0.00
On temporary support	4-22	8:30	0.02	0.48	0.19	0.01	0.01	0.48	0.19	0.01	0.01	0.01
Outside plant	4-26	10:00	4.08	83.67	31.67	2.48	0.92	83.19	31.48	2.47	0.91	1.68
Outside plant	4-28	7:15	5.97	114.84	43.42	3.33	1.26	31.17	11.75	0.85	0.34	2.27
Outside plant	5-26	11:30	34.16	341.39	129.10	9.90	3.74	226.55	85.68	6.57	2.48	6.74
Outside plant	8-05	11:50	105.15	475.51	179.82	13.79	5.21	134.12	50.72	3.89	1.47	9.39

NOTES: CS=Creep Strain; SS=Shrinkage Strain; CL=Creep Loss;SL=Shrinkage Loss; C=Creep;S=Shrinkage

(d): Details of Time Dependent Loss for NEXT Beam 4

NEXT Beam 4				Cumulative Strain		Cumulative Stress		Stage-wise Strain		Stage Wise Stress		
				CS	SS	CL	SL	CS	SS	CL	SL	
Stage	Date	Time	Days	με	με	ksi	ksi	με	με	ksi	ksi	(C+S)%AgeLoss
After Detentioning	4-26	8:00	0.00	0.00	0.00	0.00	0.00	0.00	0.00	0.00	0.00	0.00
On temporary support	4-26	8:30	0.02	0.48	0.19	0.01	0.01	0.48	0.19	0.01	0.01	0.01
Outside plant	4-28	8:30	2.02	44.64	17.69	1.30	0.51	44.16	17.50	1.29	0.50	0.89
Outside plant	5-26	10:45	30.11	323.47	128.20	9.38	3.72	278.83	110.51	8.08	3.21	6.47
Outside plant	8-05	12:03	101.17	471.98	187.07	13.69	5.43	148.51	58.87	4.31	1.71	9.44
On Abutment	8-11	8:00	107.00	477.07	189.09	13.84	5.48	5.09	2.02	0.15	0.05	9.54
Fresh Concrete Pour	9-13	9:50	140.08	498.99	197.79	14.47	5.74	21.92	8.70	0.63	0.26	9.98

NOTES: CS=Creep Strain; SS=Shrinkage Strain; CL=Creep Loss;SL=Shrinkage Loss; C=Creep;S=Shrinkage

(e): Details of Time Dependent Loss for NEXT Beam 5

NEXT Beam 5				Cumulative Strain		Cumulative Stress		Stage-wise Strain		Stage Wise Stress		
				CS	SS	CL	SL	CS	SS	CL	SL	
Stage	Date	Time	Days	με	με	ksi	ksi	με	με	ksi	ksi	(C+S)%AgeLoss
After Detentioning	4-28	8:00	0.00	0.00	0.00	0.00	0.00	0.00	0.00	0.00	0.00	0.00
On temporary support	4-28	8:30	0.02	0.01	0.19	0.01	0.01	0.01	0.19	0.01	0.01	0.01
Outside plant	5-26	11:05	28.13	313.33	124.19	9.09	3.60	313.32	124.00	9.08	3.59	6.26
Outside plant	8-5	12:07	98.17	469.20	185.10	13.61	5.39	155.87	60.91	4.52	1.79	9.38
On Abutment	8-11	11:13	104.00	474.52	188.08	13.76	5.45	5.32	2.98	0.15	0.06	9.49
Fresh Concrete Pour	9-13	9:50	136.94	497.34	197.12	14.42	5.72	22.82	9.04	0.66	0.27	9.95

NOTES: CS=Creep Strain; SS=Shrinkage Strain; CL=Creep Loss;SL=Shrinkage Loss; C=Creep;S=Shrinkage

(f): Details of Time Dependent Loss for NEXT Beam 6

NEXT Beam 6				Cumulative Strain		Cumulative Stress		Stage-wise Strain		Stage Wise Stress		
				CS	SS	CL	SL	CS	SS	CL	SL	
Stage	Date	Time	Days	με	με	ksi	ksi	με	με	ksi	ksi	(C+S)%AgeLoss
After Detentioning	4-28	8:00	0.00	0.00	0.00	0.00	0.00	0.00	0.00	0.00	0.00	0.00
On temporary support	4-28	8:30	0.02	0.01	0.19	0.01	0.01	0.01	0.19	0.01	0.01	0.01
Outside plant	5-26	12:10	28.13	313.33	124.19	9.09	3.60	313.32	124.00	9.08	3.59	6.26
Outside plant	8-5	12:07	98.17	469.20	185.10	13.61	5.39	155.87	60.91	4.52	1.79	9.38
On Abutment	8-11	11:20	104.00	474.52	188.08	13.76	5.45	5.32	2.98	0.15	0.06	9.49
Fresh Concrete Pour	9-13	9:50	136.38	497.03	197.00	14.41	5.71	22.51	8.92	0.65	0.26	9.94

NOTES: CS=Creep Strain; SS=Shrinkage Strain; CL=Creep Loss;SL=Shrinkage Loss; C=Creep;S=Shrinkage

APPENDIX D

STAGE WISE STRESS EVALUATION

Table D 1*(a-f): Stage Wise Load Related Stress (By Analytical Method)*

(a): Stress After Prestressing

NEXT BEAM		NEXT 1	NEXT 2	NEXT 3	NEXT 4	NEXT 5	NEXT 6
Duration	Unit	At Release	At Release	At Release	At Release	At Release	At Release
σ_{BI}	ksi	3.74	3.74	3.78	3.70	3.70	3.66
σ_{MI}	ksi	3.05	3.07	3.05	3.09	3.07	3.09
σ_{TI}	ksi	-0.19	-0.19	-0.19	-0.19	-0.19	-0.19

(b): Stress after Short Term Losses

NEXT BEAM		NEXT 1	NEXT 2	NEXT 3	NEXT 4	NEXT 5	NEXT 6
Date Time	Unit	10 Minutes	10 Minutes	10 Minutes	10 Minutes	10 Minutes	10 Minutes
σ_{BI}	ksi	2.37	2.37	2.39	2.35	2.35	2.34
σ_{MI}	ksi	2.05	2.06	2.05	2.07	2.06	2.07
σ_{TI}	ksi	0.53	0.53	0.53	0.53	0.53	0.53

c): Stress after placing on Temporary Support (Inside Casting Yard)

NEXT BEAM	Unit	NEXT 1	NEXT 2	NEXT 3	NEXT 4	NEXT 5	NEXT 6
Duration		30 Minutes	30 Minutes	30 Minutes	30 Minutes	30 Minutes	30 Minutes
σ_{BI}	ksi	0.19	0.19	0.19	0.18	0.18	0.18
σ_{MI}	ksi	0.13	0.13	0.13	0.14	0.13	0.14
σ_{TI}	ksi	-0.12	-0.12	-0.12	-0.12	-0.12	-0.12

(d): Stress after placing on Temporary Support (Outside Casting Yard)

NEXT BEAM		NEXT 1	NEXT 2	NEXT 3	NEXT 4	NEXT 5	NEXT 6
Duration	Unit	30 Days	4 Days	4 Days	2 Days	28 Days	28 Days
σ_{BI}	ksi	-0.033	-0.06	-0.06	-0.0326	-0.23	-0.23
σ_{MI}	ksi	-0.027	-0.05	-0.05	-0.0272	-0.19	-0.19
σ_{TI}	ksi	0.002	0.003	0.003	0.0017	0.01	0.01

(e): Stress after placing on Temporary Support and Abutment (On Site)

NEXT BEAM	Unit	NEXT 1	NEXT 2	NEXT 3	NEXT 4	NEXT 5	NEXT 6
Date Time		101 Days	6 Days	6 Days	30 Days	98 Days	98 Days
σ_{BI}	ksi	-0.209	-0.02	-0.02	-0.206	-0.12	-0.11
σ_{MI}	ksi	-0.170	-0.02	-0.02	-0.172	-0.10	-0.10
σ_{TI}	ksi	0.011	0.00	0.00	0.011	0.01	0.01

(f): Stress after placing on Temporary Support (On Site)

NEXT BEAM	Unit	NEXT 1	NEXT 2	NEXT 3	NEXT 4	NEXT 5	NEXT 6
Duration		107 Days	34 Days	6 Days	101 Days	104 Days	104 Days
σ_{BI}	ksi	-0.111	-0.17	-0.17	-0.11	0.03	0.03
σ_{MI}	ksi	-0.091	-0.14	-0.14	-0.09	0.02	0.02
σ_{TI}	ksi	0.006	0.01	0.01	0.01	-0.02	-0.02

143

(g): Stress after placing on Temporary Support

NEXT BEAM		NEXT 2	NEXT 3	NEXT 4	NEXT 5	NEXT 6
Duration	Unit	105 Days	105 Days	107 Days	137 Days	136 Days
σ_{BI}	ksi	-0.10	-0.10	0.03	-0.68	-0.67
σ_{MI}	ksi	-0.08	-0.08	0.02	-0.50	-0.50
σ_{TI}	ksi	0.01	0.01	0.02	0.44	0.44

(h): Stress after placing on Temporary Support

NEXT BEAM		NEXT 4
Duration	Unit	140 Days
σ_{BI}	ksi	-0.68
σ_{MI}	ksi	-0.50
σ_{TI}	ksi	0.44

144

APPENDIX E

STAGE WISE STRAIN EVALUATION

Table E 1*(a-f): Stage Wise Cumulative Strain (By Analytical Method)*

(a): Strain after Prestressing

NEXT BEAM Duration	Unit	NEXT 1 At Release	NEXT 2 At Release	NEXT 3 At Release	NEXT 4 At Release	NEXT 5 At Release	NEXT 6 At Release
ε_{BI}	$\mu\varepsilon$	690.16	690.16	697.20	683.11	683.11	676.07
ε_{MI}	$\mu\varepsilon$	563.41	566.93	563.41	570.45	566.93	570.45
ε_{TI}	$\mu\varepsilon$	-35.11	-35.11	-35.11	-35.11	-35.11	-35.11

(b): Strain At Stage 1

NEXT BEAM		NEXT 1 10 Minutes	NEXT 2 10 Minutes	NEXT 3 10 Minutes	NEXT 4 10 Minutes	NEXT 5 10 Minutes	NEXT 6 10 Minutes
Duration	Unit						
ε_{BI}	$\mu\varepsilon$	437.69	437.69	440.99	434.39	434.39	431.09
ε_{MI}	$\mu\varepsilon$	378.29	379.94	378.29	381.59	379.94	381.59
ε_{TI}	$\mu\varepsilon$	97.79	97.79	97.79	97.79	97.79	97.79

145

(c): Strain after placing on Temporary Support (Inside Casting Yard)

NEXT BEAM		NEXT 1	NEXT 2	NEXT 3	NEXT 4	NEXT 5	NEXT 6
Date Time	Unit	30 Minutes	30 Minutes	30 Minutes	30 Minutes	30 Minutes	30 Minutes
ε_{BI}	$\mu\varepsilon$	34.35	34.34	34.89	33.80	33.77	33.22
ε_{MI}	$\mu\varepsilon$	24.43	24.70	24.43	24.98	24.69	24.96
ε_{TI}	$\mu\varepsilon$	-22.39	-22.38	-22.38	-22.39	-22.38	-22.38

(d): Strain after placing on Temporary Support (Outside Casting Yard)

NEXT BEAM		NEXT 1	NEXT 2	NEXT 3	NEXT 4	NEXT 5	NEXT 6
Duration	Unit	30 Days	4 Days	4 Days	2 Days	28 Days	28 Days
ε_{BI}	$\mu\varepsilon$	-4.63	-8.85	-8.79	-4.69	-33.11	-33.32
ε_{MI}	$\mu\varepsilon$	0.29	0.55	0.55	0.29	2.05	2.05
ε_{TI}	$\mu\varepsilon$	-5.68	-10.77	-10.88	-5.62	-39.90	-39.49

(e): Strain after placing on Temporary Support and Abutment (On Site)

NEXT BEAM	Unit	NEXT 1	NEXT 2	NEXT 3	NEXT 4	NEXT 5	NEXT 6
Date Time		101 Days	6 Days	6 Days	30 Days	98 Days	98 Days
ε_{BI}	$\mu\varepsilon$	-36.00	-3.79	-3.83	-35.63	-19.92	-19.72
ε_{MI}	$\mu\varepsilon$	-29.39	-3.11	-3.09	-29.76	-16.54	-16.64
ε_{TI}	$\mu\varepsilon$	1.83	0.19	0.19	1.83	1.02	1.02

(f): Strain after placing on Temporary Support (On Site)

NEXT BEAM	Unit	NEXT 1	NEXT 2	NEXT 3	NEXT 4	NEXT 5	NEXT 6
Duration		107 Days	34 Days	6 Days	101 Days	104 Days	104 Days
ε_{BI}	$\mu\varepsilon$	-19.16	-28.85	-29.14	-18.97	5.69	5.59
ε_{MI}	$\mu\varepsilon$	-15.64	-23.70	-23.55	-15.84	4.09	4.14
ε_{TI}	$\mu\varepsilon$	0.97	1.47	1.47	0.97	-4.19	-4.19

147

(g): Strain after placing on Temporary Support

NEXT BEAM		NEXT 2	NEXT 3	NEXT 4	NEXT 5	NEXT 6
Time	Unit	105 Days	105 Days	107 Days	137 Days	136 Days
ε_{BI}	$\mu\varepsilon$	-17.08	-17.25	5.76	-116.77	-114.88
ε_{MI}	$\mu\varepsilon$	-14.03	-13.94	4.20	-85.67	-86.61
ε_{TI}	$\mu\varepsilon$	0.87	0.87	4.27	75.46	75.46

(h): Strain after placing on Temporary Support

NEXT BEAM		NEXT 4
Time	Unit	140 Days
ε_{BI}	$\mu\varepsilon$	-116.70
ε_{MI}	$\mu\varepsilon$	-86.56
ε_{TI}	$\mu\varepsilon$	75.46

148

APPENDIX F

STRAIN AND DATA IN FIELD

Table F 1 (a-f): Field Data for NEXT Beams

(a): Field Data for NEXT Beam 1

Date (Time)		Date: 04/26/2011 (07.00)		Date: 04/26/2011 (08.10)	
GEOKON 4200		20 Hrs After Concrete Pour		10 Minutes After Detensioning	
Gage Location	Gage Label	Strain($\mu\epsilon$)	Temperature(°C)	Strain($\mu\epsilon$)	Temperature(°C)
Midspan	1-9	2529.3	67.6	2018.9	66.0
Midspan	1-10	2447.2	68.1	1984.1	67.2
Midspan	1-11	2505.4	69.1	2008.1	64.6
Midspan	1-12	2489.3	69.5	2028.1	65.0
Midspan	1-13	2436.9	64.5	2213.8	62.4
Midspan	1-14	2520.2	58.5	2501.1	51.4
Midspan	1-15	2627.5	67.6	2398.5	63.5
Midspan	1-16	2520.8	60.0	2482.7	52.5

149

Date (Time)		Date: 04/26/2011 (08.30)		Date: 04/28/2011 (08.30)	
GEOKON 4200		Temprory Support (Casting Yard)		Temprory Support (Outside Yard)	
Gage Location	Gage Label	Strain(με)	Temperature(°C)	Strain(με)	Temperature(°C)
Midspan	1-9	1901.7	64.9	1712.3	22.7
Midspan	1-10	1891.0	66.2	1753.4	22.9
Midspan	1-11	1864.0	63.0	1674.8	22.7
Midspan	1-12	1915.9	63.7	1781.0	22.9
Midspan	1-13	2249.7	60.4	2204.7	22.3
Midspan	1-14	2493.6	47.2	2410.7	21.6
Midspan	1-15	2430.2	60.9	2405.1	22.4
Midspan	1-16	2470.4	47.0	2408.9	21.8

(a): (continued)

| Date (Time) | | Date: 05/26/2011 (12:15) | | 8/5/2011(11:35) | |
| GEOKON 4200 | | Temprory Support (Outside Yard) | | Temprory Support (Outside Yard) | |
Gage Location	Gage Label	Strain(με)	Temperature(°C)	Strain(με)	Temperature(°C)
Midspan	1-9	1645.6	20.7	1561.2	23.0
Midspan	1-10	1725.0	20.5	1630.8	23.3
Midspan	1-11	1584.2	22.8	1485.9	24.1
Midspan	1-12	1727.1	22.8	1623.0	24.5
Midspan	1-13	2211.4	27.2	2151.0	27.5
Midspan	1-14	2400.7	34.2	4337.5	30.1
Midspan	1-15	2394.7	30.0	2328.7	28.0
Midspan	1-16	2416.6	35.7	2345.5	32.3

151

(b): Field Data for NEXT Beam 2

Date (Time)		Date: 04/22/2011 (07.00)		Date: 04/22/2011 (8.10)	
GEOKON 4200		20Hrs After Concrete is poured		10 Minutes After DE tensioning	
Gage Location	Gage Label	Strain(με)	Temperature(°C)	Strain(με)	Temperature(°C)
Midspan	2-9	2451.9	68.4	1988.1	66.2
Midspan	2-10	2369.4	69.4	1965.0	67.4
Midspan	2-11	2457.8	67.7	2012.8	65.2
Midspan	2-12	2399.9	67.5	1989.9	67.4
Midspan	2-13	2536.6	57.2	2503.0	52.8
Midspan	2-14	2625.0	60.4	2410.4	59.6
Midspan	2-15	2458.6	58.3	2292.6	55.0
Midspan	2-16	2485.1	66.3	2293.3	65.1
Midspan	2-17	2329.9	64.1	2284.9	58.7

Date (Time)		Date: 04/22/2011 (08.30)		Date: 04/26/2011 (10.00)	
GEOKON 4200		Temprory Support (Casting Yard)		Temprory Support (Outside Yard)	
Gage Location	Gage Label	Strain(με)	Temperature(°C)	Strain(με)	Temperature(°C)
Midspan	2-9	1881.7	63.3	1755.5	12.4
Midspan	2-10	1880.8	64.5	1813.4	12.2
Midspan	2-11	1900.4	63.4	1765.6	13.1
Midspan	2-12	1894.1	64.2	1815.7	12.7
Midspan	2-13	2491.7	49.1	2491.4	17.5
Midspan	2-14	2431.8	58.1	2439.4	15.7
Midspan	2-15	2643.2	52.2	2623.1	16.8
Midspan	2-16	2321.1	61.2	2340.6	15.2
Midspan	2-17	2274.0	54.7	2289.1	16.2

(b) (continued)

Date (Time)		Date: 04/28/2011 (07.15)		26/5/2011(11:45)	
GEOKON 4200		Temprory Support (Outside Yard)		Temprory Support (Outside Yard)	
Gage Location	Gage Label	Strain(με)	Temperature(°C)	Strain(με)	Temperature(°C)
Midspan	2-9	1764.5	21.2	1685.3	20.8
Midspan	2-10	1806.8	21.3	1769.4	20.5
Midspan	2-11	1772.0	21.5	1701.9	20.3
Midspan	2-12	1807.2	21.8	1767.6	20.0
Midspan	2-13	2460.3	21.0	2447.0	33.7
Midspan	2-14	2412.3	21.3	2390.4	29.8
Midspan	2-15	2596.2	20.5	2581.7	33.7
Midspan	2-16	2314.4	21.6	2300.3	27.4
Midspan	2-17	2264.3	21.3	2261.6	30.9

(b) (continued)

Date (Time)		8/5/2011(11:50)	
GEOKON 4200		Temprory Support (Outside Yard)	
Gage Location	Gage Label	Strain($\mu\varepsilon$)	Temperature($°C$)
Midspan	2-9	1625.7	22.9
Midspan	2-10	1697.5	23.0
Midspan	2-11	1639.5	22.8
Midspan	2-12	1694.4	22.9
Midspan	2-13	2394.5	29.7
Midspan	2-14	2327.2	28.1
Midspan	2-15	2521.3	30.8
Midspan	2-16	2261.5	25.7
Midspan	2-17	2198.7	27.4

(c): Field Data for NEXT Beam 3

Date (Time)		Date: 04/22/2011 (07.00)		Date: 04/22/2011 (08.10)	
GEOKON 4200		20 Hrs After Concrete is Poured		10 Hrs After De tensioning	
Gage Location	Gage Label	Strain(με)	Temperature(°C)	Strain(με)	Temperature(°C)
Midspan	3-1	2672.9	68.6	2167.7	68.4
Midspan	3-2	2515.1	69.2	2057.9	67.8
Midspan	3-3	2561.3	67.1	2065.1	64.9
Midspan	3-4	2487.9	67.7	2044.8	66.2
Midspan	3-5	2278.3	62.5	2255.9	55.3
Midspan	3-6	2477.5	68.2	2306.2	67.3
Midspan	3-7	2518.4	61.8	2491.6	59.9
Midspan	3-8	2450.2	63.8	2261.4	61.0
Midspan	3-9	2508.2	59.6	2480.0	53.6

(c) (Continued)

Date (Time)		Date: 04/22/2011 (08.30)		Date: 04/26/2011 (10.00)	
GEOKON 4200		Temprory Support (Casting Yard)		Temprory Support (Outside Yard)	
Gage Location	Gage Label	Strain($\mu\varepsilon$)	Temperature(°C)	Strain($\mu\varepsilon$)	Temperature(°C)
Midspan	3-1	2063.9	66.1	1923.7	14.6
Midspan	3-2	1972.9	67.7	1888.8	14.0
Midspan	3-3	1965.1	62.9	1825.3	12.8
Midspan	3-4	1959.6	64.4	1889.9	12.4
Midspan	3-5	2266.2	48.3	2262.4	19.8
Midspan	3-6	2340.7	64.0	2374.4	15.0
Midspan	3-7	2479.1	57.4	2543.0	18.0
Midspan	3-8	2274.1	58.3	2310.3	15.2
Midspan	3-9	2469.3	48.3	2506.7	17.2

(c) (Continued)

Date (Time)		Date: 04/28/2011 (7:15)		5/26/2011(11:30)	
GEOKON 4200		Temprory Support (Outside Yard)		Temprory Support (Outside Yard)	
Gage Location	Gage Label	Strain(με)	Temperature(°C)	Strain(με)	Temperature(°C)
Midspan	3-1	1938.3	21.6	1828.4	25.7
Midspan	3-2	1884.2	21.8	1813.4	24.8
Midspan	3-3	1834.9	21.4	1764.0	20.7
Midspan	3-4	1880.9	21.5	1847.8	20.5
Midspan	3-5	2232.1	21.1	2218.9	35.9
Midspan	3-6	2334.2	21.6	2355.1	27.7
Midspan	3-7	2513.7	20.7	2514.0	32.4
Midspan	3-8	2287.2	21.6	2271.4	27.7
Midspan	3-9	2479.1	21.2	2481.3	33.1

(c) (Continued)

Date (Time)		8/5/2011(11:55)	
GEOKON 4200		Temprory Support (Outside Yard)	
Gage Location	Gage Label	Strain($\mu\varepsilon$)	Temperature(°C)
Midspan	3-1	1758.0	27.2
Midspan	3-2	1729.9	26.9
Midspan	3-3	1688.1	23.1
Midspan	3-4	1760.8	23.3
Midspan	3-5	2128.7	34.9
Midspan	3-6	2260.3	28.8
Midspan	3-7	2437.2	31.5
Midspan	3-8	2220.3	27.5
Midspan	3-9	2393.9	31.1

(d): Field Data for NEXT Beam 4

Date (Time)		Date: 04/26/2011 (07.00)		Date: 04/26/2011 (08.10)	
GEOKON 4200		20 Hrs After Concrete Pour		Temprory Support (Inside Yard)	
Gage Location	Gage Label	Strain(με)	Temperature(°C)	Strain(με)	Temperature(°C)
Midspan	4-1	2441.2	70.3	1892.8	65.8
Midspan	4-2	2423.5	70.0	1927.0	65.9
Midspan	4-3	2528.7	67.3	1977.3	65.7
Midspan	4-4	2463.1	70.7	1953.3	66.3
Midspan	4-5	2384.2	61.5	2369.5	55.6
Midspan	4-6	2334.8	67.5	2149.3	64.5
Midspan	4-7	2573.5	60.1	2547.5	55.7
Midspan	4-8	2577.0	68.5	2365.7	64.0
Midspan	4-9	2486.5	61.4	2426.0	54.4

Date (Time)		Date: 04/26/2011 (8.30)		Date: 04/28/2011 (8.30)	
GEOKON 4200		Temporary Support (OutsideYard)		Temporary Support (Outside Yard)	
Gage Location	Gage Label	Strain(με)	Temperature(°C)	Strain(με)	Temperature(°C)
Midspan	4-1	1783.3	64.4	1600.8	22.5
Midspan	4-2	1822.8	64.4	1675.3	23.0
Midspan	4-3	1852.6	64.3	1658.4	22.8
Midspan	4-4	1859.2	64.6	1719.6	22.7
Midspan	4-5	2355.7	51.1	2303.0	21.9
Midspan	4-6	2179.9	62.7	2442.3	22.3
Midspan	4-7	2544.0	52.1	2505.4	21.6
Midspan	4-8	2395.5	61.2	2363.2	22.5
Midspan	4-9	2467.7	50.4	2330.5	21.7

(d) (Continued)

Date (Time)		Date: 05/26/2011 (10.45)		8/5/2011(12:03)	
GEOKON 4200		Temprory Support (Outside Yard)		Temprory Support (Outside Yard)	
Gage Location	Gage Label	Strain(με)	Temperature(°C)	Strain(με)	Temperature(°C)
Midspan	4-1	1493.7	24.9	1378.2	28.1
Midspan	4-2	1650.0	19.5	1545.4	23.1
Midspan	4-3	1606.2	19.5	1499.0	23.0
Midspan	4-4	1646.2	25.6	1533.3	28.3
Midspan	4-5	2301.4	29.4	2197.2	34.0
Midspan	4-6	2176.1	24.8	2082.7	29.7
Midspan	4-7	2524.9	30.3	2456.4	32.3
Midspan	4-8	2383.3	25.8	2317.0	27.9
Midspan	4-9	2397.5	24.8	2356.2	30.0

(d) (Continued)

| Date (Time) | | 8/11/2011(8:00) | | 9/13/2011 (7:15) | |
| GEOKON 4200 | | NEXT beam on Abutment | | After Fresh Concrete Pour | |
Gage Location	Gage Label	Strain(με)	Temperature(°C)	Strain(με)	Temperature(°C)
Midspan	4-1	1442.4	21.2	1541.6	20.1
Midspan	4-2	1563.6	22.0	1635.7	21.4
Midspan	4-3	1544.8	21.7	1641.4	20.9
Midspan	4-4	1562.3	21.6	1642.0	20.5
Midspan	4-5	2198.3	17.8	2244.5	22.1
Midspan	4-6	2050.2	19.8	1944.7	23.0
Midspan	4-7	2480.9	20.3	2460.1	22.5
Midspan	4-8	2302.1	20.1	2185.0	23.5
Midspan	4-9	2345.9	17.9	2340.1	23.2

(d) (Continued)

Date (Time)		9/22/2011(7:40)	
GEOKON 4200		9 Days After Fresh Concrete Pourr	
Gage Location	Gage Label	Strain($\mu\varepsilon$)	Temperature($°C$)
Midspan	4-1	1569.8	19.5
Midspan	4-2	1657.9	19.5
Midspan	4-3	1656.1	19.7
Midspan	4-4	1674.7	19.4
Midspan	4-5	2252.8	20.3
Midspan	4-6	1969.9	19.5
Midspan	4-7	2480.3	20.7
Midspan	4-8	2215.3	20.0
Midspan	4-9	2342.1	20.7

164

(e) : Field Data for NEXT Beam 5

Date (Time)		Date: 04/28/2011 (07.00)		Date: 04/28/2011 (08.10)	
GEOKON 4200		20hrs After Concrete is Poured		10 minutes After Detensioning	
Gage Location	Gage Label	Strain(με)	Temperature(°C)	Strain(με)	Temperature(°C)
Mid-span	5-1	2579.0	67.4	2090.0	65.2
Mid-span	5-2	2582.6	69.1	2142.4	67.5
Mid-span	5-3	2588.5	66.7	2084.7	64.9
Mid-span	5-4	2638.9	68.2	2199.9	66.6
Mid-span	5-5	2536.8	58.8	2500.3	54.1
Mid-span	5-6	2621.9	67.2	2437.6	63.6
Mid-span	5-7	2689.6	61.3	2668.1	58.6
Mid-span	5-8	2725.9	65.2	2538.5	62.2
Mid-span	5-9	2411.4	59.6	2372.3	54.1

(e) (Continued)

Date (Time)		Date: 04/28/2011 (08.30)		Date: 05/26/2011 (11.05)	
GEOKON 4200		Temprory Support (Casting Yard)		Temprory Support (Outside Yard)	
Gage Location	Gage Label	Strain(με)	Temperature(°C)	Strain(με)	Temperature(°C)
Mid-span	5-1	1968.9	61.8	1767.9	19.5
Mid-span	5-2	2044.8	64.2	1902.3	19.6
Mid-span	5-3	1953.7	62.7	1756.9	19.4
Mid-span	5-4	2093.6	64.3	1972.0	19.3
Mid-span	5-5	2505.2	49.8	2446.7	26.5
Mid-span	5-6	2468.7	61.1	2459.3	23.4
Mid-span	5-7	2664.7	57.2	2641.1	29.6
Mid-span	5-8	2567.0	60.0	2505.5	25.7
Mid-span	5-9	2366.9	48.0	2313.4	27.5

(e) (Continued)

| Date (Time) | | Date: 08/05/2011 (12.07) | | 8/11/2011(11:13) | |
| GEOKON 4200 | | Temprory Support (Outside Yard) | | Temprory Support (Outside Yard) | |
Gage Location	Gage Label	Strain(με)	Temperature(°C)	Strain(με)	Temperature(°C)
Mid-span	5-1	1670.7	22.8	1705.7	20.9
Mid-span	5-2	1795.8	23.0	1816.4	21.4
Mid-span	5-3	1668.2	22.4	1701.9	21.3
Mid-span	5-4	1880.3	22.5	1890.4	21.4
Mid-span	5-5	2337.1	31.8	2352.8	19.9
Mid-span	5-6	2369.2	26.7	2348.7	20.6
Mid-span	5-7	2562.4	31.2	2541.8	19.8
Mid-span	5-8	2441.1	25.4	2421.7	20.2
Mid-span	5-9	2253.9	29.3	2192.3	20.0

(e) (Continued)

Date (Time)		9/13/2011		9/22/2011	
GEOKON 4200		After Fresh concrete Pour		After 9 days of Concrete pour (Not in Scope of Thesis)	
Gage Location	Gage Label	Strain(με)	Temperature(°C)	Strain(με)	Temperature(°C)
Mid-span	5-1	1801.8	20.6	1808.6	19.5
Mid-span	5-2	1874.1	21.3	1889.0	19.3
Mid-span	5-3	1805.4	20.6	1838.2	19.6
Mid-span	5-4	1959.0	20.9	1974.6	19.2
Mid-span	5-5	2340.5	23.1	2353.2	20.7
Mid-span	5-6	2234.5	23.5	2267.4	19.7
Mid-span	5-7	2545.6	22.6	2560.5	20.5
Mid-span	5-8	2306.7	23.3	2340.7	19.4
Mid-span	5-9	2239.0	22.9	2253.7	20.2

(f): Field Data for NEXT Beam 6

Date (Time)		Date: 04/28/2011 (07:00)		4/28/2011(08:10)	
GEOKON 4200		20hrs After Concrete is Poured		10 minutes After Detensioning	
Gage Location	Gage Label	Strain(με)	Temperature(°C)	Strain(με)	Temperature(°C)
Mid-span	6-1	2590.0	68.7	2146.7	67.3
Mid-span	6-2	2592.1	69.4	2189.9	68.5
Mid-span	6-3	2508.9	68.4	2098.6	66.6
Mid-span	6-4	2458.5	67.8	2015.0	65.7
Mid-span	6-5	2515.2	66.6	2281.1	65.1
Mid-span	6-6	2516.2	67.9	2310.9	64.7

Date (Time)		Date: 04/28/2011 (08:30)		5/26/2011(11:05)	
GEOKON 4200		Temprory Support (Inside Yard)		Temprory Support (Outside Yard)	
Gage Location	Gage Label	Strain($\mu\epsilon$)	Temperature($°C$)	Strain($\mu\epsilon$)	Temperature($°C$)
Mid-span	6-1	2007.9	64.9	1814.9	19.9
Mid-span	6-2	2071.7	66.9	1956.0	19.6
Mid-span	6-3	1964.2	66.3	1826.3	21.6
Mid-span	6-4	1858.3	64.1	1650.8	21.8
Mid-span	6-5	2311.6	64.2	2310.5	25.7
Mid-span	6-6	2357.0	60.8	2317.3	27.9

Date (Time)		8/05/2011(12:10)		8/11/2011(11:20)	
GEOKON 4200		Temprory Support (Outside Yard)		NEXT beam on Abutment	
Gage Location	Gage Label	Strain($\mu\epsilon$)	Temperature($°C$)	Strain($\mu\epsilon$)	Temperature($°C$)
Mid-span	6-1	1720.5	22.9	1754.5	21.3
Mid-span	6-2	1861.6	22.7	1872.6	21.4
Mid-span	6-3	1719.7	24.4	1725.9	23.3
Mid-span	6-4	1552.5	24.4	1584.0	22.9
Mid-span	6-5	2224.0	27.7	2206.2	20.4
Mid-span	6-6	2224.6	28.8	2208.5	21.6

(f) (Continued)

Date (Time)		9/13/2011(09:40)		9/22/2011 (16:30)	
GEOKON 4200		After Concrete pour		9 Days After Concrete Pour (Not in Scope of Thesis)	
Gage Location	Gage Label	Strain($\mu\varepsilon$)	Temperature(°C)	Strain($\mu\varepsilon$)	Temperature(°C)
Mid-span	6-1	1541.6	20.1	1569.8	19.5
Mid-span	6-2	1635.7	21.4	1657.9	19.5
Mid-span	6-3	1641.4	20.9	1656.1	19.7
Mid-span	6-4	1642.0	20.5	1674.7	19.4
Mid-span	6-5	2244.5	22.1	2252.8	20.3
Mid-span	6-6	1944.7	23.0	1969.9	19.5

171

APPENDIX G

STRAIN VARIATION FOR DIFFERENT STAGES

To get the strain variation, temperature as well as strain both is measured. The filed data will be used to evaluate individual load related strain and cumulative strain at different stages.

Equation 6.1 will be used to obtain the true load related strains.

$$\mu_{True} = (R1-R0)\ B + (T1-T0)\ (C1-C2) \qquad \text{.....Equation G.1}$$

Where,

μ_{True} = true load related strain.

R_1 = measured strains at present stage.

R_0 = measured strains at previous stage.

B = 0.975 is calibration factor

T_1 = measured temperature at present stage.

T_0 = measured temperature at previous stage

C_1 = 12.2 micro strain/^{o}C Thermal coefficient of expansion for wire

C_2 = 10.0 micro strain/^{o}C Thermal coefficient of expansion for wire

172

Based on Equation E.1 individual true load related strains are calculated. The individual load related strain are listed in Table E.1 and E.2.

Table G 1*(a-f): Stage Wise True Load Related Strain for NEXT Beams*

(a) *Wise True Load Related Strain for NEXT Beam1*

GEOKON 4200	Date	04/26/2011	4/26/2011	4/26/2011	4/28/2011	5/26/2011	8/5/2011
	Time	7:00	8:10	8:30	8:30	0:15	11:35
	Instrument Depth from BF	20 hrs After Pour	ES+R	C+S	C+S	C+S	C+S
Gage Label	y	Strain(με)	Strain(με)	Strain(με)	Strain(με)	Strain(με)	Strain(με)
1-9	3.75	-214	-501	-117	-278	-69	-77
1-10	8.25	-221	-454	-93	-229	-33	-86
1-13	29.50	-192	-222	31	-128	17	-58
1-11	3.75	-234	-495	-144	-273	-88	-93
1-12	8.00	-244	-460	-112	-221	-53	-98
1-15	29.50	-205	-232	25	-109	7	-69

NOTES: ES=Elastic Shortening Loss; R= Relaxation Loss; C=Creep;S=Shrinkage; BF =Bottom Fiber

173

(b): Stage Wise True Load Related Strain for NEXT Beam 2

GEOKON 4200	Date	04/22/2011	4/22/2011	4/22/2011	4/26/2011	4/28/2011	5/26/2011	8/5/2011
	Time	7:00	8:10	8:30	10:00	10:15	11:45	11:50
	Instrument Depth from BF	20 hrs After Pour	ES+R	C+S	C+S	C+S	C+S	C+S
Gage Label	y	Strain($\mu\varepsilon$)	Strain($\mu\varepsilon$)	Strain($\mu\varepsilon$)	Strain($\mu\varepsilon$)	Strain($\mu\varepsilon$)	Strain($\mu\varepsilon$)	Strain($\mu\varepsilon$)
2-9	3.750	-243	-457	-110	-235	28	-78	-53
2-10	8.125	-245	-399	-88	-181	14	-38	-65
2-14	29.500	-173	-211	18	-86	-14	-3	-65
		0	0	0	0	0	0	0
2-11	3.750	-251	-439	-114	-242	25	-71	-55
2-12	8.125	-245	-400	-100	-190	12	-43	-65
2-16	29.500	-241	-190	19	-82	-11	-1	-42

NOTES: ES=Elastic Shortening Loss; R= Relaxation Loss; C=Creep;S=Shrinkage; BF =Bottom Fiber

174

(c): Stage Wise True Load Related Strain for NEXT Beam 3

GEOKON 4200	Date	04/26/2011	4/22/2011	4/22/2011	4/26/2011	4/28/2011	5/26/2011	8/5/2011
	Time	7:00	8:00	8:30	10:00	7:15	11:30	11:55
	Instrument Depth from BF	20 hrs After Pour	ES+R	C+S	C+S	C+S	C+S	C+S
Gage Label	y	Strain(με)	Strain(με)	Strain(με)	Strain(με)	Strain(με)	Strain(με)	Strain(με)
3-1	3.50		-493	-106	-250	30	-98	-65
3-2	8.13		-449	-83	-200	13	-62	-77
3-6	29.50		-169	26	-75	-25	34	-69
3-3	3.50		-489	-102	-247	28	-71	-90
3-4	8.25		-435	-87	-182	11	-34	-90
3-8	29.50		-190	6	-60	-8	-2	-77

NOTES: ES=Elastic Shortening Loss; R= Relaxation Loss; C=Creep;S=Shrinkage; BF =Bottom Fiber

(d): Stage Wise True Load related Strain NEXT Beam 4

GEO KON 4200	Date	04/26/2011	4/26/2011	4/26/2011	4/28/2011	5/26/2011	8/5/2011	8/11/2011	9/13/2011	9/22/2011
	Time	7:00	8:00	8:30	8:30	10:45	12:03	8:00	9:50	16:30
	Depth from BF	20 hrs. After Pour	ES+R	C+S	C+S	C+S	C+S	C+S	Fresh Concrete+ C+S	C+S (Not in Scope)
Gage Label	y	Strain(με)	Strain(με)	Strain(με)	Strain(με)	Strain(με)	Strain(με)	Strain(με)	Strain(με)	Strain(με)
4-1	4.3	-163	-545	-110	-270	-99	-106	47	94	26
4-2	8.0	-199	-493	-105	-235	-32	-94	15	69	17
4-6	29.5	-174	-187	26	167	-254	-80	-53	-96	17
4-3	4.0	-185	-541	-125	-281	-58	-97	42	92	12
4-4	7.8	-185	-507	-95	-228	-65	-104	14	75	29
4-8	29.5	-188	-216	23	-117	27	-60	-32	-107	22

NOTES: ES=Elastic Shortening Loss; R= Relaxation Loss; C=Creep;S=Shrinkage; BF =Bottom Fiber

(e): Stage Wise True Load related Strain NEXT Beam 5

GEOKON 4200	Date	04/28/2011	4/28/2011	4/28/2011	5/26/2011	8/5/2011	8/11/2011	9/13/2011	9/22/2011
	Time	7:00	8:00	8:30	11:05	12:07	11:03	8:00	9:50
	Instrument Depth from BF	20 hrs After Pour	ES+R	C+S+R	C+S+R	C+S+R	C+S+R	Fresh Concrete+C+S	C+S (Not in Scope)
Gage Label	y	Strain($\mu\varepsilon$)	Strain($\mu\varepsilon$)	Strain($\mu\varepsilon$)	Strain($\mu\varepsilon$)	Strain($\mu\varepsilon$)	Strain($\mu\varepsilon$)	Strain($\mu\varepsilon$)	Strain($\mu\varepsilon$)
5-1	4.25	-186	-482	-126	-289	-88	30	93	4
5-2	7.875	-190	-433	-102	-237	-96	17	56	10
5-6	29.50	-196	-188	25	-92	-81	-33	-105	24
5-3	3.875	-164	-495	-133	-287	-80	30	99	30
5-4	8.125	-195	-432	-109	-218	-82	7	66	11
5-8	29.50	-159	-189	23	-135	-63	-30	-105	25

NOTES: ES=Elastic Shortening Loss; R= Relaxation Loss; C=Creep;S=Shrinkage; BF =Bottom Fiber

177

(f): Stage Wise True Load related Strain NEXT Beam 6

GEOKON 4200	Date	04/28/2011	4/28/2011	4/28/2011	5/26/2011	8/5/2011	8/11/2011	9/13/2011	9/22/2011
	Time	7:00	8:00	8:30	8:30	10:45	12:03	8:00	16:30
	Instrument Depth from BF	20 hrs After Pour	ES+R	C+S	C+S	C+S	C+S	C+S+Deck	C+S (Not in Scope)
Gage Label	y	Strain(με)	Strain(με)	Strain(με)	Strain(με)	Strain(με)	Strain(με)	Strain(με)	Strain(με)
6-1	4.25	-223	-435	-141	-287	-85	30	112	17
6-2	8.00	-230	-394	-119	-217	-85	8	81	22
6-6	29.50	-191	-232	28	-86	-80	-33	-117	27
6-3	4.00	-230	-404	-132	-233	-98	4	106	26
6-4	7.75	-213	-437	-156	-295	-90	27	140	29
6-5	29.50	-186	-207	36	-111	-88	-32	-114	14

NOTES: ES=Elastic Shortening Loss; R= Relaxation Loss; C=Creep;S=Shrinkage; BF =Bottom Fiber

STAGE WISE CUMULATIVE STRAIN

Table H 1(a-f): Stage Wise Cumulative Strain for NEXT Beams

(a): Stage Wise Cumulative Strain for NEXT Beam 1

	Date	04/26/2011	4/26/2011	4/26/2011	4/28/2011	5/26/2011	8/5/2011
	Time	7:00	8:00	8:30	8:30	10:45	12:03
GEOKON 4200	Instrument Depth from BF	20 hrs After Pour	Inside CY	Inside CY	Outside CY	Outside CY	Outside CY
Gage Label	y	Strain($\mu\epsilon$)	Strain($\mu\epsilon$)	Strain($\mu\epsilon$)	Strain($\mu\epsilon$)	Strain($\mu\epsilon$)	Strain($\mu\epsilon$)
1-9	3.75	-214	-715	-832	-1109	-1179	-1256
1-10	8.25	-221	-674	-767	-997	-1029	-1115
1-13	29.50	-192	-414	-383	-511	-494	-552
1-11	3.75	-234	-729	-873	-1146	-1234	-1327
1-12	8.00	-244	-704	-816	-1037	-1090	-1188
1-15	29.50	-205	-437	-412	-521	-514	-583

NOTES: ES=Elastic Shortening Loss; R= Relaxation Loss; C=Creep;S=Shrinkage; BF =Bottom Fiber

GEOKON 4200	Date	04/22/2011	4/22/2011	4/22/2011	4/26/2011	4/28/2011	5/26/2011	8/5/2011
	Time	7:00	8:00	8:30	10:00	10:15	11:45	11:50
	Depth from BF	20 hrs After Pour	Inside CY	Inside CY	Outside CY	Outside CY	Outside CY	On Site BP
Gage Label	y	Strain(με)	Strain(με)	Strain(με)	Strain(με)	Strain(με)	Strain(με)	Strain(με)
2-9	3.750	-243	-700	-810	-1045	-1017	-1095	-1149
2-10	8.125	-245	-644	-732	-913	-899	-938	-1002
2-14	29.500	-173	-384	-366	-452	-466	-469	-534
2-11	3.750	-251	-691	-804	-1046	-1022	-1093	-1148
2-12	8.125	-245	-645	-745	-935	-923	-966	-1031
2-16	29.500	-241	-431	-412	-495	-506	-507	-549

\

(c): Stage Wise Cumulative Strains NEXT Beam 3

GEOKON 4200	Date	04/26/2011	4/26/2011	4/26/2011	4/28/2011	5/26/2011	8/5/2011	8/11/2011
	Time	7:00	8:00	8:30	8:30	10:45	12:03	8:00
	Depth from BF	20 hrs After Pour	Inside CY	Inside CY	Outside CY	Outside CY	Outside CY	On Site BP
Gage Label	y	Strain(με)	Strain(με)	Strain(με)	Strain(με)	Strain(με)	Strain(με)	Strain(με)
3-1	3.50		-493	-599	-849	-820	-918	-983
3-2	8.13		-449	-532	-732	-719	-782	-859
3-6	29.50		-169	-143	-218	-242	-208	-277
3-3	3.50		-489	-591	-837	-809	-879	-970
3-4	8.25		-435	-522	-705	-693	-728	-818
3-8	29.50		-190	-184	-243	-252	-254	-331

(d): Stage Wise Cumulative Strains NEXT Beam 4

GEOKON 4200	Date	04/26/2011	4/26/2011	4/26/2011	4/28/2011	5/26/2011	8/5/2011	8/11/2011	9/13/2011	9/22/2011
	Time	7:00	8:00	8:30	8:30	10:45	12:03	8:00	9:50	16:30
	Depth from BF	20 hrs. After Pour	Inside CY	Inside CY	Outside CY	Outside CY	Outside CY	On Site BP	On Site AP	On Site AP
Gage Label	y	Strain(με)	Strain(με)	Strain(με)	Strain(με)	Strain(με)	Strain(με)	Strain(με)	Strain(με)	Strain(με)
4-1	4.3	-163	-708	-818	-1088	-1187	-1293	-1245	-1151	-1125
4-2	8.0	-199	-692	-797	-1032	-1065	-1159	-1143	-1074	-1057
4-6	29.5	-174	-362	-336	-169	-423	-503	-557	-653	-636
4-3	4.0	-185	-726	-851	-1131	-1190	-1286	-1245	-1152	-1141
4-4	7.8	-185	-691	-787	-1015	-1080	-1185	-1171	-1096	-1066
4-8	29.5	-188	-404	-381	-498	-471	-531	-562	-669	-647

BF – Depth from Bottom fiber; CY – Casting Yard; BP- Before Pour; AP – After Pour of Fresh concrete

182

(e): Stage Wise Cumulative Strains NEXT Beam 5

GEOKON 4200	Date	04/28/2011	4/28/2011	4/28/2011	5/26/2011	8/5/2011	8/11/2011	9/13/2011	9/22/2011
	Time	7:00	8:00	8:30	11:05	12:07	11:03	8:00	9:50
	Instrument Depth from BF	20 hrs After Pour	Inside CY	Inside CY	Outside CY	Outside CY	Outside CY	On Site BP	On Site AP
Gage Label	y	Strain(με)	Strain(με)	Strain(με)	Strain(με)	Strain(με)	Strain(με)	Strain(με)	Strain(με)
5-1	4.25	-186	-668	-793	-1082	-1170	-1140	-1047	-1042
5-2	7.875	-190	-622	-725	-962	-1058	-1042	-986	-975
5-6	29.50	-196	-384	-359	-451	-532	-565	-670	-647
5-3	3.875	-164	-659	-792	-1079	-1159	-1128	-1029	-999
5-4	8.125	-195	-627	-736	-953	-1036	-1028	-962	-951
5-8	29.50	-159	-348	-325	-461	-524	-555	-660	-635

f): Stage Wise Cumulative Strains NEXT Beam 6

GEOKON 4200		04/26/2011	4/26/2011	4/26/2011	4/28/2011	5/26/2011	8/5/2011	8/11/2011	9/13/2011
	Date								
	Time	7:00	8:00	8:30	8:30	10:45	12:03	8:00	16:30
	Depth from BF	20 hrs After Pour	Inside CY	Inside CY	Outside CY	Outside CY	Outside CY	On Site BP	On Site AP
Gage Label	y	Strain(με)	Strain(με)	Strain(με)	Strain(με)	Strain(με)	Strain(με)	Strain(με)	Strain(με)
6-1	4.25	-223	-659	-799	-1086	-1172	-1142	-1031	-1013
6-2	8.00	-230	-624	-743	-960	-1045	-1037	-956	-934
6-6	29.50	-191	-423	-395	-481	-561	-594	-711	-684
6-3	4.00	-230	-634	-766	-999	-1096	-1093	-987	-960
6-4	7.75	-213	-650	-806	-1102	-1192	-1164	-1024	-995
6-5	29.50	-186	-393	-357	-468	-557	-588	-702	-688

BIBLIOGRAPHY

1. **Alaa Helba, John B. Kennedy.** *Collapse Loads of Continuous Skew Composite Bridges.*. 5, 1994, Journal of Structural Engineering, Vol. 120, pp. 1395-1415.

2. **Scott A. Civjan, P.E., Christine Bonczar, Sergio F. Breña, Jason DeJong, Daniel Crovo.** *Integral Abutment Bridge Behavior: Parametric Analysis of a Massachusetts Bridge.* 1, January/February 2007, Journal of Bridge Engineering, Vol. 12, pp. 64-67.

3. **Sergio F. Breña, Christine H. Bonczar, Scott A. Civjan, Daniel S. Crovo.** *Evaluation of Seasonal and Yearly Behavior of an Integral Abutment Bridge.* 3, May/June 2007, Journal of Bridge Engineering, Vol. 12, pp. 296-305.

4. **Murat Dicleli, Semih Erhan.** *Effect of Soil and Sub structure Properties on Live-Load Distribution in Integral Abutment Bridges.* 5, 2008, Journal Bridge Engineering, Vol. 13, p. 527.

5. **Toorak Zokaie.** *AASHTO-LRFD Live Load Distribution Specifications.* 2, May 2000, Journal of Bridge Engineering, Vol. 5, pp. 131-138.

6. **Bishara, A.G, Liu, M.C and and El-Ali, N.D.** *Wheel Load distribution on Simply Supported Skew I-Beam Composite Bridges.* 2, 1993, ASCE Journal of Structural Engineering, Vol. 119, pp. 399-419.

7. University of Illinois Bulletin Engineering Experiment Station.*Studies of Slab and Beam Highway Bridges – Part II: Test of Simple- Span Skew I- Beam Bridges,.* 375,

8. **Newmark, N.M and Peckham, W.M.** *Live load distribution equations for integral Bridge sub structures.* **Erhan S., Dicleli M.** 5, 2009, Engineering Structures, Vol. 31, pp. 1250-1264.

9. **Zaher Yousif and Riyadh Hindi**. *AASHTO-LRFD Live Load Distribution for Beam-and-Slab Bridges: Limitations and Applicability.***,** J. Bridge Eng. 12, 765 (2007); doi:10.1061/(ASCE)1084-0702(2007)12:6(765) (9 pages)

10 , **Paul J. Barr, Marc O. Eberhard, and John F. Stanton.***Live-Load Distribution Factors in Prestressed Concrete Girder Bridges*J. Bridge Eng. 6, 298 (2001); doi:10.1061/(ASCE)1084-0702(2001)6:5(298) (9 pages)

11. **Devin K. Harris.** *Assessment of flexural lateral load distribution methodologies for stringer Bridges.* Engineering Structures, Volume 32, Issue 11, November 2010, Pages 3443-3451

12 . A**li R. Khaloo and H. Mirzabozorg.** *Load Distribution Factors in Simply Supported Skew Bridges* J. Bridge Eng. 8, 241 (2003); doi: 10.1061/(ASCE)1084-0702(2003)8:4(241) (4 pages)

13 . **Yochia Chen.** *Distribution of vehicular loads on Bridge girders by the FEA using ADINA: modeling, simulation, and comparison Original* Computers & Structures, Volume 72, Issues 1-3, July-August 1999, Pages 127-139

14. *Fifth edition 2010 AASHTO LRFD Bridge design specification*

15. *NCHRP Report 592 Simplified Live Load distribution factor equation.*